Student thesis series INES nr 258

Aerosol Light Absorption Measurement Techniques: A Comparison of Methods from Field Data and Laboratory Experimentation

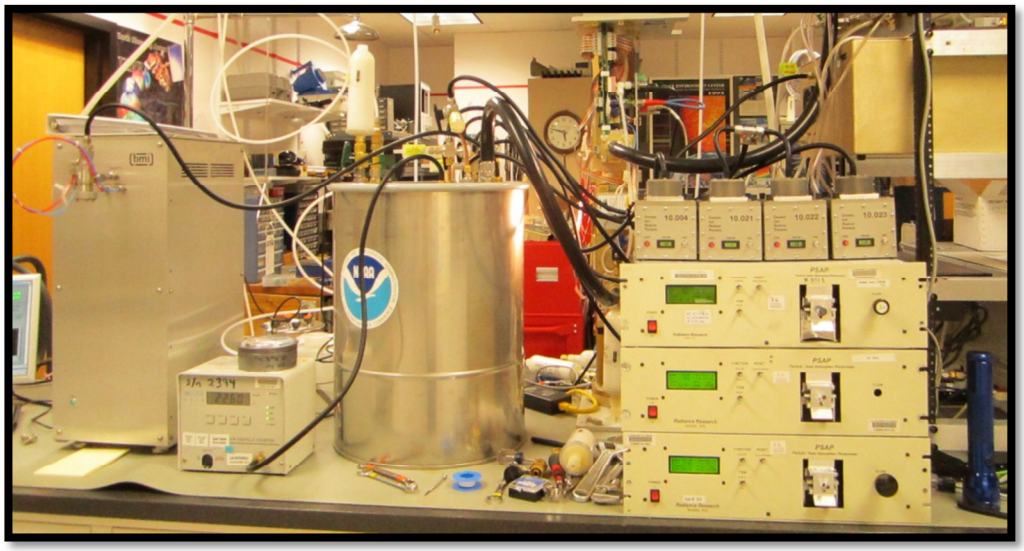

Christine Walsh

2012
Department of Earth and Ecosystem Sciences
Physical Geography and Ecosystems Analysis
Lund University
Sölvegatan 12
S-223 62 Lund
Sweden

Christine Walsh (2012). "Aerosol Light Absorption Measurement Techniques: A Comparison of Methods from Field Data and Laboratory Experimentation"

Master Degree Thesis, 30 credits in *Atmospheric Sciences and Biogeochemical Sciences*

Department of Earth and Ecosystem Sciences
Physical Geography and Ecosystems Analysis, Lund University

Cover photo Credit: C. Walsh

A Master's Thesis presented to

Department of Physical Geography and Ecosystems Analysis

Centre for Geographical Information Systems

of

LUND
UNIVERSITY

By

Christine Walsh

In partial fulfilment of the requirements

for the degree of Master's in

Atmospheric Sciences and Biogeochemical Cycles

Supervisors:

Thomas Holst of Lund University

John Ogren of the National Oceanic and Atmospheric Administration

I. Acknowledgments

There are a great number of people I feel gratitude towards in the completion of this project. There are many faces of inspiration I have had the pleasure of meeting along the way and I am pleased for the opportunity to thank a few of them.

Thank you to the many brilliant professors and staff of the Physical Geography department in Lund University; most particularly my supervisor, Thomas Holst for all your insight and guidance. I also wish to express my appreciation to Harry Lankreijer and Helena Erikkson for all your assistance in my realizing my educational pathway during my time in Lund. I am also very grateful to Antti Lauri, Kaale Hämeri, and Bjarke Mölgaard of University of Helsinki and Christina Isaxon of LTH at Lund University for accepting me into their wonderful and infinitely helpful atmospheric aerosol-introducing courses.

Naturally, I am incredibly grateful to everyone at the National Oceanic and Atmospheric Administration Global Monitoring Division of Boulder, Colorado who were so open to providing this sensational opportunity for me. Notably, my gratitude is felt for my supervisor, John Ogren, as well as Betsy Andrews, Patrick Sheridan, Anne Jefferson, and Derek Hageman for welcoming me into your offices and laboratory, and being so willing to share your incredible knowledge-base on such a fascinating subject. I have valued your patience in my questions, inquiries, and insight-seeking conversations. Thank you Dan Lack and Justin Langridge for such an engaging dataset and for your interest in collaboration.

Thank you to every teacher along the way who encouraged my zest for remaining an everlasting student; especially Mrs. Kelly Meyer (for her early encouragement in my love for writing), Mr. Matthew Achor and Mrs. Marilyn Nowicki (for instilling a passion for science), and Mr. Jay Bell (for helping me to acknowledge the inevitability of graduate school).

And of course, thank you to my family and friends all over the globe for remaining a never-ceasing foundation of encouragement and support; thank you to my mom and dad, and to Robbie and Kathy; your support has meant the world to me. And finally, thank you Brandon Henry, for the collaboration in realizing a once-distant dream.

II. Abstract

Atmospheric aerosols are of great importance climatically due in part to their ability to scatter and absorb solar radiation. However, their influence in our changing climate holds the greatest uncertainty of all atmospheric components. With this in mind, there remains a necessity for advancement in monitoring and measurement techniques. The aim of this investigation is to consider the current measurement techniques for aerosol absorption and compare instrument performance in a variety of conditions. Filter-based measurements and various referencing techniques for establishing values of the aerosol absorption coefficient (σ_{ap}) are examined. The report discusses the various instrumentation, mathematical techniques, and uncertainties associated with each through applications employed during a field campaign, the California Air Quality and Climate Nexus Campaign (CalNex; April-May 2010) and a laboratory experiment at the National Oceanic and Atmospheric Administration (NOAA) in Boulder, Colorado (April 1st, 2012- May 2, 2012). The filter-based instruments, particle soot absorption photometer (PSAP) and the continuous light absorption photometer (CLAP), are compared in performance to the in-situ techniques of the photoacoustic spectrometer (PAS) and absorption obtained via the difference method (σ_{ap} = extinction (σ_{ep}) – scattering (σ_{sp})). A potential bias of filter-based instruments during high organic aerosol (OA) loading was investigated during in-flight sampling over the Los Angeles metro region, yielding only one bias occurrence for the analysis on a daytime flight. Possible discrepancies in utilization of the difference method as a reference for filter-based σ_{ap} are investigated in laboratory data, as a 5% inconsistency between σ_{ep} and σ_{sp} during white aerosol runs yields questionable reference σ_{ap} results. Potential benefits of the novel Corrected Two-Stream (CTS) correction method for filter-based instruments in various conditions are also investigated for both datasets, with obvious advantages during the changing conditions of a grey to white aerosol laboratory run. A comparison of the CLAP and PSAP filter-based method during laboratory experimentation was also examined, demonstrating the highly-correlated measurements of the two instruments. The aim of this investigation is not to decide which of these instruments or methodologies for the quantification of σ_{ap} should be deemed “the best method”, but rather to provide real-world examples of their applications, capabilities, and limitations.

Keywords: Aerosol, Absorption, Filter-based Instruments, In-situ Techniques, Difference Method, Filter-based Correction

III. Table of Contents

IV. List of Tables and Figures

List of Tables:

List of Figures:

1: Introduction

1.1: Aerosols in the Atmosphere

The term atmospheric aerosol refers to the multi-phase collection of solid and/or liquid particles that are suspended in the air around us. These are either emitted directly (primary aerosols) or formed due to processing with volatile components of the surrounding air (secondary aerosols) (Seinfeld and Pandis, 2006). The aerosols of the global atmosphere are composed of diverse characteristics and qualities; each particle with unique shape, size, chemical composition, and optical properties. Aerosols in our atmosphere have a wide range of potential sources; both natural and anthropogenic in origin. Ranging in size from the just-stable molecule clusters of a few nanometers (nm) to the short-lived particles heavily-influenced by gravity (up to 100 micrometers (μm)), aerosols are responsible for a large array of atmospheric marvels, such as fog, haze, clouds, fumes, smoke, and mist (Hinds, 1999). Particles at the smaller end of the size range are vital to the development of clouds, while the less abundant larger particles have higher concentrations near the sea or dust sources. For climate science, particles ranging from 0.05 to 10 μm are of greatest interest, due to their interaction with sunlight (Kahn et al., 2009).

Due to their diversity in sources and characteristics, aerosols are both highly spatially and temporally variable. Lifetimes of aerosols ranges from a few minutes to a few weeks, depending on their size and composition, atmospheric conditions, and subsequent atmospheric processing. Therefore, the influence of atmospheric particulates based on concentration and composition is not constant on a global scale (Seinfeld and Pandis, 2006). For instance, locally peaked concentrations of aerosols can be observed in the morning hours during high levels of traffic, fluctuating in magnitude as the day continues on. Also, the concentrations are higher closer to the roadways and will decrease as a function of increasing distance (Wrobel et al., 2000; Zhu et al., 2002; Virtanen et al., 2006). Aerosol concentrations will not only vary on an hourly and daily basis, but also experience seasonal and yearly fluctuations. This regional heterogeneity creates a substantial challenge for the quantification and characterization of aerosols in scientific study (Seinfeld and Pandis, 2006; Kahn et al., 2009).

The scientific investigation of aerosols in the atmosphere is essential, due to both their direct and indirect effect on climate. The indirect effect, described in detail by Twomey (1974),

Ramanathan et al (2001), and Feingold (2003), is the aerosol interactions with cloud development, characteristics, and lifetimes. Despite the climactic importance of these relationships, of greater interest to this investigation is the interaction of aerosols with solar radiation, known as the direct effect. Determined by the wavelength of incident radiation, the size of the particle, and the particle's refractive index, aerosols can change the direction and/or intensity of light via scattering and absorption (Seinfeld and Pandis, 2006). In doing so, aerosols can have effects on visibility (Malm et al., 1994), as well as the radiative balance of the Earth (Rasool and Schnedier, 1971; Charlson et al., 1992; Ramanathan and Vogelman, 1997).

The warming or cooling of the aerosol direct climate forcing is dependent on the amounts of scattering or absorption. An essential tool for the quantification of the direct effect is the single scattering albedo (SSA or ω):

$$SSA = \frac{Scattering}{Exticition} = \frac{Scattering}{Scattering + Absorption} \quad (1)$$

where SSA will range from 0 (purely absorbing, dark particles) to 1 (purely scattering particles); however, there is no particle in existence that will truly be quantified at 0 or 1 (Seinfeld and Pandis, 2006). With that, the asymmetry parameter (g) provides insight on whether the particle will completely backscatter light (-1), uniformly scatter light (0), or completely forward- scatter light (+1) (Seinfeld and Pandis, 2006). Whether the aerosol will warm or cool the surrounding air will be dependent on the SSA and the asymmetry parameter, as well as the brightness or darkness of the surface beneath it (Ramanathan et al., 2001).

Typically, scattering aerosols have reflective components, such as sulphates, organics, and nitrates. Alternatively, absorbing aerosols are most often from primary sources, such as the soot created during combustion processes, which are then modified in the atmosphere when other species react/condense upon them (Seinfeld and Pandis, 2006). Absorbing aerosols are of climactic importance due to their contribution to atmospheric warming, with black carbon (BC), or completely absorbing aerosol, said to contribute up to 20-50% as warming by CO_2 (IPCC, 2007; Ramanathan and Carmichael, 2008). When found within cloud cover, the absorption of light by aerosols causes the instability and dissipation of clouds. Known as the semi-direct effect,

absorbing aerosols contribute to the warming of the atmosphere (Ramanathan et al., 2001). It is well-known that atmospheric aerosols have comparable influence on climate to that of highly studied greenhouse gases (Seinfeld and Pandis, 2006). However, as the fraction of light that is absorbed by aerosols is typically smaller in magnitude compared to scattering by aerosols, accurate measurements remain a challenge in practice (Lack et al., 2008; Müller et al., 2011).

1.2: Uncertainty of Atmospheric Aerosols

Currently, the drive to develop understanding in this field is strong, with a range of approaches bringing various components together. While in situ field campaigns yield knowledge on the concentrations and compositions of aerosol at or near the surface, remote sensing via satellite can provide vertical profiles essential for understanding radiative influence of aerosols. The coupling of long-term observation sites, short-term field campaigns, and monitoring via satellites yield a more comprehensive estimate of current global radiative forcing by atmospheric aerosols. All of these components are essential for the better-constraint of present global models aiming to predict future climate implications (IPCC, 2007; Kahn et al., 2009).

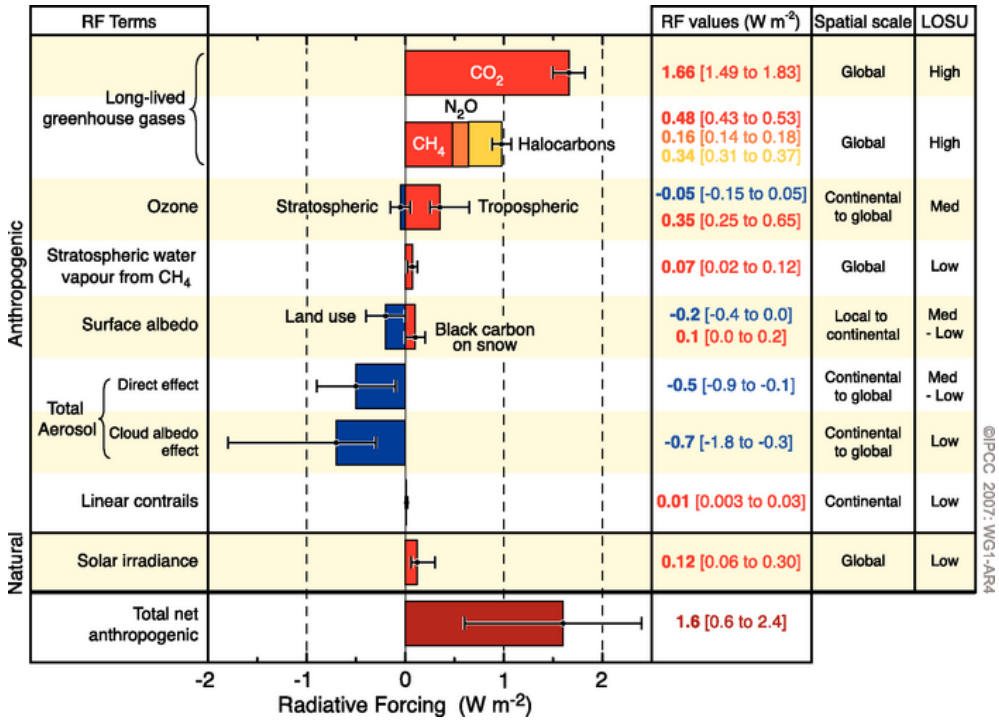

Figure 1.1: Components of natural and anthropogenic climate forcings as determined by the Intergovernmental Panel on Climate Change (IPCC). As can be seen, the uncertainty bars associated with atmospheric aerosols remain the largest. Figure from Climate Change 2007: The Physical Basis. Printed with permission from the IPCC and the World Meteorological Organization.

The current consensus is that the scattering of light by the indirect effect of aerosols is the dominant radiative process, causing a net cooling effect (IPCC, 2007). As can be seen in figure 1.1 from the IPCC's WGI: The Physical Science Basis, the climate forcing of atmospheric aerosols remains the largest uncertainty in the determination of current climate sensitivity (IPCC, 2007; Schwartz et al., 2006). Due to the difficulties in measurement with spatial and temporal variation of atmospheric aerosols, further scientific investigation is essential for climate and atmospheric research.

1.3: Importance of Instrument Inter-comparison

With that, there remains a necessity for advancement in monitoring and measurement techniques. In order to do so, proper evaluation of the tools and instruments utilized in the quantification of aerosol properties is essential. Relevant to the aim of this investigation, both established and novel techniques for the measurement of aerosol absorption will be considered.

Currently, there is no instrumentation for studying aerosol absorption that offers reliable measurements, simplicity in use, and reasonable cost as a single entity (Moosmüller et al., 2009). As these are the important factors to consider when deciding what to use for measurement purposes, it is important to evaluate the differences in results for the properties of interest. Instruments for more exclusively for intensive field campaigns (in situ) can be expensive and complex in operation, but more accurate and precise. Those intended for long-term monitoring within a network need to be affordable and simple to operate, but may yield less accuracy and precision. Therefore, instruments used in short-term campaigns are often utilized as reference measurements for those utilized in long-term monitoring.

Due to the differences in the techniques for measurement of aerosol optical properties, there can be discrepancies in observations made by each instrument. Even when operated simultaneously and under the same conditions, differences in instrument output can be observed. Although it is to be considered in greater detail in further sections, an example of such is the suggestion that biases in certain instrumentation may exist due to concentrations of organic matter (Lack et al., 2008, Cappa et al., 2008). Furthermore, the various corrections that must be applied to instrument output have potential to contribute to uncertainty (Bond et al., 1999); a concept considered in the development of new techniques for corrections (Müller et al., 2012- in draft). If

a better understanding of the climatic influence of aerosols is the goal, awareness in the accuracy of instrumentation utilized to quantify aerosol interaction with light is vital. Reducing the ambiguity in data used for the determination of aerosol radiative forcing will assist in the better estimation of current and future climate conditions.

1.4: Scientific Research Questions

Therefore, a comparison of various instrumentation's data output is proposed as the focus of this master's thesis as a means to better quantify the uncertainty of measurement in absorption of energy by atmospheric aerosols. The scientific research questions to be investigated are as follows:

a. What are the differences and similarities in absorption measurements from filter-based methods versus in-situ methods when operated simultaneously, under the same conditions?

b. What conditions during measurement can cause the greatest divergence or commonalties in measurements?

c. Are there observed differences based on the type or composition of aerosol (i.e. organics, nitrates, etc)?

d. Can an advanced correction scheme reduce the differences between the filter-based and in-situ measurements of light absorption?

In order to effectively investigate these questions, filter-based measurements and various referencing techniques for establishing values of aerosol absorption will be examined. The report will discuss the various instrumentation, mathematical techniques, and uncertainties associated with each through applications employed during a California-based field campaign and National Oceanic and Atmospheric Administration (NOAA) laboratory experiment. For the development of this investigation, the various techniques for measuring absorption by aerosols will be discussed in further detail for both the field campaign (utilizing the photoacoustic spectrometer for filter-based referencing) and the laboratory experiment (utilizing the difference method for filter-based referencing). The data accrued during the field campaign and laboratory experiment

also provides the opportunity to investigate instrumentation uncertainty, potential biases, and novel corrections schemes. Within the laboratory experiment, a comparison of various filter-based instruments will additionally be presented. The aim of this investigation is not to decide which of these instruments or methodologies should be deemed “the best method” for measuring aerosol absorption, but rather to provide real-world examples of their applications and capabilities.

An introduction to instrumentation and associated methodologies for measuring aerosol absorption is presented in sections 2.1-2.4, as well as the advantages and disadvantages for each technique. Section 2.5-2.6 describes the opportunities for inter-comparison. Followed by this is the description of analysis methodology (section 3.1-3.2), as well as the analysis results and discussion (sections 4.1-4.2). From this, conclusions of the thesis work are made in section 5.

2. Background

2.1: Introduction to various techniques of aerosol optical measurements

Currently, there are several measurement approaches for the quantification of aerosol absorption of solar radiation. The first technique to be considered is the utilization of instruments for long-tem monitoring of aerosols within a global network. These instruments are typically less expensive and require less maintenance. However, since they do not measure the aerosol while sustained in an airborne state, corrections must be made to account for the potential artifacts collected during sampling. Two versions of the filter-based instruments will be discussed as an example of this type of technology.

Other approaches for absorption measurements are optimized for a short-term, intensive field campaigns. Typically, instruments utilized in this regard are complex, more expensive, and require an expert for operation. Because of this, they are calibrated to yield high quality, precise data during the duration of measurements. Photoacoustic spectrometry and difference-based methods employing in-situ techniques are discussed as examples of the utilization of such instrumentation. As these measurements are taken without the use of a filter (i.e. the aerosols remain in their suspended state), the comparison of the difference method or the photoacoustic technique is commonly utilized as an independent indication of filter-based performance (Moosmüller et al., 2009).

2.2: Filter-based Techniques

The most commonly-utilized technique for measuring aerosol absorption for long term observations is the use of filter-based instruments (Arnott et al., 2003). As a simplistic explanation, the measurement is obtained when a sample of air traverses through a filter at a known rate of flow, depositing absorbing aerosols, and changing the intensity of light observed on the other side. Here, the particle soot absorption photometer (PSAP) and the continuous light absorption photometer (CLAP) are introduced as examples of this technology, with corrections to this measurement technique discussed in section 2.2.3.

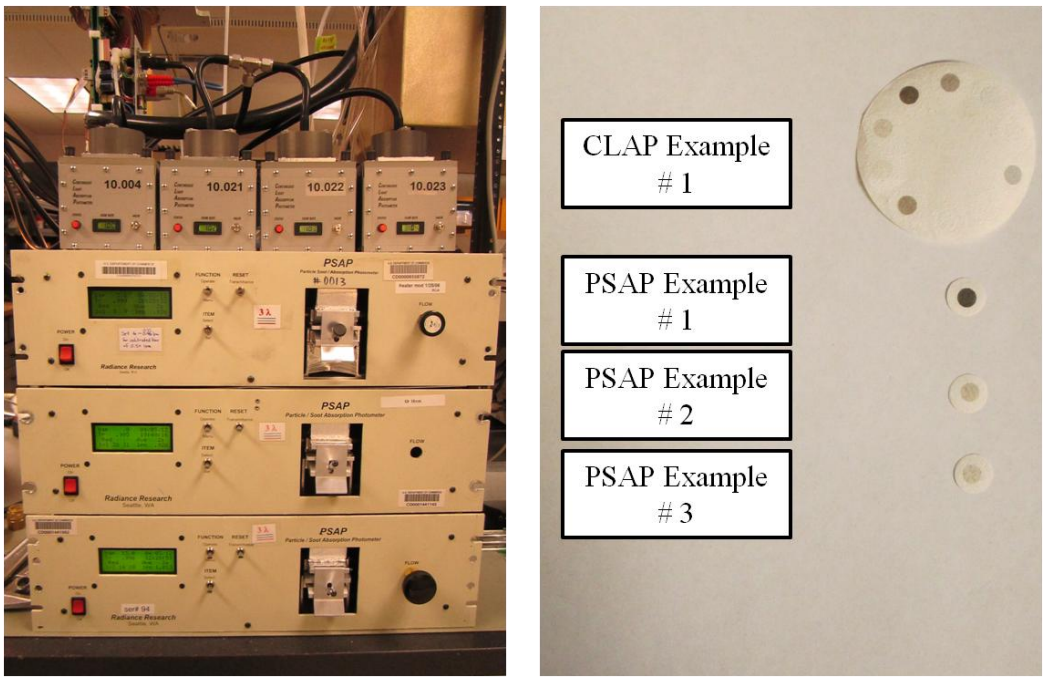

Figure 2.1: Photo of 4 CLAP instruments (top; left) and 3 PSAP instruments (bottom; left) in a laboratory setting. Currently, the CLAP and the PSAP will measure the absorption coeffient (σ_{abs}) simultanously at NOAA observatories and measurement stations. Examples of CLAP (top; right) and PSAP (bottom; right) filters after measurements. The filters utilized in the PSAP and the CLAP are glass filters with a cellulose backing (Pallflex type E70-2075W), differing only in diameter (10 mm and 47 mm, respectively). Photo credit: C. Walsh

2.2.1: The Particle Soot Absorption Photometer (PSAP)

The particle soot absorption photometer (PSAP; Radiance Research, Seattle, Washington) (shown in figure 2.1) is a field-deployable, real-time instrument that monitors the changes in light transmittance at one (565 nm) or three (467, 530, 660 nm) wavelengths at an operating flow around 1 liter/min (Bond et al., 1999). Absorbance is calculated based on Beer's law (shown in equation 2), which describes the change in light transmission through the filter as a function of particle deposition:

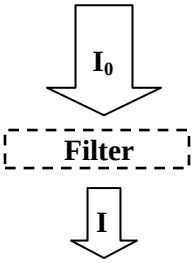

$$Abs = \ln\left(\frac{I_o}{I}\right) \quad (2)$$

where *Abs* is the optical depth (i.e. filter + particles), I_o / I is the average transmittance of the filter in time zero and current time period.

The uncorrected absorption coefficient (σ'_{ap}) is calculated based on the change in light intensity for a known volume of sampled air:

$$\sigma'_{ap} = \left({}^{A}/_{V}\right) ln\left(\frac{Io}{I}\right) \quad (3)$$

where in this equation, I_0 is the intensity at time zero and I is intensity at time zero plus the interval change in time. A is the area of the sample spot and V is the volume of sample air pulled through the filter during a known time interval for I (Bond et al., 1999).

A manufacturer's calibration is included in the output value of the PSAP (σ_{PSAP}) that incorporates the potential effects on observations as the filter becomes loaded with particles. This includes exaggeration of absorption levels by the filter and nonlinearities in the reaction of the instrument as loading continues (Bond et al., 1999):

$$\sigma_{PSAP} = \frac{\sigma'_{ap}}{2(0.5398\tau + 0.355)'} \quad (4)$$

where τ is the filter transmission, which is reset each time a new filter is installed. A value of τ =1 indicates that the filter is unloaded. Ideally, based on findings by Bond et al. (1999), the transmittance should be above 0.7. To ensure that the change in transmittance is not due to a change in the LED light strength, a reference filter is used. The sample flow is first run through the particle-loaded filter, with cleaned air then passing through the reference filter. The filters utilized in the PSAP are 10 mm diameter, glass filters with cellulose backing (Pallflex type E70-2075W). The total uncertainty for 10 second averages of PSAP data is estimated to be between 20-30% (Bond et al., 1999; Sheridan et al., 2005; Langridge et al., 2011).

2.2.2: The Continuous Light Absorption Photometer (CLAP)

Like the PSAP, the continuous light absorption photometer (CLAP; National Oceanic and Atmospheric Administration) (figure 2.1(left)) is another filter-based technique. Similar in concept to the PSAP, it differs in that the instrument cycles through a filter in 10 different measurement locations (as shown in figure 2.1 (right) above). Eight of these 10 are sampling spots, with the remaining two as reference locations where only filtered air will pass through

them. The rotation of sampling sites allows for the ideal minimum transmittance of 0.7 to be achieved for eight times as long as the PSAP (NOAA CLAP User's Manual, 2012; draft in progress). This notion is ideal for some of the monitoring locations that are in remote areas, where less maintenance requirements would be beneficial. 47 mm diameter, glass filters (Pallflex type E70-2075W) are utilized in the CLAP; the same as the PSAP in every aspect except diameter. Designed for durability, the filters are composed of two superimposed fibrous layers; borosilicate glass and a cellulose backing. Although the CLAP lowers the relative humidity of the sample with an internal heater, the cellulose backing will draw water during high humidity circumstances (NOAA CLAP User's Manual, 2012; draft in progress).

CLAP instruments are operated with a 1.0 l/min volumetric sampling flow rate in order to maintain the particle deposition characteristics. A quality-assurance test is achieved with a white filter check, which is a feature of the instrument that resets based on the installation of a new filter. With that, calibrations of flow into the instrument are accomplished with high-precision flow meters (NOAA CLAP User's Manual, 2012; draft in progress). Uncertainties estimated for the CLAP are similar to the PSAP at 20-30% for 10 second ambient measurements (NOAA Aerosol Group Homepage, 2012). However, an important aspect of the filter-based techniques, such as the CLAP, is their lower detection limits in comparison to in situ techniques. This becomes essential for the monitoring of ambient air with lower absorption concentrations (Müller et al., 2011).

Currently, there are around 20 CLAP instruments deployed at NOAA measurement facilities globally. These instruments are often lent for field campaigns and laboratory experimentation. At present, the two filter-based instruments operate simultaneously, within the NOAA Earth System Research Laboratory/ Global Monitoring Division's (ERSL/GMD) basic aerosol instrumentation system (see NOAA Aerosol Group Homepage for detailed instrumentation schematics). However, this is to assure that the comparisons between the two are comparable, as the PSAP instruments will be eventually decommissioned from NOAA facilities. Initial the comparisons of co-located data from the CLAP and the PSAP suggest very good agreement (further results and discussion to follow in section 4.2.1-4.2.2)

2.2.3: Correction Schemes for Filter-Based Measurements

2.2.3a: The Bond Correction Scheme

In order to obtain the finalized value for the absorption coefficient for filter-based methods, a set of corrections have to be made to account for sampling artifacts. These corrections are described in detail by Bond et al. (1999), Virkkula et al. (2005a), and Ogren (2010) and are routinely applied to the filter-based measurements of aerosols.

For instance, scattering by particles can cause an absorption artifact by affecting the transmittance. Although the filters are designed to minimize scattering, the particles collected on the optically diffuse environments may still be subject to scattering. There are three potential effects due to scattering:

1. The filter is loaded with non-absorbing particles
2. Increased opportunity for absorption via light scattered by previously deposited particles
3. Backscattering of particles, which is a size-dependent characteristic

The multiple scattering effects will increase the absorption from the true value within the filter-based instrument (Bond et al., 1999). Additionally, corrections must be made for the slight differences in spot size that can occur in manufacturing. It must also be taken into account that any transmittance values below 0.5 are considered invalid and need to be removed from data (www.ersl.NOAA.gov/gmd/aero). As transmittance decreases, the PSAP sensitivity in measurement will also decrease.

These are accounted for in an empirical equation suggested by the PSAP manufacturer (equation 4) and has been modified by Bond et al. (1999), Virkkula et al. (2005a), Sheridan et al. (2005), and Ogren (2010) as follows:

$$\sigma *_{ap,PSAP} = 0.873 \left[\frac{b^*}{1.0796\ x\ Tr + 0.71}\right] x \frac{1}{1.22} \quad (5)$$

where $\sigma_{ap,PSAP}$ is the corrected absorption coefficient for multiple scattering effects and 0.873 is the value that accounts for the difference in exposed filter area from that of the manufacturer's assessment and the correction developed by Bond et al. (1999) (Ogren, 2010). Tr is the filter

transmission (equal to 1 for an unloaded, newly installed filter) and b^* is uncorrected absorption measurement from the instrument. The manufacturer's correction (Weiss correction; equation 4) is within the brackets, with 1.22 representing a further scaling factor established by Bond et al. (1999).

$\sigma_{abs,PSAP}$ is the fully corrected absorption coefficient when the assumed "apparent absorption" is applied. Apparent absorption is an absorption measurement that has been caused by scattering influences. The scattering by particles already collected on the filter is corrected by assuming the absorption is around 2% of the 1.22 scaling factor, or 1.6% (Bond et al., 1999).

$$\sigma_{ap,PSAP} = \sigma^*_{ap,PSAP} - 0.016\, x\, \sigma_{sp} \quad (6)$$

The σ_{sp} term is typically measured from an integrating nephelometer (instrument explained in greater detail in section 2.4.3). The measurement of aerosol absorption by the PSAP then has an estimated uncertainty 20-30% after these corrections are applied (Bond et al., 1999). Further uncertainties associated with the Bond Correction Scheme will be discussed in section 2.6.2.

2.2.3b: The CTS Correction Scheme

Alternatives to the correction scheme developed by Bond et al. (1999) have been proposed, offering a novel method of correcting the filter-based techniques using an iterative process that begins with a totally-particle free filter. As particles are collected, each measurement is then affected by the particles previously deposited. The Corrected Two-Stream Method (CTS) correction scheme proposed by Müller, Virkkula, and Ogren (2012; draft in progress) is one that aims to account for this effect of previously deposited particles through utilization of properties beginning with a completely white filter and the monitoring of the property changes as particles are deposited as follows:

$$\delta_{f+p} = \left(\overline{F}_s(\delta_s, g)\cdot\delta_s + \overline{F}_a(\delta_a)\cdot\delta_a\right)\cdot F_f\left(\delta_e, \varpi_f, g\right) \quad (7)$$

where δ_{f+p} is the optical depth of the filter and particles, δ_s and δ_a are the scattering and absorption optical depths of the particles deposited on the filter, δ_e is extinction optical depth ($\delta_s + \delta_a$), ω is the single scattering albedo (SSA), and g is the asymmetry parameter. The terms F_s, F_a, and F_f are responses functions to scattering, absorption, and apparent absorption (an indicated

absorption caused by scattering influences) respectively. Having the terms F_s and F_a, as response functions makes them easier to directly measure during sampling. Equation (7) is then calculated as an iterative algorithm that yields the CTS-corrected δ_a for all of the particles collected on the filter. This is followed by corrections for spot size and flow rate as:

$$\sigma_a(t) = \frac{A}{Q} \cdot \frac{d}{dt} \delta_a(t) \tag{8}$$

where Q is the flow rate (m/s) and A is the spot area.

2.3: Photoacoustic Technique

A common technique for measuring aerosol absorption in short term field campaigns is the use of photoacoustic instrumentation. This technique has been utilized to quantify absorption of both aerosol and gases and is typically utilized as a reference measurement for filter-based techniques (Moosmüller et al., 2009). Without the use of filters, these measurements are obtained through the inevitable temperature increase of particles as they absorb light, and the subsequent release of heat to the surroundings. The increase in temperature can be characterized into aerosol optical behaviors by the detection of sound that the change in pressure creates (Moosmüller et al., 2009). Here, the photoacoustic spectrometer is discussed.

2.3.1: The Photoacoustic Spectrometer (PAS)

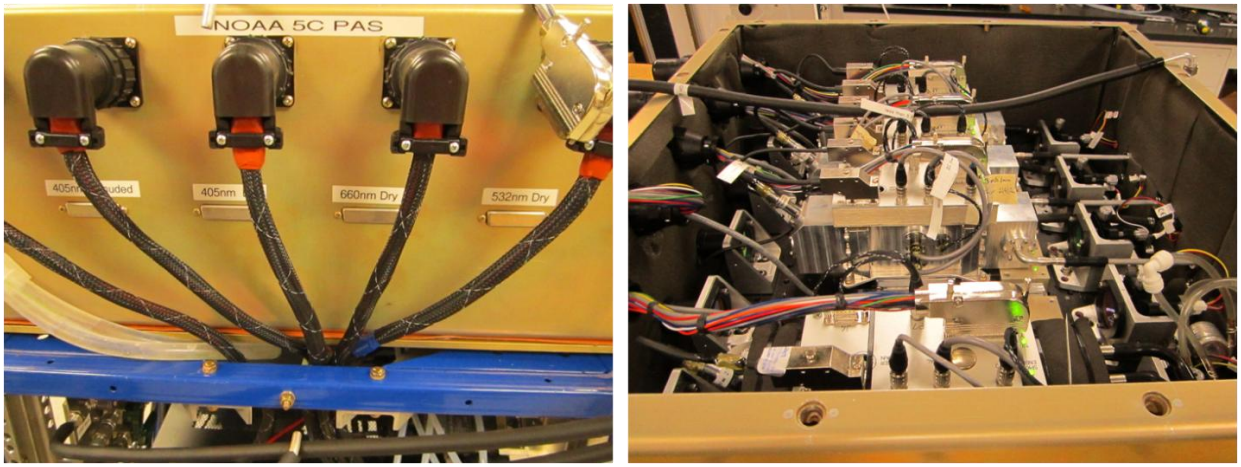

Figure 2.2: The Photoacoustic Spectrometer (PAS) utilized in the CalNex campaign. The front view (left) shows the various sampling channels, including different wavelengths (405, 532, and 600 nm). The inside of the instrument (right) houses the measurement instrumentation. Precautions were taken to provide extra isolation from airplane noise in the form of padded walls. Photo credit: C. Walsh.

As described by Lack et al. (2006), the photoacoustic spectrometer (PAS; figure 2.2) measures aerosol absorption directly, with a continuous sample flow through a cavity with resonance (two 25 mm resonators) and a frequency-moderated laser beam (F_R). As absorption occurs, a change in pressure will cause a pressure wave that can be acoustically detected via highly sensitive microphones (Knowles Acoustics EK3132; Itasca, Illinois). The signal from the microphone is linear in proportion to the absorption coefficient, if the detection occurs within the acoustic period of $1/F_R$ (Arnott et al., 2003). Any delay in the acoustic detection will be related to other occurrences, such as detected energy returned during evaporation of volatile components (Arnott et al., 2003). The major uncertainty associated with the PAS is possibility of volatile species evaporating from the aerosol (Arnott et al., 2003; Lack et al., 2006). This has been shown to occur at high levels of relative humidity, causing a photoacoustic response. However, this bias can potentially be avoided through the drying of aerosols to 65-70% RH, as well as the cut-off of particles larger than 2 μm (Arnott et al., 2003; Raspet et al., 2003).

Depending on the conditions of instrument utilization, the reported accuracies for the PAS is between 5-10% (Lack et al., 2006). This value will not only depend on whether the instrument is deployed in the field or within a laboratory setting, but also the method of calibration utilized. There are two methods of calibration used as described by Lack at al. (2006). For microphone calibration, the known-absorption by gas-phase ozone passed through the PAS and cavity ringdown instrument (introduced in section 2.4.1) is correlated to the response of the microphone. The measurements are made simultaneously, with the correlation of the two utilized instruments for the calibration of the PAS. NO_2 can also be used in this manner of calibration; however, the used of NO_2 requires different assumptions discussed in greater detail in Lack et al. (2006). Pressure dependencies are also accounted for by passing air into the sample lines (pre-measurement) while the pressure of the system is reduced from ambient conditions (about 100 kPa) to 40 kPa, and then using a ratio calculation for calibration.

In the particular application of the instrumentation during the CalNex field campaign (to be explained in greater detail in section 2.6.1 and 3.1), special attention had to be paid to adjusting for accuracy during airborne measurements. Measures were taken to isolate the PAS from in-flight extraneous noises and vibrations. Multiple layers of isolating foam rubber were installed to the housing of the instrument; an acoustically and thermally isolated box. With that, frequent

calibrations were essential, as stable operating conditions fluctuate with pressure and temperature changes (Lack et al., 2011).

2.4: The Difference Method

Finally, aerosol absorption values can be obtained via a combination of methods that measure aerosol light scattering and extinction of light by aerosols. Absorption is calculated from the difference in measured extinction (scattering + absorption) and scattering. The measurements of both extinction and scattering are made simultaneously, under the same operating conditions, and with the same sample in order to reduce any potential discrepancy within the volume of interest (Moosmüller et at., 2009). Absorption coefficients obtained from the difference-method are viewed as another form of reference measurement for the filter-based techniques.

2.4.1: The Cavity Ringdown Spectrometer (CRDS)

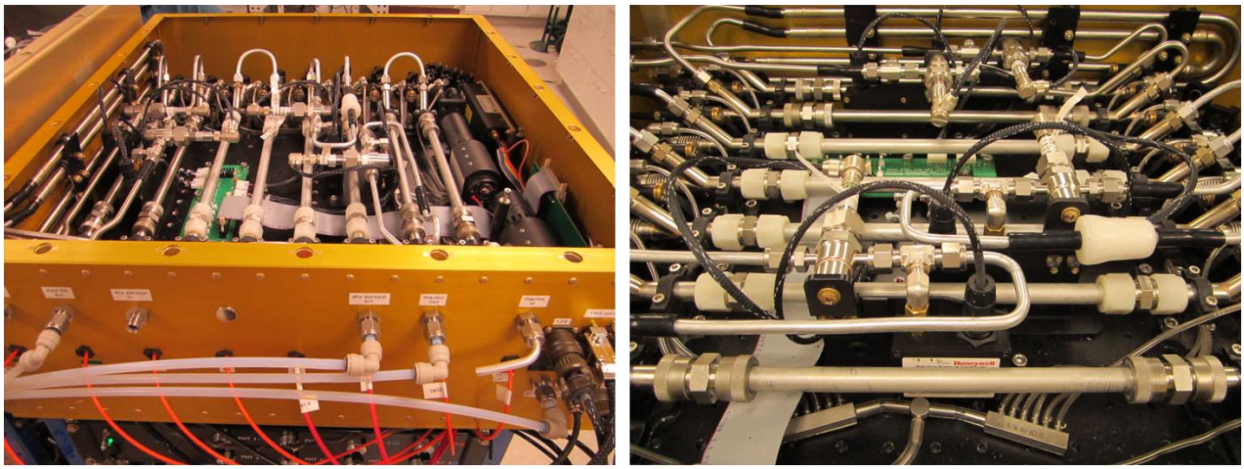

Figure 2.3: The Cavity Ringdown Spectrometer (CRDS) utilized in the CalNex field campaign. The front view (left) shows the various channel inputs for sampling with different wavelengths (405, 532, and 662 nm) and humidites (10%, 70%, and 95%). The inside view (right) shows the 8 separate measurement cells of this modified CRDS, which included two cells for gas-phase measurements. Photo credit: C. Walsh.

The conservation of energy states that any change in a beam of light has to be accounted for by the addition of scattering (σ_{sp}) and absorption (σ_{ap}) by the particle. Therefore, extinction (σ_{ep}) by aerosols is defined as:

$$\sigma_{ep} = \sigma_{sp} + \sigma_{ap} \quad (9)$$

A technique first described by O'Keefe and Deacon (1988), the cavity ringdown spectrometer (CRDS; figure 2.3) is a spectroscopy method that measures the extinction by aerosols with high

sensitivity at one or more wavelengths. Langridge et al. (2011) deployed a CRDS that measured at three wavelengths (405, 532, and 662 nm), as well as multiple relative humidities (10%, 70%, and 95%). Aerosol extinction is measured by observing fluctuations in a constant ring-down time within an optical cavity, once the sample is introduced (Strawa et al., 2003; Moosmüller et al., 2005). It has been utilized for measurement of atmospherically-important components, such as gas species and aerosol particles. The CRDS measures the extinction using short pulses of a laser beam in an optically-stable cavity produced with the use of two highly reflective concave mirrors (Langridge et al., 2011). The intensity of light from the short pulses will degrade over time as it continues to travel distances of multiple kilometers between the mirrors within the cavity. The ringdown time (τ), or the rate of decay of the light within the cavity, is determined with (τ) and without (τ_0) absorbing or scattering species present, and the extinction coefficient (α) is then calculated by:

$$\alpha = \frac{R_L}{c}\left(\frac{1}{\tau} - \frac{1}{\tau_0}\right) \quad (10)$$

where c is the speed of light and R_L is a ratio of the actual physical cavity length to the length when the sample is present. This component is included to account for the sample not occupying the complete mirror-to-mirror area (Langridge et al., 2011).

The CRDS utilized in the field campaign of CalNex (section 2.6.1 and 3.1) has been expanded upon from the traditional instruments described in the references cited in the previous paragraph. Here, the CRDS is composed of 8 separate measurement cells with varying humidites and wavelengths, as well as 2 for gas phase measurements (Langridge et al., 2011). Measures were taken to stabilize for pressure changes, as well as changes in temperature and humidity. Total uncertainties were determined to be 1-2% for 1 second dry measurements and up to 20% at RH of 95%.

2.4.2: The Cavity Attenuated Phase Shift (CAPS) Extinction Monitor

The Cavity Attenuated Phase Shift (CAPS; figure 2.4) extinction monitor is a recently developed instrument that monitors levels of aerosol extinction at 656 nm through spectroscopy techniques (Massoli et al., 2010). The CAPS consists of a 26 cm cavity with highly reflective mirrors

(99.98%) at each end, each isolated from the potential contact with aerosol particles via purge flow air that is constantly maintained in front of them.

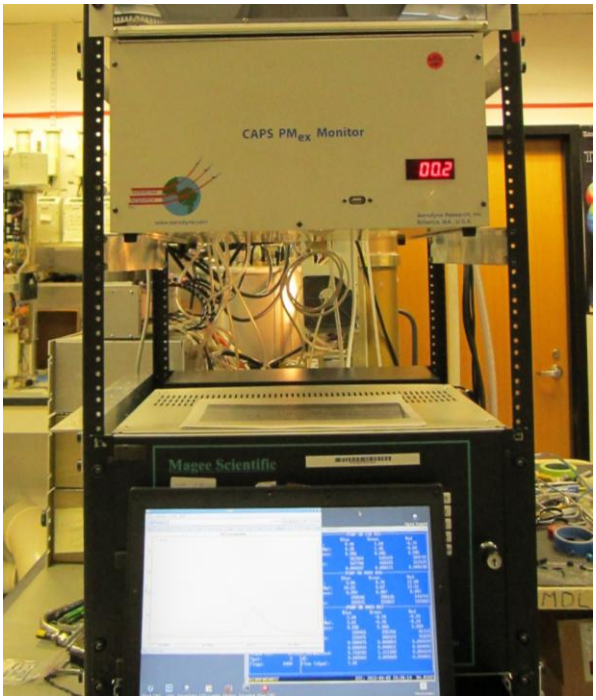

Figure 2.4: The Cavity Attenuated Phase Shift (CAPS) utilized in the NOAA laboratory experiment. The aerosol extinction coefficient (σ_{ep}) is measured and displayed on the front panel for quick view. Photo credit: C. Walsh.

The sample length within the cavity due to the high reflectivity of the mirrors becomes around 2 km, with the sample flow rate maintained at 0.85 l/min. A broadband LED-source light shines into the cavity through one mirror, arriving at the other as a distorted wave from the original (phase shift). The light is then collected at the end of the cavity via a vacuum photodiode detector, where a band-pass filter of 10 nm characterizes the spectral range of the sample (Massoli et al., 2010). The measured extinction is related to the phase shift through:

$$\cot\theta = \cot\theta_o + (c/\pi * f) * \sigma_{ep} \quad (11)$$

where θ is the measured phase shift, θ_o is the phase shift under particle-free conditions, *c* is the speed of light, and *f* is the modulation frequency. The instrument regularly shifts from sampling to particle-free air to sustain optimal instrument performance. Instrument temperature and temperature are also continuously monitored for fluctuations from the ambient conditions of operation (Massoli et al., 2010).

2.4.3: The Integrating Nephelometer

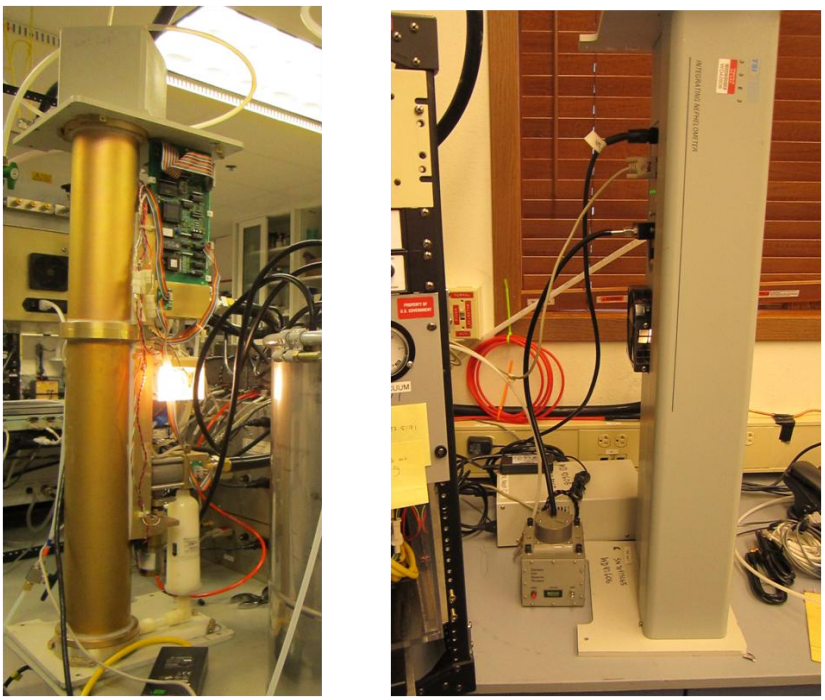

Figure 2.5: The Integrating Nephelometer utilized in the NOAA laboratory experiment (left), as well as pictured at the Storm Peak Laboratory in Steamboat Springs, Colorado (right). The nephelometer measures the aerosol scattering coefficient (σ_{sp}). Photo credit: C. Walsh.

Ideal for both short-term and long-term measurements, the integrating nephelometer (TSI 3563; St. Paul, MN) (figure 2.5) measures the scattering coefficient (σ_{sp}) of aerosol particles, while concurrently measuring the hemispheric backscattering at 3 wavelengths (450, 550, and 700 nm) (Anderson and Ogren, 1998). This is achieved through the detection of light scattering due to aerosols and the subtraction of light scattering by the carrier gas, the walls of the instrument, and noise created by the detector (Heintzenberg and Charlson, 1996). The sample travels within the nephelometer 90 cm long aluminum tube (10 cm in diameter), until it reaches the receiving optics housing at the other end. The light collected is then split into the blue, green, and red wavelengths and received in the photomultiplier housing. Stabilization is obtained via a reference chopper containing three zones: dark (where no light is allowed through), signal (measurement is taken), and calibrate (where only 0.1% of light is allowed through for lamp stability testing) (NOAA Aerosol Group Homepage, 2012). This chopper rotates 23 times per second.

The σ_{scat} is the measured scattering by the nephelometer, which distinguishes scattering from Mie (particles) from the scattering due to Rayleigh (gas). The σ_{sp} is generated by subsequently subtracting as:

$$\sigma_{scat} = \sigma_{rg} + \sigma_{sp} \tag{12}$$

$$\sigma_{sp} = \sigma_{scat} - \sigma_{rg} \tag{13}$$

where σ_{rg} is scattering from the carrier gas and σ_{sp} is scattering from particles. Calculations for the nephelometer involve several steps including signal processing for all three colors, as well as corrections for the use of a non-perfect 180° light source and truncation errors (Anderson and Ogren, 1998). The truncation error refers to the limitations of the instrument in measuring all scattering from 0-180°. The instrument configuration result in an underestimation of the σ_{sp}, since it limits light detection to the angular range between 7° to 170° instead of the full 0-180. The raw data is corrected for this limitation based on particle size via a linear relationship between what is measured and the measurements not included:

$$C_{ts} = \frac{\sigma_{sp,true}}{\sigma_{sp,neph}} \tag{14}$$

where C_{ts} is the truncation correction applied, $\sigma_{sp,true}$ is the actual scattering by particles and $\sigma_{sp,neph}$ is the scattering measured by the nephelometer. There are a number of truncation corrections suggested for use, with a variety of methods for adjustments (Anderson and Ogren, 1998; Moosmüller and Arnott, 2003; Bond et al., 2009; Massoli et al., 2009b). Further discussion will follow in section 4.2.3. The reader is referred to the NOAA aerosol's group homepage for more details of theory, operation, and mechanics of the integrating nephelometer (NOAA Aerosol Group Homepage, 2012).

2.5: Reasons for Inter-Comparison

Each technique for the measurement of absorption by aerosols has associated uncertainties. Despite obtaining a measurement for the same parameter, comparison of filter-based, photoacoustic, and difference derived absorption coefficients are not always highly correlated, leading to uncertainty in our understanding of the true value of absorption (Moosmüller et at.,

2009). This uncertainty needs to be better scrutinized in order to determine why these differences in instrument output occur. As discussed previously, qualities of the filter-based technique may cause artifacts in estimation for various reasons. As the filter becomes loaded, the potential for overestimation becomes an issue (Bond et al., 1999). However, this is not the only issue of concern. It's also possible that the deposition of particles on a filter can cause a change in morphology and alteration in particle properties. If the particle is coated with liquid-like organic material (such as may be present due to incomplete combustion of biomass), the potential for this coating to spread within the filter is a significant concern for accuracy in measurement (Subramanian et al., 2007).

Cappa et al. (2008) and Lack et al. (2008) have also investigated the potential for an overestimation bias based on the amount of organic aerosol (OA) present in the filter measurement. In companion articles, the potential for this bias is discussed based on both laboratory and field evidence where comparisons of PSAP and PAS measurements are made. During these campaigns, the high loading of organic aerosols (OA > 12.5 $\mu g/m^3$) was associated with large discrepancies between the measurement techniques. It was shown that the PSAP overestimated absorption by 50-80% at very high OA loading conditions. In order to determine whether this is a constant feature associated with filter-based instruments, continued investigation is vital.

Other concerns about measurement accuracy lie in the necessity for empirical corrections for filter-based techniques (further explained in section 2.6.2). Since several factors require correction with the filter-based instruments, the uncertainty obtained of measurements is systematically increased. Because of this, the CTS correction scheme has been proposed as an alternative for the typically applied Bond Correction for filter-based instruments. As the CTS is a novel algorithm that currently has not been published for wide use by the scientific community, in-house investigation on its application may provide further insight on its potential.

The utilization of photoacoustic spectrometry or the difference method as a reference for the absorption coefficient measured by filter-based is common practice; although, neither method has been deemed "the better way" to do so (Sheridan et al., 2005; Moosmüller et al., 2009). However, the technologically-advanced PAS and instruments utilized in the difference-based

methods also possess potential uncertainties and errors in measurement. Uncertainties in photoacoustic measurement can arise from interference during sampling (Moosmüller et al., 2009). Difference-based techniques may be uncertain due to the proliferation of error in the differencing of two different techniques. Obtaining the absorption from the difference of extinction – scattering can increase noise in the outcome significantly with measurements associated with low SSA (Moosmüller et al., 2009). Uncertainty will also stem from the subtraction of two larger numbers (extinction and scattering) to obtain a significantly smaller number (absorption), possibly necessitating a correction factor (Bond et al., 1999).

2.6: Opportunities for Inter-Comparison

A comparison of instrumentation and applied methods for determining aerosol absorption becomes essential in order to address current uncertainties associated with atmospheric aerosol optical properties. As mentioned previously, the climatic impact of aerosols remains the most significant uncertainty in the IPCC's assessments of current and future climate effects. As a means of reducing this gap in knowledge, a detailed characterization of instrument capabilities in comparison to one another is imperative. Increasing the awareness of the capabilities and potential uncertainties in measurements of aerosol optical properties can aid in better understanding of aerosol influence on the changing climate (Moosmüller et al., 2003).

2.6.1: CalNex Field Campaign

In April-May 2010, a substantial scientific undertaking was conducted within the state of California, entitled the California Air Quality and Climate Nexus Campaign (CalNex). With the cooperation of the California Air Resources Board (CARB), the California Energy Commission (CEC) and the National Oceanic and Atmospheric Administration (NOAA), scientific measurements aimed at increased understanding of air quality and climate processes were collected throughout the state and along the eastern Pacific coastal region (NOAA Research Plan, 2008). CalNex was designed to gain vital scientific knowledge for development of more comprehensive climate-related policy via a range of atmospheric disciplines and from various sources and locales. With the inclusion of data collected during airborne flights, on maritime ships, and within field locations, a better understanding of the spatial and temporal variation in atmospheric chemistry and processing could be developed.

For the measurements of atmospheric aerosol properties and radiative effects, the NOAA Lockheed WP-3D Orion aircraft was deployed with onboard instrumentation for obtaining measurements within the planetary boundary layer and free troposphere. Typically flown for severe weather and meteorology-related measurements, the four-engine WP-3D is capable of long range scientific investigation. This capacity created an ideal platform for the study of atmospheric processing of urban and industrial plumes (NOAA Research Plan, 2008). Although there was a wide range of measurement methods conducted during the CalNex campaign, the instruments and measurements of relevance to this analysis were the PSAP, CLAP, PAS, and CRDS on-board the WP-3D, as well as supporting instrumentation mentioned in the next section.

Despite the original intention of this thesis to focus on an inter-comparison of the CLAP and PAS measurements from the CalNex field campaign, CalNex was the first deployment for the CLAP instrument and the instrument was not operated by the developing team. Therefore, it is not surprising that measurement problems occurred, but were not recognized or resolved during the deployment. After observation of significant discrepancies between the PSAP and the CLAP during CalNex (which, as mentioned in section 2.2.2, is not the case at the NOAA surface-based field sites), further extensive analysis deemed the aerosol absorption data collected by the CLAP invalid (illustrated in figures appendix A1 and A2). However, a laboratory-based instrument comparison that utilizes the CLAP was conducted at NOAA in the spring of 2012 and will be described further within the laboratory results and discussion.

2.6.1b: Supporting instrumentation in CalNex Field Campaign:

Besides the relevant onboard instrumentation described in detail in sections 2.2-2.4, other supporting measurements were taken onboard the WP-3D that will be important during analysis. The aerosol mass spectrometer (AMS) is the first field-deployable MS that is capable of distinguishing the elemental composition of ions that compose an aerosol particle (DeCarlo et al., 2006). The AMS instrument provides the mass spectra of aerosol as a mixture of nucleated particles (in μg per std m^3 of air) emitted from different sources or formed due to various processes (condensation, cloud processing, etc.) (Jimenez at al., 2003). The associated uncertainty is estimated to be around 30% (Jayne et al., 2000; Jimenez et al., 2003).

For additional evaluation of air quality during the analysis, the single particle soot photometer (SP2) was periodically utilized. The SP2 identifies black carbon in the accumulation mode size range of 90-700 nm, accounting for 70-90% of the accumulation mode mass distribution particles (Stevens et al., 2003; Schwartz et al., 2006). The total uncertainty for 1-second data collected by the SP2 is around 40% (Langridge et al., 2012; paper submitted).

2.6.2: NOAA Laboratory Experiment

On April 1st, 2012- May 2nd, 2012, an aerosol absorption measurement experiment was conducted at NOAA's Earth Systems Research Laboratory aerosol laboratory in Boulder, Colorado. The scientific aim of the investigation was similar to that of the Reno Aerosol Optics Study (RAOS; Sheridan et al., 2005), where various types of aerosol were generated in order to better characterize current instrument abilities under a controlled laboratory setting. Instruments of relevance to this investigation that were utilized in the laboratory were 3 PSAP's, 4 CLAP's, 1 integrating nephelometer, and one CAPS (lab set up to be detailed in section 3.2.1 and supporting instrumentation discussed below). The experiment aimed to specifically address uncertainties associated with the Bond Correction scheme for filter-based instrumentation.

Currently, the Bond Correction scheme attempts to address the potential artifacts in measurements for filter-based instruments; however, it is associated with a number of uncertainties. The hypotheses proposed by Bond et al. (1999) are investigated in this laboratory setting in several ways. First, the Bond Correction assumes the transmittance may only decrease to a level of 0.7 in order to obtain measurement. The NOAA experimentation attempts to define a dynamic range beyond this level. Second, the Bond Correction assumes a certain penetration depth associated with the velocities at which the particles will reach the instruments (i.e. flow rates). Here, the flow rates were varied in attempts to better understand changes in output as a result of differences in flow. Finally, the sensitivity of the Bond Correction to particles previously deposited on the filter was addressed. This was achieved through the abrupt changes in particle types deposited on the filters (i.e. a filter loaded with white particles is then exposed to small amount of black particles). It has been suggested that this sort of scenario affects the accuracy in the Bond Correction (Virkkula et al., 2005b).

The NOAA experiment utilized a wide range of techniques to examine these hypotheses. However, the aim of this investigation is less focused on the potential adjustments to the Bond Correction and more interested in the instrumentation and methodologies associated with the measurement of aerosol absorption. Therefore, the data utilized from the NOAA laboratory experiment for the purposes of this thesis will be directed towards the scientific questions outlined in section 1.4. It is also important to note that the laboratory analysis in this document is based on data obtained while the experiment was in process. Due to time restrictions of this project, the analysis is based on data that may be transformed as analysis continues. The data analyzed in this report was obtained from laboratory runs and post-processing between April 1st, 2012- April 27th, 2012, which was before the conclusion of the laboratory experimentation. Final results from the experiment may be slightly different due to instrument adjustments.

2.6.2b: Supporting NOAA Laboratory Instrumentation

The instrumental set up will be discussed in the methodology (section 3.2.1). However, quite an extensive array of instrumentation was utilized to address the scientific questions of the NOAA laboratory experiment. The supporting instrumentation that are not used in the analysis described here are as follows (readers are encouraged to follow references for more information):

The Multi-Angle Absorption Photometer (MAAP; Thermo Fisher Scientific Inc., Waltham, MA) is a novel filter-based instrument that obtains the aerosol absorption coefficient at 670 nm through reported values of the black carbon (BC) mass density. The measurement is corrected in real time for scattering artifacts through the simultaneous measurement of transmittance and reflectance. Automatic filter changes via a filter-tape are installed within the instrument (Petzold and Schönlinner, 2004; Moosmüller et al., 2009).

The Aethalometer (Magee Scientific Company, Berkeley, CA) is a filter-based instrument continuously measures light absorption of carbon particles at seven wavelengths (from 370-950 nm). Most commonly, these instruments are used at long-term monitoring stations where minimal maintenance is essential. This is allowable in part due to the continuous filter-tape component (www.mageesci.com; Weingartner et al., 2003).

The Scanning Electrical Mobility Spectrometer (SEMS; BMI Aerosol Solutions) measures the particle sample size distribution by means of particle migration within an electrical field towards a charged rod. The size of the particles is determined by the strength of the electrical mobility the particle possess and the location in which it is drawn to the rod. The instrument is optimal for particles between 0.01 -2.0 μm and can continuously scan over that size range in a rapid fashion from 15 seconds to 10 hours (www.brechtel.com/sizing.html; Wang and Flagan, 1990).

The mixing chamber is also connected to a Condensation Particle Counter (CPC; TSI, St. Paul, MN), where the amount of particles passing through the sample line is counted through means of alcohol-induced growth. The particles will pass through a heated saturator, where alcohol (n-butanol is vaporized and diffused into the sample stream. As the temperature decreases from the heated region, the alcohol will condense onto the particles, causing growth to a countable size for an optical counter (NOAA Aerosol Group Homepage, 2012; Agarwal and Sem, 1980).

3. Methodology

3.1: Experimental Design and Analysis: CalNex

3.1.1: Experimental Design: CalNex

During the CalNex field campaign, a total of 21 scientific flights were conducted over the state of California. Each flight had various scientific aims from many aspects of atmospheric sciences, each within different regions of interest. Typical flight duration was around 7 hours, with flight path and altitude depending on the scientific aim of the particular flight. Along with data collected from the scientific instruments onboard, the WP-3D's flight details were also provided (i.e. pressure and altitude changes, GPS positioning information, etc.).

However, not every flight yielded useable data for all instruments of interest to this analysis. Therefore, flights for more in depth analysis were chosen based on the availability and quality of data from the PSAP, PAS, and AMS with simultaneous measurements. It is necessary to have data from all three instruments in order to compare the PAS and PSAP absorption measurements and then relate the comparison to the AMS chemical composition and concentration data. Without each of these components available, only partial inferences could be made. Table 3.1 gives details of the chosen flights; including the date, location, and scientific objectives from each.

The flight tracks of the days included in the analysis are shown in figure 3.1. As described in table 3.1, theses flights vary in scientific aim, as well as location. The city of Los Angeles was flown over a number of times; it was of particular interest due to the large population of just under 3,800,800 people (US Census Bureau, 2010) and the associated pollution and emissions. Rural areas, such as the agricultural regions within the San Joaquin Valley, were also explored. Air masses from the Pacific Ocean and coastal characteristics were also considered during a number of flights.

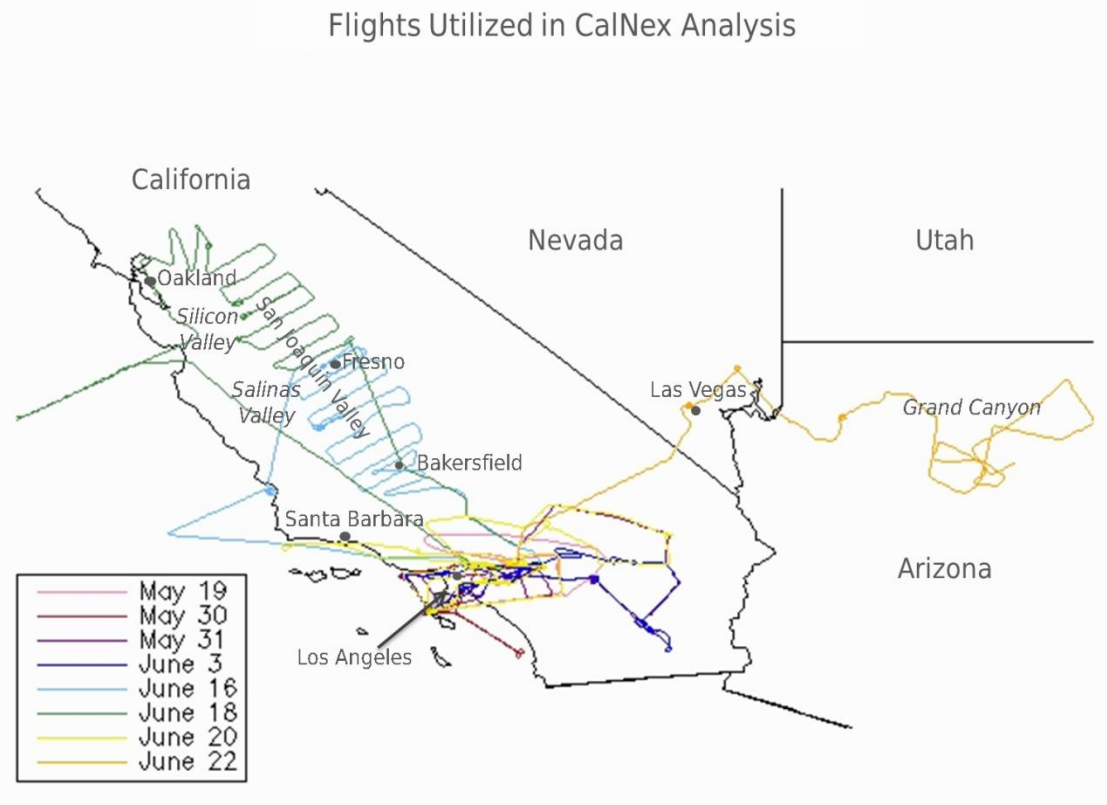

Figure 3.1: The flight tracks of the 8 CalNex flights utilized in analysis. Regions are labeled in italics, with cities distinguished by points. Of the 8 flights, 5 were concentrated within the Los Angeles region with 3 flights outside of this area. Flight times varied by scientific aim, as described in table 3.1.

Table 3.1: The flight dates, locations, and scientific aim utilized in analysis of the CalNex field campaign. Of the 21 flights over southern California in the campaign, 8 were chose for this investigation. Selection was based in the availability of the PSAP, PAS, and AMS data in order to make instrument comparisons of absorption (σ_{ap}) measurements and relate to the AMS chemical composition and concentration data.

Flight Day	Day of Year	Location	Aim
May 19, 2010	139	Los Angeles Region	Observe aging of LA plume from east to west
May 30, 2010	150	Los Angeles	Nighttime and Sunrise chemistry
May 31, 2010	151	Los Angeles Region	Nighttime and Sunrise chemistry; pollution plume export to Mojave Desert and Salton Sea
June 3, 2010	154	Los Angeles Region	Nighttime chemistry; pollution plume export
June 16, 2010	167	San Joaquin Valley, Fresno, Bakersfield, Santa Barbara	Survey of regions (urban and rural emissions), observe and compare planetary boundary layer in contrasting regions
June 18, 2010	169	San Joaquin Valley, Salinas Valley, Silicon Valley, Oakland	Survey of mixed agriculture and dairy farm regions, Oakland emissions and plume export
June 20, 2010	171	Los Angeles Region	Observe aging LA plume
June 22, 2010	173	CA → Denver (Via Las Vegas)	Pollution plume on way to and over Las Vegas, air quality over Grand Canyon, plumes from NM and CO forest fires

Data for aerosol absorption were collected at 3 wavelengths (467 nm (blue), 530 nm (green) and 660 nm (red)) for the PSAP and 3 wavelengths (404 nm (blue), 532 nm (green), and 659 nm (red)) for the PAS. Aerosol extinction was measured via the CRDS at 3 wavelengths (405 nm, 532 nm, and 662 nm) and at various relative humidites (10%, 70%, and 95%). However, only the green wavelengths are utilized within this analysis due to the unavailability of data from the blue and red PAS and CRD wavelengths.

3.1.2: Data Analysis Technique: CalNex

Each of the instruments of interest onboard the CalNex flights have different methods for obtaining the final measurements. Certain potential artifacts, manufacturing discrepancies, instrument sensitivities, etc. have to be empirically accounted for in final, corrected measurements.

As mentioned in section 2.2.3, the filter-based mechanisms require a number of empirical corrections to be applied to the raw data output. The PSAP data has the Weiss correction (equation 4) built within the instrument's output by the manufacturer. Following this, the PSAP requires the application of equation 5 to correct for differences in spot sizes and potential for overestimation of absorption by the influence of scattering particles (Bond et al., 1999; Ogren, 2009). Because there was no direct measurements of aerosol scattering on-board the WD-P3, the scattering coefficient must be obtained via equation 15 for the correction applied from Bond et al (1999). For comparison purposes, the CTS correction scheme was also applied to the filter-based data set (equation 7 and 8). The scattering coefficient was calculated for the purposes of the Bond and CTS Correction schemes via:

$$\sigma_{sp} = \sigma_{ep,CRD} - \sigma_{ap,PAS} \quad (15)$$

For the corrections and calibration techniques of the other onboard instruments, the reader is referred to more detailed sources of descriptions of the instruments and their operation (e.g., Lack et al., 2012; Langridge et al., 2011). The PAS utilized in the CalNex campaign is described in greater detail in the Lack et al. (2012), and the CRDS utilized in the CalNex campaign is detailed in the companion paper by Langridge et al. (2011). It is important to note that precautions to stabilize the instruments from airplane noise levels were a priority during this

campaign. This was in order to minimize any errors in measurements, due to the instruments' utilization of acoustic resonance for measurement.

After the empirical corrections are applied to the filter-based methods, all data are examined for potential spikes and noise. This process is done within the NOAA aerosols group data analysis interface CPX2, where the entire flight dataset can be visually inspected for all parameters simultaneously. Here, edits can be made by the user to invalidate certain instances within the flight where obvious unreasonable peaks are noted, followed by a note of justification in a message log. Once the editing of data was completed, the data sets were then passed as final and could be extracted for use in Interactive Data Language (IDL; Exelis Visual Information Systems, Boulder, Colorado). For each flight, 30 second averaged data files were generated, with subsequent scripts created for further statistical analysis within the IDL program. PSAP data were limited in use by laboratory-defined instrument-to-noise levels, as discussed in 4.1.1.

3.2: Experimental Design and Analysis: NOAA Laboratory Experiment

3.2.1: Experimental Design: NOAA Laboratory Experiment

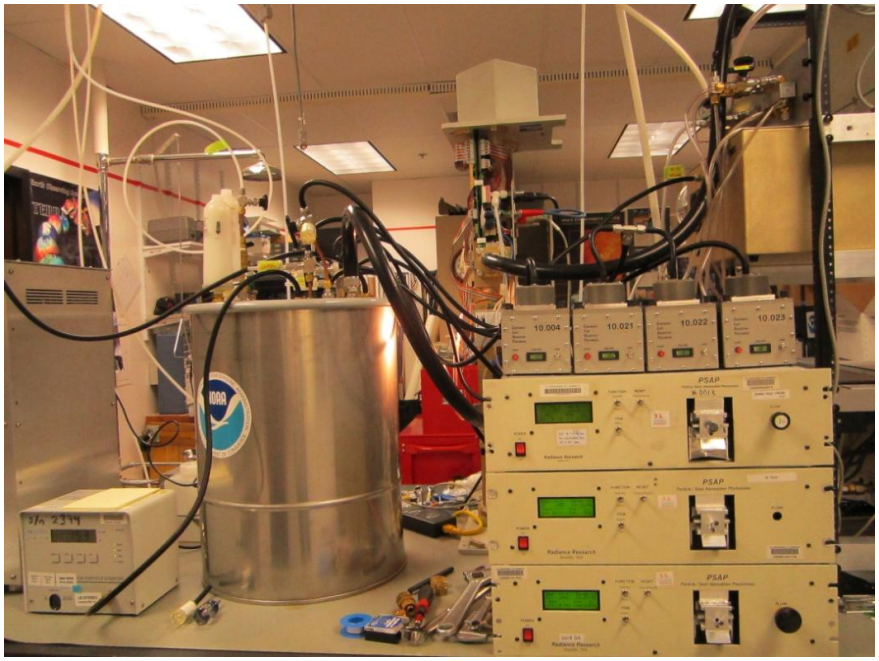

Figure 3.2: A portion of the NOAA experimental set up, showing the CLAPs, PSAPs, CPC, and mixing chamber. Photo credit: C. Walsh.

As discussed in section 2.6.2, the matrix of tests established for the NOAA laboratory experiment was specific and extensive (partially pictured in figure 3.2). However, the dynamic

range of alterations in sampling conditions for testing of various hypotheses is beyond the scope of this report. Rather, the material included here will be limited to a demonstration of how the filter-based methods measure compare to each other when operated simultaneously, as well as an applied example of the difference-based method as an absorption reference. As mentioned in 2.4, the difference-based method is often used as an absorption reference standard for the filter-based methods; it is therefore essential to explore results from pairs of instruments for which the difference method can be applied. For this section of the investigation, the instruments included the one of the 4 CLAPs, one of the 3 PSAPs (the same PSAP utilized in the CalNex campaign), the nephelometer, and the CAPS.

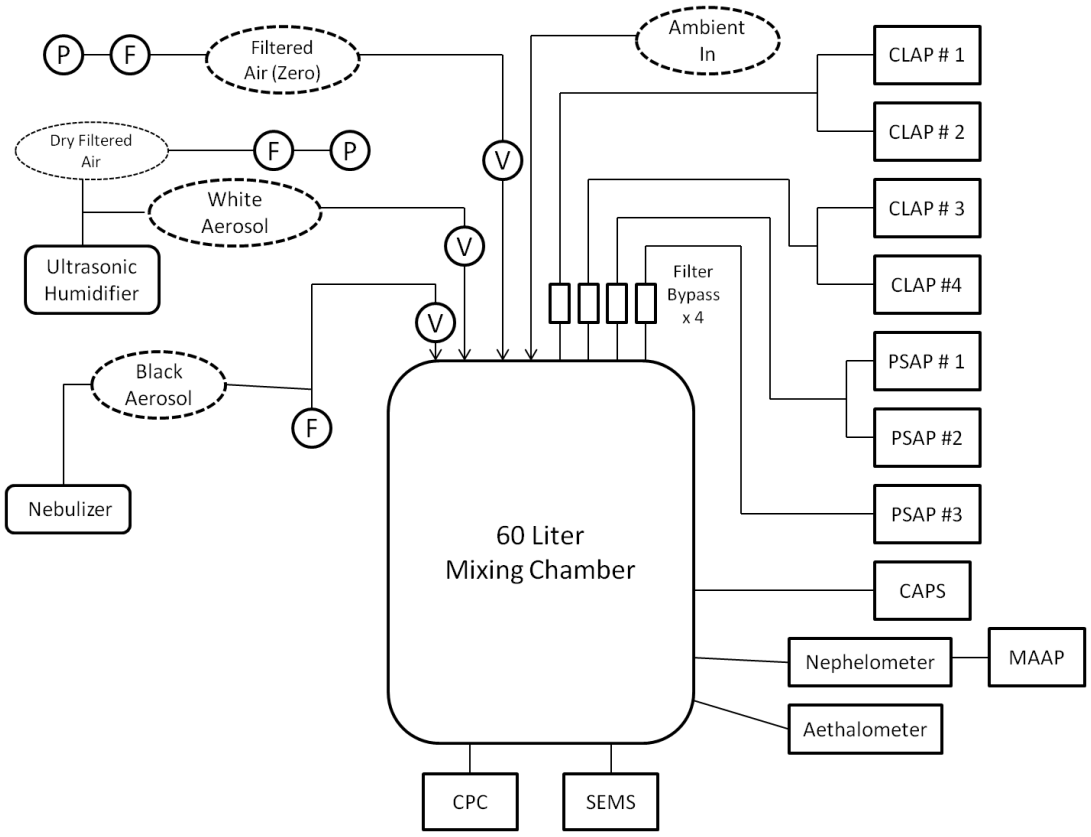

Figure 3.3: The instrumental layout for the NOAA laboratory experiment. The investigation by the NOAA aerosols group was extensive in aim, requiring the wide range of instruments for analysis. For this investigation, analysis was focused on the scientific questions posed in section 1.4 Utilized instruments included CLAP #1, PSAP #1, the integrating nephelometer, and the CAPS.

The schematic of the laboratory layout is depicted in figure 3.3. The left side of the figure shows the various methods for generating and sampling aerosol. Three types of aerosol, as well as filtered and ambient air, were introduced to the 60 liter mixing chamber via a network of

individual tubes connected at separate inlets. The 60 liter mixing chamber remained below ambient pressure, with the sample air being pulled out from instrument sampling lines at various flow rates. Maintaining this delicate balance required lengthy trial and error in pump and valve adjustments before and during sampling runs.

White aerosol particles were generated from a dilute solution of ammonium sulfate in filtered water by means of a commercially-available ultrasonic humidifier. The output of the humidifier was mixed with dry, filtered air in order to assure efficient delivery of the aerosol sample through the sample lines and to the mixing chamber. Ammonium sulfate is an ideal white aerosol because it has negligible absorption in the visible wavelengths and assumes a near-spherical shape when dry. Measurement of the white aerosol run will assist in the better quantification of absorption artifacts; where up to several inverse Mm of "absorption" can be measured due to scattering effects of a purely scattering aerosol. Black aerosol was generated with fullerene soot diluted with distilled water via a nebulizer. This method, as opposed to black soot generated via kerosene lamp burning, is ideal due to the stability in particle size and gradual growth and decline in number. The mixed aerosol was a combination of these two methods. Both the white and black aerosol generators were equipped with separate sampling lines to minimize unintended mixing prior to delivery at the mixing chamber.

Generated aerosol particles were delivered to the mixing chamber, where the CPC and SEMS sampled off additional sampling ports in order to measure the particle number concentration and the size distribution, respectively. Within the mixing chamber, three fans served to circulate the sample so that it was well-mixed prior to sampling by the multiple instrument connected to the chamber. Each run was defined by the type of particle generated, the intended SSA, the flow rate of the sample, and the level of filter transmittance reached.

3.2.2: Data Analysis Technique: NOAA Laboratory Experiment

Table 3.2 shows the aerosol types, materials, and run comments for the runs utilized in the data analysis. Ambient and filtered air runs were not utilized for the analysis due to the very clean nature of the aerosol. The air sampled in Boulder, Colorado yields low absorption levels, and the "real atmosphere" test for aerosol instrumentation has already been explored via the CalNex analysis. Typically, a filtered air run is utilized for better instrument calibration and

understanding of instrument noise. As such, the filter air run was utilized in order to establish the instrument-to-noise for the PSAP used for the CalNex campaign (discussed in section 4.1.1), but not utilized in further analysis. For the experimental runs included here, the flow rates were not altered to test for variation in filter penetration as mentioned in section 2.6.2 and remained a consistent distribution to all instruments of about 30 l/min for each run.

Table 3.2: Descriptions of the runs from the NOAA laboratory experiment utilized in the analysis. One of each type of aerosol run was utilized in analysis, excluding the ambient and filter-based air runs. The generated material and run comments are listed.

Aerosol Type	Generated Material	Run Comments
White	Ammonium Sulfate (AS)	AS deposited on fresh filter
Black	Fullerene Soot (FS)	Transmittance dropped to 0.67 on filter-based instruments
Mixed (Grey)	AS + FS	Transmittance dropped to 0.50 on filter-based instruments
White on Grey	AS on top of previously-deposited AS + FS	AS laid on top of grey overnight

Corrections for the filter-based instruments applied in the laboratory experiment are the same as described above in section 3.1.2. Both the Bond correction scheme and the CTS correction scheme are considered, most specifically for the conditions where the Bond correction scheme has suggested issues in accuracy (discussed in section 2.6.2). The integrating nephelometer was corrected for truncation errors assuming submicron distribution (Anderson and Ogren, 1998). All instruments were adjusted to report at standard temperature and pressure (STP) conditions (0° C, 1013.25 hPa). For all other instrument calibrations and corrections, readers are referred to the references associated with instrument descriptions within the background sections 2.2.4 and 2.6.2b.

Before data analysis, all instruments utilized in the laboratory were wavelength adjusted to 656 nm; the standard operating wavelength for the CAPS. Since the single wavelength CAPS was an integral part of the reference absorption measurement, all other instruments were adjusted to the red wavelength for simplicity in analysis. Data were first run through a “quick plots” and “quick statistics” script developed for R (an open-source statistical data analysis program), to provide first looks at the experiment data at the end of a run. These figures were not only beneficial in identifying potential issues with laboratory activities (i.e., undesired changes in flow or aerosol characteristics) and decision making for subsequent runs, they also assisted in determining which

runs provided valid data for analysis. Analysis of laboratory data is similar to what has been previously described in section 3.1.2. Data were inspected in the CPX2 program to edit spikes and identify sub-run segments. Once data editing was completed, the R script to generate figures and statistics was re-run for one minute averages on the edited data and it is these results that were evaluated. For the lab experiment, the R and CPX2 figures will be utilized, while CalNex analysis will rely on the IDL figures and statistics.

The reference absorption for the laboratory experiment was obtained from the difference method. For this, the σ_{ap} is obtained from the extinction measured from the CAPS minus the scattering measured from the integrating nephelometer.

$$\sigma_{ap} = \sigma_{ep,CAPS} - \sigma_{sp,neph} \quad (16)$$

4. Results and Discussion

4.1: CalNex Results and Discussion:

4.1.1: PSAP versus PAS Measurements during Concurrent Sampling

With an instrument noise level of 1.1 Mm^{-1} for 30 second averages, as determined in laboratory testing of instrument-to-noise levels, the justification to limit the analysis to σ_{ap} greater than 1 Mm^{-1} is justified. Only absorption data above the instrument noise level is utilized. The investigation was also limited by CRDS extinction measurements; only when extinction levels were greater than 10 Mm^{-1} (which corresponds to σ_{ap} of 1 Mm^{-1} for an assumed SSA of 0.9) were absorption values considered. Extinction levels below 10 Mm^{-1} are an indication of very clean air measurements. During clean area periods, genuine observation of the variability between instruments is difficult to distinguish. Therefore, excluding these ranges of measurements provide a more clear depiction of similarities and differences in measurements for the bulk of the data collected.

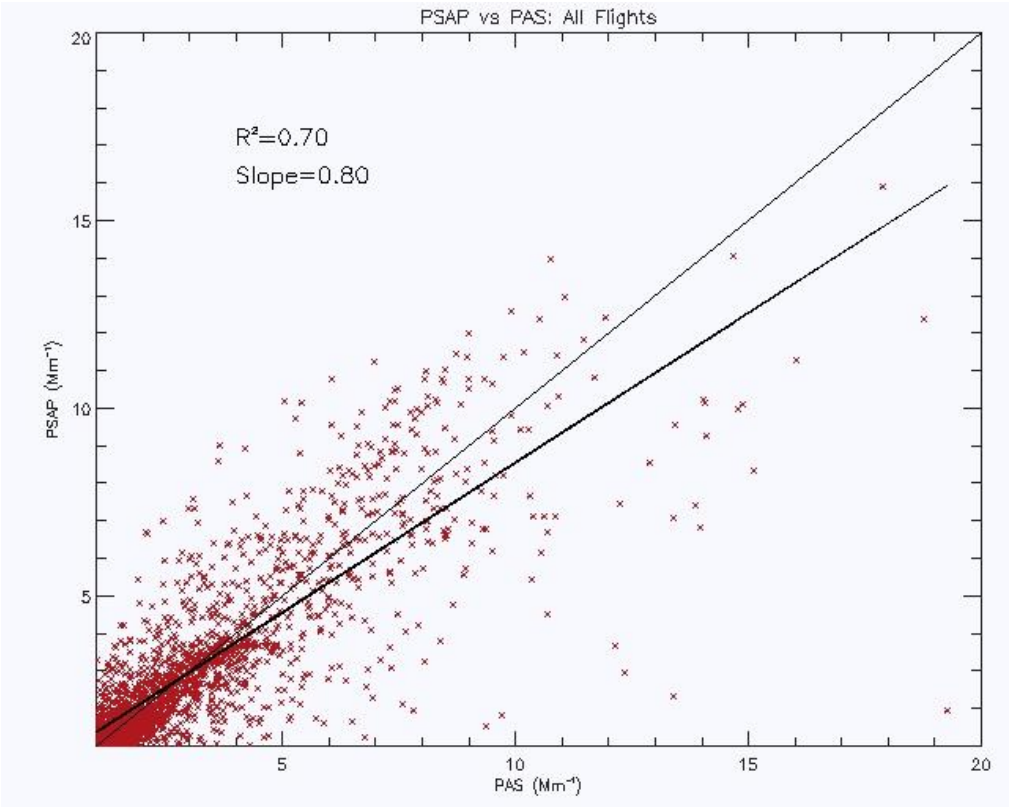

Figure 4.1: Regression between the PSAP and the PAS absorption coefficient (σ_{ap}) in 30-second averages for all analyzed flights in CalNex. The instruments are linearly correlated with a slope of 0.80 and an R^2 of 0.70.

The comparison between the PSAP and the PAS absorption coefficient (σ_{ap}) for all flights analyzed (for 30 second averages) is shown in figure 4.1. The PSAP and the PAS are linearly correlated, with the slope for the entire dataset of 0.80 and an R^2 value of 0.70. The equation for the least fit line is y=0.80x+0.36, with the PSAP absorption tending to be less than the PAS absorption. If the two instruments agreed perfectly, the data points would fall on the 1:1 line where the slope would be 1.0 and there is no offset.

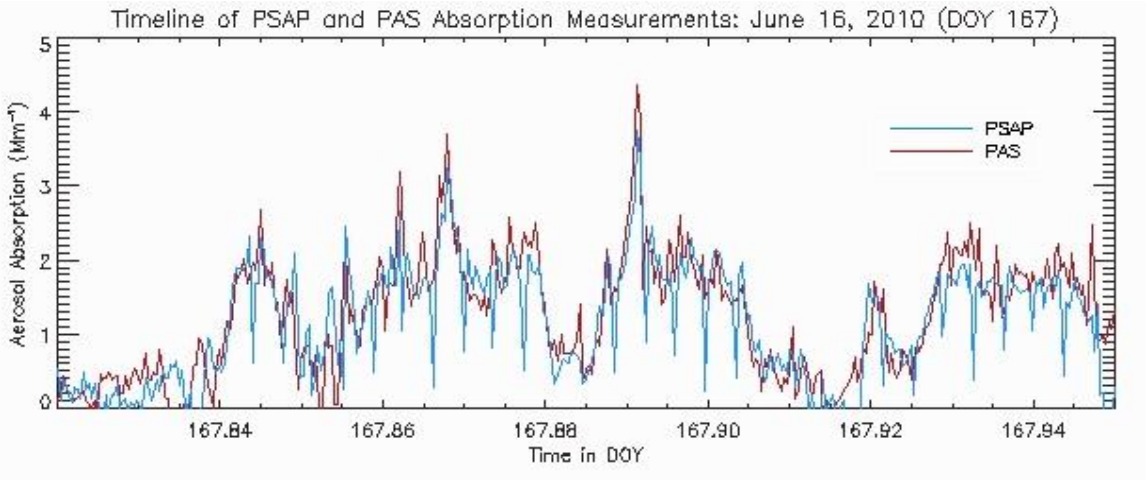

Figure 4.2: Time series example of data collection in by the PSAP and PAS for a segment of the June 16th, 2010 (DOY 167) flight. Both instruments follow closely in shape and magnitude of σ_{ap} measurements. The PSAP was subject to periodic zeroing for calibration purposes; however, these instances are not included in further analysis.

An example of the absorption data collected from the PSAP and PAS simultaneously while operating under the same conditions is shown in figure 4.2. The periodic zeroing in the PSAP measurements occurred at regular intervals in order to assist in the calibration of resonance properties of the PAS and CRDS (however, these zeroing periods are not included within the regression analysis to follow). It is clear that the σ_{ap} values from both instruments follow each other closely in shape and magnitude. This is a typical characteristic for the entire dataset. However, variances in measurement occur throughout the time series where further examination is appropriate in order to clarify any potential biases and/or remedies for divergence. Day 167 (June 16th, 2010) depicted in 4.2 was a flight where a substantial portion of the investigation was flown over the agricultural regions of the San Joaquin Valley, with flight time over the cities of Fresno and Bakersfield, as well as the Pacific Ocean. Despite the variability in potential aerosol type within these regions, the measurements from the PSAP and PAS instruments were well correlated throughout (had the CLAP been fully functional during the CalNex field campaign, it

would have been expected to be nearly in-sync with the PSAP measurements, as shown in laboratory experiment results). It is not expected that the PSAP and PAS instruments should report an identical data stream (as is evident during the first 30 minutes of the flight in figure 4.2).

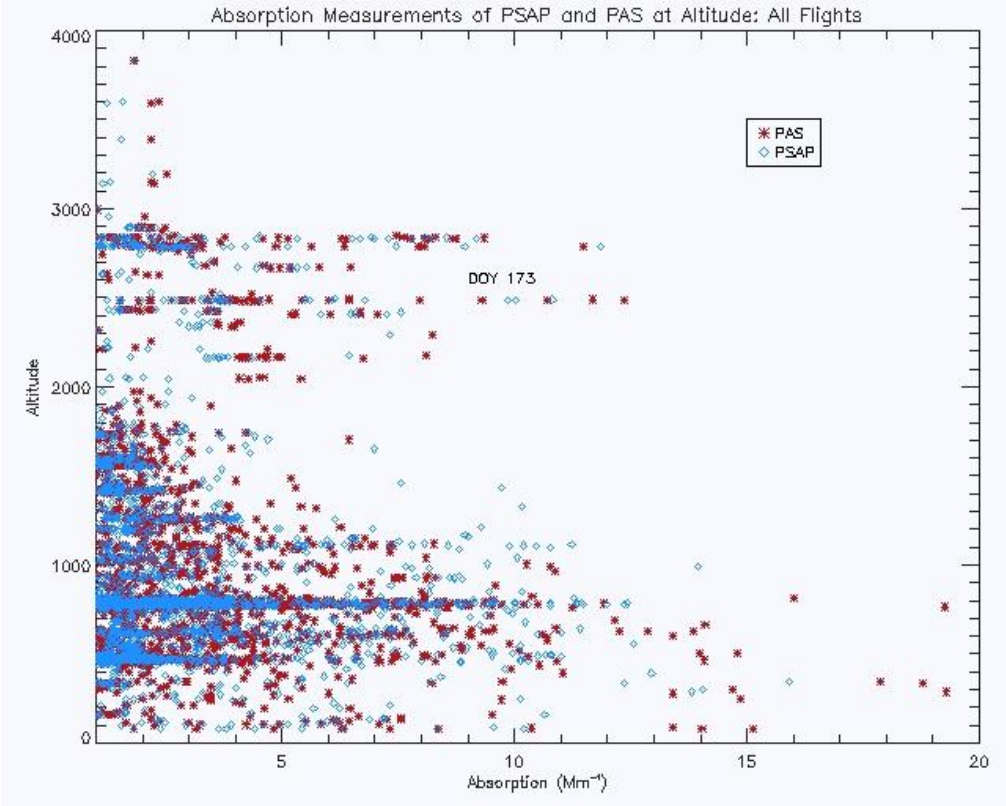

Figure 4.3: Aerosol σ_{ap} levels based on altitude for the PSAP (blue diamonds) and PAS (red asterisks). Most of the atmospheric aerosol burden resides within the planetary boundary layer (0 to ≈ 1000 m), where a fairly constant concentration is maintained due to turbulent processes. Plumes, such as the one that occurred on DOY 173 (to be further discussed in section 4.1.2), have to potential to be pushed aloft to higher altitudes.

As mentioned in section 1.1, aerosols within the atmosphere are highly variant on spatial and temporal scales. It is therefore an important consideration during airborne studies to identify in which altitude ranges the greatest burden of aerosols resides. Figure 4.3 shows the aerosol σ_{ap} levels based on altitude for both the PSAP and the PAS. This figure illustrates how aerosols are mostly observed within the planetary boundary layer or "mixed layer" (0 to ≈ 1000 m) where turbulent processes maintain a fairly constant concentration profile, with the potential for plumes to be aloft at higher altitudes. A greater range of σ_{ap} is observed within the planetary boundary layer, with an obvious decline in absorption between 1000 and 2000 m. Higher levels of σ_{ap} were observed between 2500-3000 m, which has been determined to be an altitude where plumes from

distant forest fires were detected (DOY 173; to be discussed in greater detail in section 4.1.2). The development of regional vertical profiles from aircraft studies and lidar measurements can be coupled with on-ground and long-term research findings to establish a more comprehensive view of atmospheric constituents (Arnott et al., 2006; Kahn et al., 2009). As figure 4.3 suggests, the pollution of the Los Angeles and Southern California area can be affected by sea breezes and the nearby mountain range, often causing plumes to be pushed aloft (Wakimoto and McElroy, 1986; Lu and Turko, 1994). The concentration of these plumes will be related to the strength of the emission source, as well as the distance travelled from the source region. These distances can be quite large, despite the relatively short lifetimes of atmospheric aerosols. As stated in the atmospheric aerosol climate review by Kahn et al. (2009), particles traveling 5 m/s can travel up to 3000 km/week. Plume concentrations aloft will also be influenced by meteorological factors, such as wind speed, precipitation, and the depth of the mixed layer. Additionally, the altitude of the boundary layer is not constant over time and will fluctuate based on various conditions: location, season, terrain, etc. (Oke, 1978). Due to this potential heterogeneity within a vertical profile, scientific investigations via aircraft studies have indispensable value for the measurement of atmospheric components.

As the data obtained through airborne aerosol investigations is so critical to atmospheric and climate studies, the evaluation of instrument performance when operated at altitudes and during changes in pressure is vital to this type of field-based study. For this, a linear regression was developed depicting the relationship between the PSAP and the PAS based on measurements at different altitude ranges (figure 4.4). Figure 4.4 shows the results of comparison of the PSAP and PAS measurements for four different altitude levels, with the average absorption ratios (R_{abs} = $\sigma_{ap,PSAP}$ / $\sigma_{ap,PAS}$) and standard deviations given in table 4.1. The analysis includes both level flight legs and profiles within their respective altitude ranges. A variety of correlation coefficients and R_{abs} between the instruments as a function of altitude is observed, yielding further insight on the instrument comparison in relation to the vertical absorption profile shown in figure 4.3.

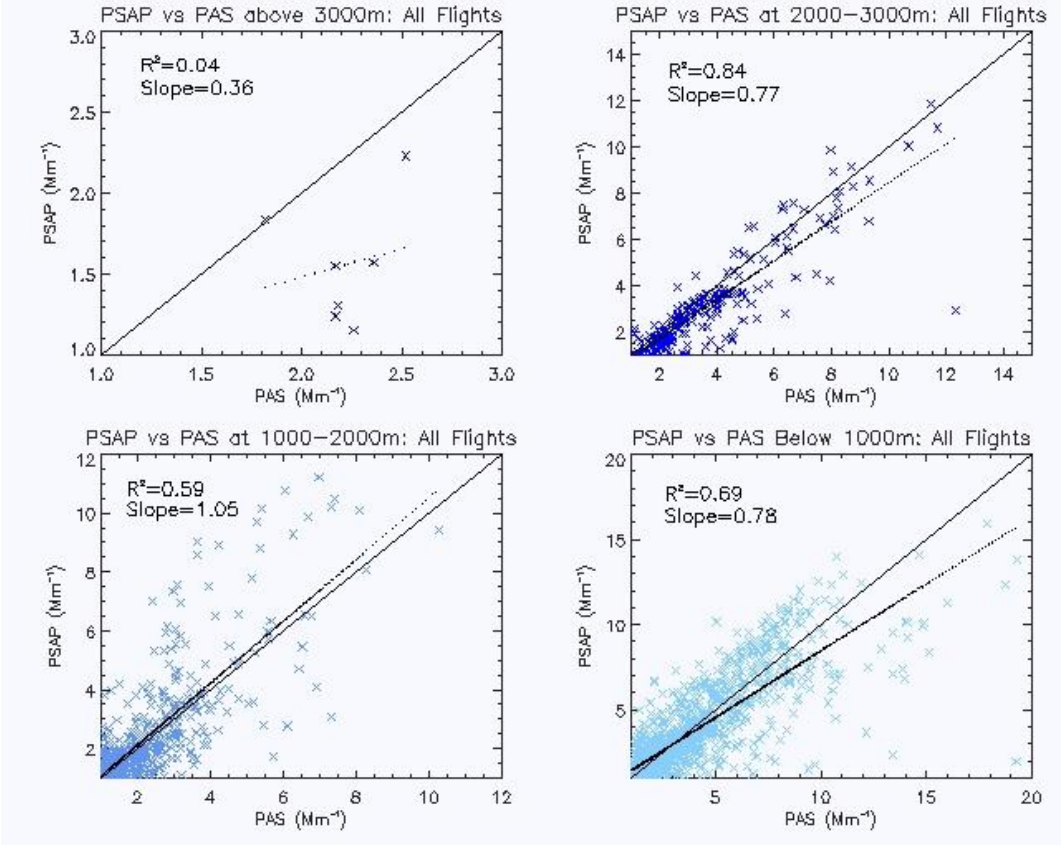

Figure 4.4: Regressions between the PSAP and the PAS σ_{ap} measurements based on four different altitude levels. The analysis includes both level flight legs and profiles within each altitude range.

Table 4.1: The average absorption ratios (R_{abs} = $\sigma_{ap,PSAP}$ / $\sigma_{ap,PAS}$) and standard deviations at the four different altitude ranges shown in figure 4.4.

Altitude	>3000 m	2000-3000 m	1000-2000 m	<1000 m
Absorption Ratio (R_{abs})	0.70 (± 0.18)	0.87 (± 0.23)	1.07 (± 0.44)	1.03 (± 0.37)

The scatter of points in the 1000-2000m range, where the PSAP measured significantly higher absorption values than the PAS is due to a flight on May 19th (DOY 139), where level flight was not often observed. These DOY 139 measurements occurred during significant ascents and descents, which suggests further investigation of pressure-related issues through the segmentation of flight characteristics into level legs and profiles (other possible reasons further discussed in section 4.1.2). However, this level of detailed analysis was not explored in this investigation, primarily because filtering the low instrument signal to noise ratio σ_{ap} measurements resulted in a low number of observations to analyze at an altitude above 3000 m. Despite the small number of reasonable observations above 3000 m, it is apparent that the

measurements observed at this level are potentially below the detection limit. The uncertainty associated with these measurements would increase with altitude, due to potential instrument sensitivities to changes in pressure. As noted in section 2.3.1, certain measures were established to minimize the effect of pressure changes on the PAS instrument during in-flight conditions (Langridge et al., 2011; Lack et al., 2012). The PSAP measurements can also be effected by the changes in pressure, as the filter has the capacity to bend and thereby altering measurement properties (Anderson et al., 2003). However, this effect is considered negligible in most cases when pressure does not greatly fluctuate.

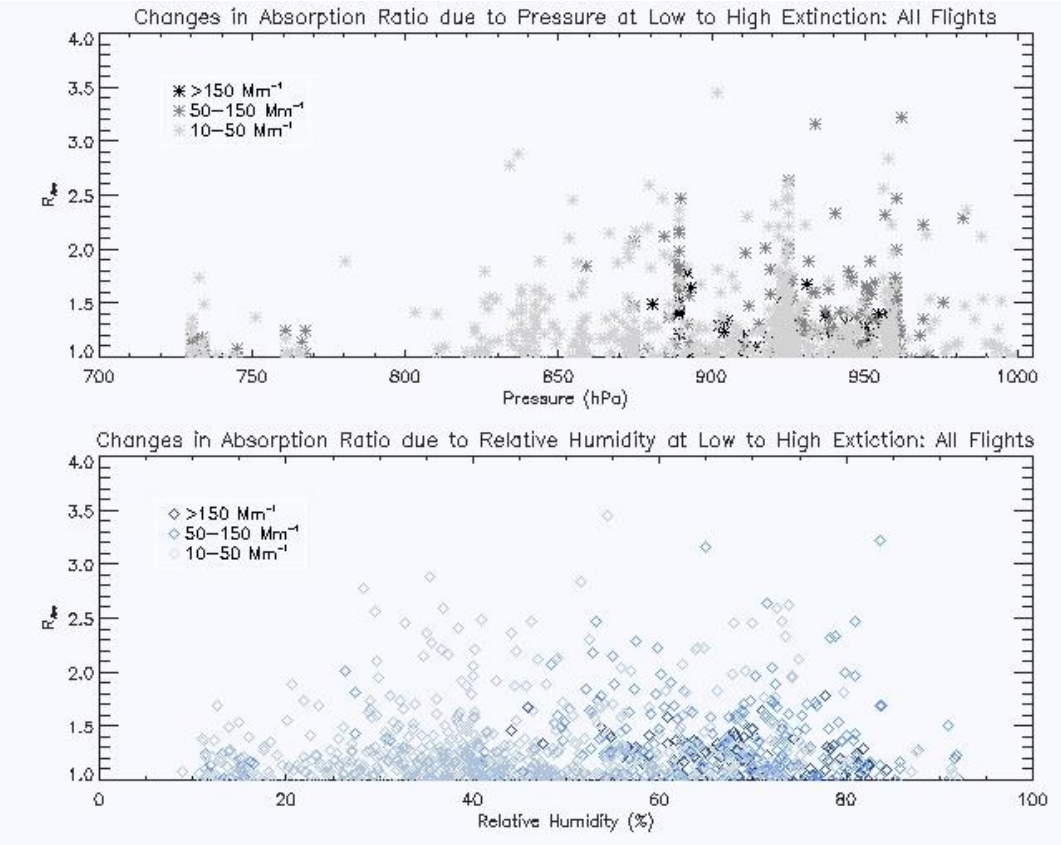

Figure 4.5: The changes in R_{abs} based on pressure (ρ) (top) and relative humidity (RH) (bottom) for all analyzed CalNex flights. Levels of atmospheric aerosol extinction are distinguished to provide insight on "clean" or "dirty" air, which could potentially influence instrument variability.

The change in the R_{abs} based on pressure (ρ) and relative humidity (RH) is investigated further in figure 4.5. Measurements observed during various levels of extinction are distinguished to yield insight on whether the sample was taken within "clean" or "dirty" air, which could also have influence on instrument variability during high or low ρ or RH. It's apparent that the extinction

levels were mostly between 10-50 Mm^{-1} for these flights, yielding no clear pattern within these figures. Only a very slight pattern is observed, with the majority of measurements made during medium to high extinction levels occur during periods at higher ρ. This would be due to the higher pollution levels near the surface and within the mixing layer discussed earlier. The traces of observed absorption at lower pressure (i.e. higher altitude) are likely related to the plumes aloft shown in figure 4.3. Only a very slight tendency is also observed in figure 4.5 (bottom) in relation to extinction levels; however, it appears that levels of RH do not have a substantial effect on R_{abs} of measurements. It appears as though the changes in relative humidity have similar effects on both instruments, creating no obvious fluctuations in the values measured between them. One would assume that the measurements made in low RH would present the most stable results, with increasing uncertainty with rising RH levels; hence why samples are often dried before entering instrumentation (Arnott et al., 2003). At higher humidites there is a potential for liquids to reach the filter and alter its shape, possibly spreading and changing the dynamics of the measurement (Subramanian et al., 2007). It does however appear that the measurements distinguished by levels of extinction appear to split the distribution into two parts; with the low extinction corresponding to low RH and vice-versa for high extinction. This could be associated with the liquid-like coatings on higher-absorbing organic aerosols; however this is only speculation, as it appears that R_{abs} is not highly dependent on RH or ρ in this case. It could also be the lower RH air is simply cleaner, and yields lower levels of absorption. In an airborne study over Asia conducted by Anderson et al. (2003), the PSAP sensitivities to RH and pressure were investigated via the consecutive measurements of two PSAP's in flight. One of these was sampling outside air, while the other sampled only filtered air. This provided the opportunity to quantify PSAP sensitivity to pressure and RH. It was noted that humidity changes, even at low levels, will increase the PSAP noise. It was also shown that PSAPs perform the best in level flight legs, and ambient gradients of RH teamed with changes in altitude increase PSAP noise. In this regard, further analysis utilizing only level flight leg segments could prove beneficial for the CalNex campaign.

4.1.2: Addressing the Potential Organic Aerosol Filter-Based Bias

As mentioned in section 2.5, it has been suggested that potential biases in filter-based measurements can occur as a function of atmospheric organic aerosols; a concept first described

in detail by Subramanian et al. (2007) and Lack et al. (2008). The bias was not described as a consistent occurrence in all cases. However, many papers have cited this argument, claiming this bias to be a regular feature of filter-based collected data. The bias of filter-based measurements has been mentioned in a number of studies involving a filter-based instrument, as well as within the absorption instrument reviews by Moosmüller et al., 2009 and Müller et al., 2011. Since the publication of the ground-breaking Lack et al. (2008) paper, little evidence to refute this finding as a fixed characteristic of filter-based measurements has been explored or presented. Further analysis of this potential bias is essential, since the assumption that a filter-based instrument will report this bias under all conditions could prove detrimental to the acceptance of long-term records of absorption from PSAPs. Of course, the bias would need to be more aggressively addressed in existing and future data sets if it were found to occur in all cases. The development of a robust correction scheme would be essential.

Table 4.2: The classification of organic aerosol (OA) based on the definitions utilized by Lack et al. (2008); first established by Zhang et al. (2007). The classification of "heavily polluted" (>12.5 µg m^{-3}) is not utilized in further analysis, as the large majority of OA observed during the CalNex campaign remained in the "urban" category. Levels of OA above 12.5 µg m^{-3} were only observed during one instance in the analyzed flights.

Organic Aerosol	Low OA	Medium OA	High OA	Very High OA
Classification	Rural/ Remote	Urban Downwind	Urban	Heavily Polluted
AMS OA Mass (µg m^{-3})	0 to 2.5	2.5 to 5	5 to 12.5	>12.5

Table 4.2 gives the classification of organic aerosol (OA), based on the definitions utilized by Lack et al. (2008), which were established by Zhang et al. (2007). However, the classification of "heavily polluted" (>12.5 µg m^{-3}) has been omitted within this analysis, as levels of organics above 10 µg m^{-3} were not often observed within the CalNex campaign. The highest levels of >12.5 µg m^{-3} were observed only a very small number of times during the campaign; for instance, during flights over the heavily populated city of Los Angeles and during observations of forest fire plumes. Moreover, the occurrences become less in number when they are averaged in 30 second intervals. Therefore, the "heavily polluted" category was not included in this analysis and the single occurrence where organics are considered "heavily polluted" is analyzed within the "urban" category.

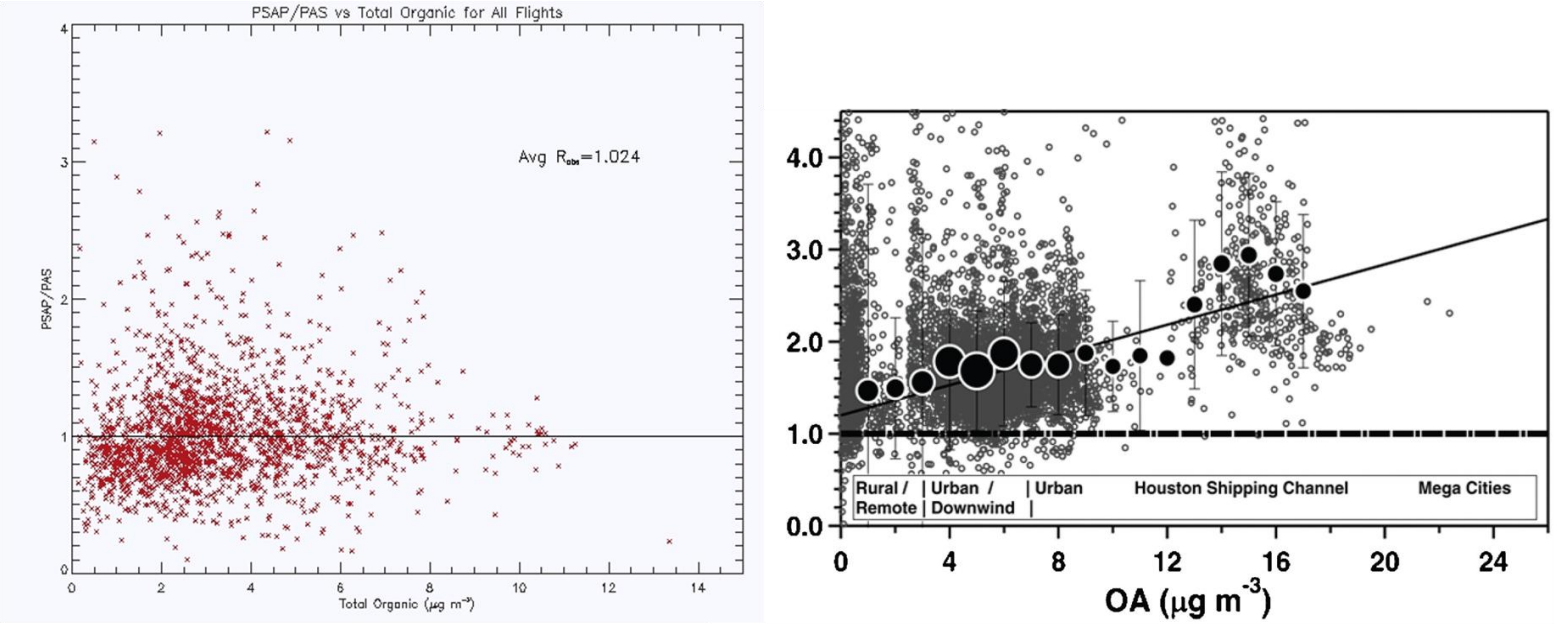

Figure 4.6: The ratio of the PSAP absorption to the PAS absorption (R_{abs}) as a function of the level of AMS OA mass concentration (left), where OA levels measured between 0-14 μg m^{-3}. The counterpart figure from the Lack et al. (2008) (right) Houston investigation shows the observed filter-based bias as OA levels increased above 12.5 μg m^{-3}. Figure reprinted with permission from American Association for Aerosol Research.

Figure 4.6 (left) shows the ratio of the PSAP absorption to the PAS absorption (R_{abs}) as a function of the level of AMS OA mass concentration. The CalNex dataset measured OA concentrations between 0-14 μg m^{-3}. This contrasts with figure 4.6 (right) (from Lack et al. (2008) during the TexAQS-GoMACCS campaign in Houston, Texas), where the organics reached levels of 22 μg m^{-3}. Despite the organics concentration remaining under 11 μg m^{-3} for most of the CalNex campaign, an important distinction between these two field experiments can be noted. As the OA mass concentration increases, the CalNex dataset does not demonstrate an increasing trend in the ratio of absorption by the $\sigma_{ap,PSAP}$ /P $\sigma_{ap,PAS}$ nor are the R_{abs} values as high as those shown in the Lack et al. (2008) counterpart figure 4.6 (right). Thus bias in filter-based absorption measurement attributed to OA by Lack et al. (2008) does not appear to affect the CalNex dataset. The comparison of figure 4.6 (left) and the Lack et al. counterpart (4.6; right) suggests distinctly different results in terms of an OA bias for the two different campaigns. The CalNex campaign does not suggest an increase in R_{abs} upon reaching the levels of OA where the Houston campaign began to see a bias in the R_{abs}. During the CalNex campaign, the ratio actually appears to move closer to a value of 1 at higher OA. Overall, it does not appear that the

absorption measured by the PSAP during CalNex has a dependence on the level of organics within the sampled air.

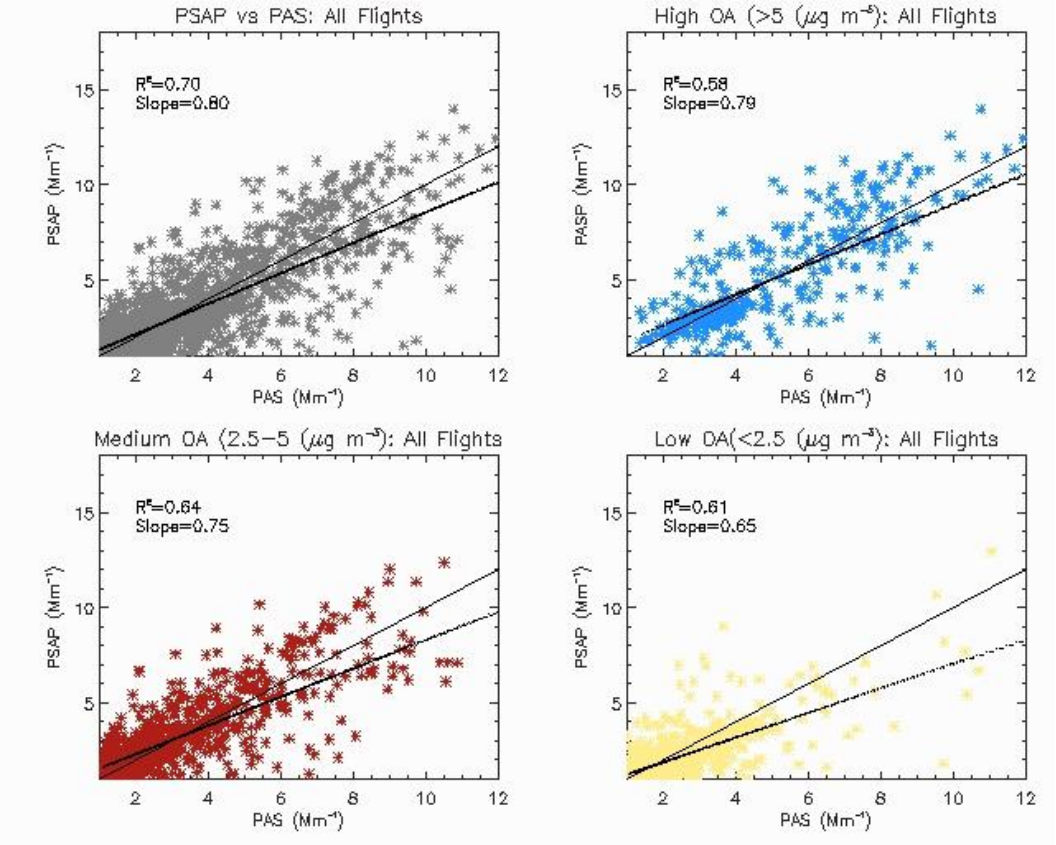

Figure 4.7: The regressions between the PSAP and PAS at four different levels of OA for all flights. Categories of OA are based on the same classification utilized in Lack et al. (2008), with the one occurrence of "highly polluted" OA levels (>12.5 µg m^{-3}) included in "high OA" category.

Table 4.3: The R_{abs} values and standard deviations for each category of OA analyzed in figure 4.7.

	All Flights	High OA	Medium OA	Low OA
Absorption Ratio (R_{abs})	1.02 (± 0.38)	1.04 (± 0.58)	1.07 ±0.38)	0.97 (±0.37)

In order to further investigate this finding, the separation of PSAP versus PAS measurements at different levels of OA (based on table R2 from Zhang et al. (2007)) are shown in figure 4.7. Table 4.3 gives the corresponding R_{abs} for each level of organics. As mentioned, the difference between the two instrument's measurements becomes larger at lower levels of absorption. The lower levels in absorbing particles create more difficult conditions for discerning genuine differences between instrument performances, due to the instrument noise discussed in section 4.1.1. These low levels of aerosol absorption are most prominently observed during flights at

night (DOY 150), over rural areas (DOY 167 and 169), and during periods of flights over the ocean (e.g. DOY 151). The aerosol observed during these time periods will potentially consist of more oxidized (aged) aerosol and secondary organic aerosol due to less distance from anthropogenic combustion emissions and greater influence by natural sources (Ng, et al., 2010). During the periods where higher OA levels are observed (>5 μg m^{-3}), the R_{abs} (1.04) most closely resembles the overall average of 1.02, creating a point of contrast with the Lack et al. (2008) bias observed in the Houston Region. The materials generally observed in polluted regions will create a different range of absorption measurements due to the variance in emission types and secondary organic aerosol precursors. Despite the magnitude of OA during CalNex not being at the same level as in the Houston region, this creates an interesting opening for further discussion on where the differences may lie between the Houston versus Los Angeles investigations.

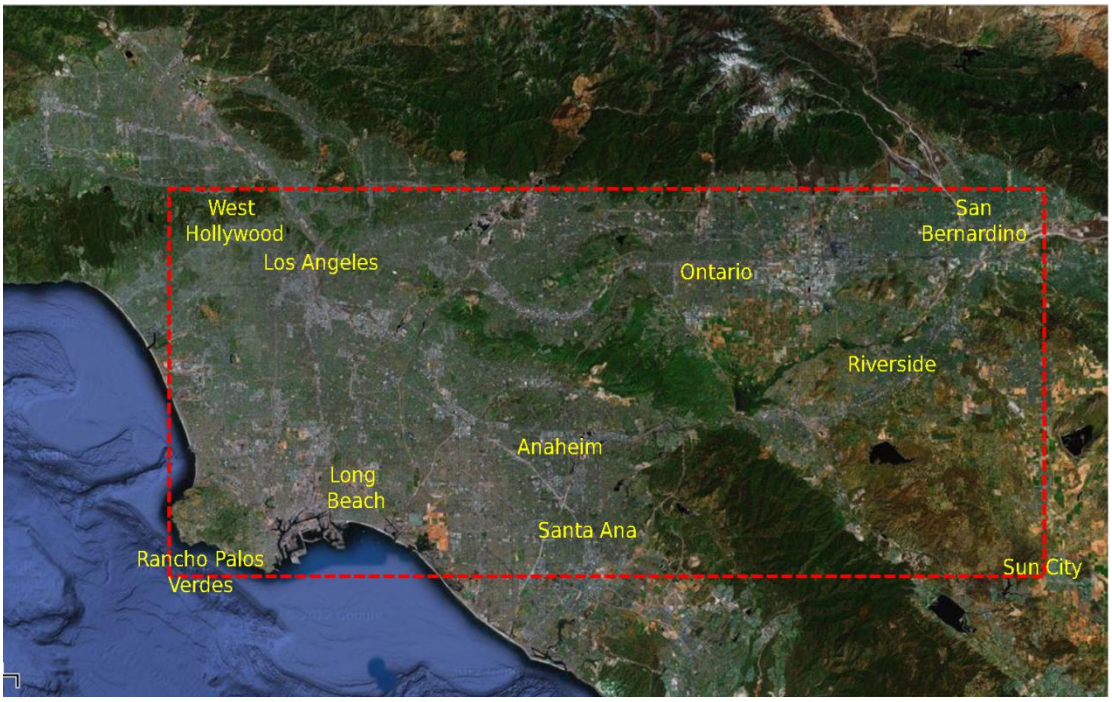

Figure 4.8: Map of the defined Los Angeles, California metro region utilized in analysis. Boundaries were defined to include as much populated area as possible, while minimizing the amount of included ocean area. Area photo obtained from Google (public domain).

Figure 4.8 shows the Los Angeles metro region defined for this analysis and investigated in greater detail below. As reported by the US Census Bureau (2010), the Los Angeles metro region is the 13th largest in the world by population and the 2nd largest within the United States. The Los Angeles-Long Beach-Riverside area (commonly known as the Greater Los Angeles Area) has an

estimated population of 17,786,419 as of the 2010 Census. In contrast, the Houston metro area is the 6th largest in the United States, with an estimated population of 5,946,800 (US Census Bureau, 2010). The metro region of Los Angeles defined in this investigation has been defined to range from the West Hollywood-Rancho Palos Verdes line to the west, to the San Bernardino-un City the east. These boundaries were established in order to minimize the amount of included ocean-based aerosol, while maximizing the inclusion of populated regions. The chosen study area expands just beyond Riverside to include the San Bernardino area, as that area was often included within the CalNex flight tracks due to the variance in emission types from local industry and populations.

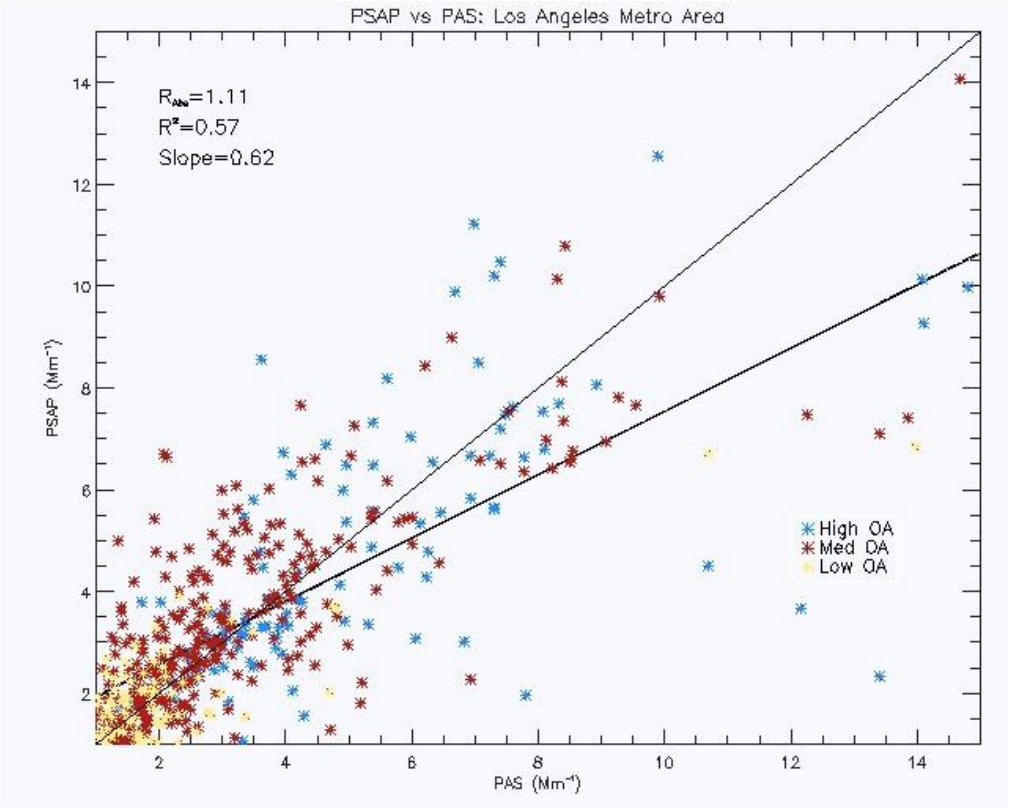

Figure 4.9: The regression of the PSAP and the PAS for measurements obtained within the defined Los Angeles metro region (defined in figure 4.8). Levels of OA are distinguished to better associated R_{abs} values with associated OA concentration.

Figure 4.9 shows the results of the regression analysis based on data only gathered within the defined boundaries of 4.8. The value of R_{abs} increases slightly from 1.02 in all flights to 1.11 when limited only to measurements made within the Los Angeles region. Again the organics were distinguished to better discern the amount of OA associated with R_{abs} quantities. The R_{abs}

values limited to the Los Angeles region also do not appear to depend on the levels of organics based on figure 4.9. The range of observations scattered in figure 4.9 appears to have no obvious pattern hinting at a bias in PSAP measurements.

This raises an interesting point of discussion: what characteristic of Houston's OA is so markedly different from the Los Angeles OA? Both regions are heavily populated, with high degrees of anthropogenic influence. The Houston metropolitan area is home to a substantial amount of shipping and industry, yielding emission plumes that may not be as prevalent in the Los Angeles Region (Lack et al., 2008; Massoli et al., 2009a). However, the Los Angeles region is touted as one of the most heavily polluted regions in the United States (American Lung Association, 2011). One important aspect which was not considered in the Houston campaign is the differences between daytime and nighttime chemistry, primarily due to photochemical effects. It is possible that the daytime emissions (i.e. traffic and other human-based activities), as well as subsequent atmospheric processing (e.g., photochemical reactions) play a role in the observation of the observed organic bias. Three out of the five analyzed flights where LA was either the direct focus or a significant portion of the flight were flown from the middle of the night to sunrise. This would mean the peak hours of pollution and photochemical response within the atmosphere would have been missed for these flights.

Figure 4.10 investigates this potential for the bias dependence of photochemical activities by separating the daytime flights versus the nighttime flights; a notion that has not been previously investigated in past work. Here, a filter-based bias is now seen within the data, previously hidden in the comprehensive analysis of all flights. A R_{abs} value of 1.17 and a slope of 1.19 is seen during the daytime hours, yielding an important distinction from the overall analysis. During the nighttime hours, a R_{abs} of 1.08 and a slope of 0.57 are observed, suggesting no bias towards the filter-based instrument. This finding is further investigated in figure 4.11, where the two daytime flights are considered individually.

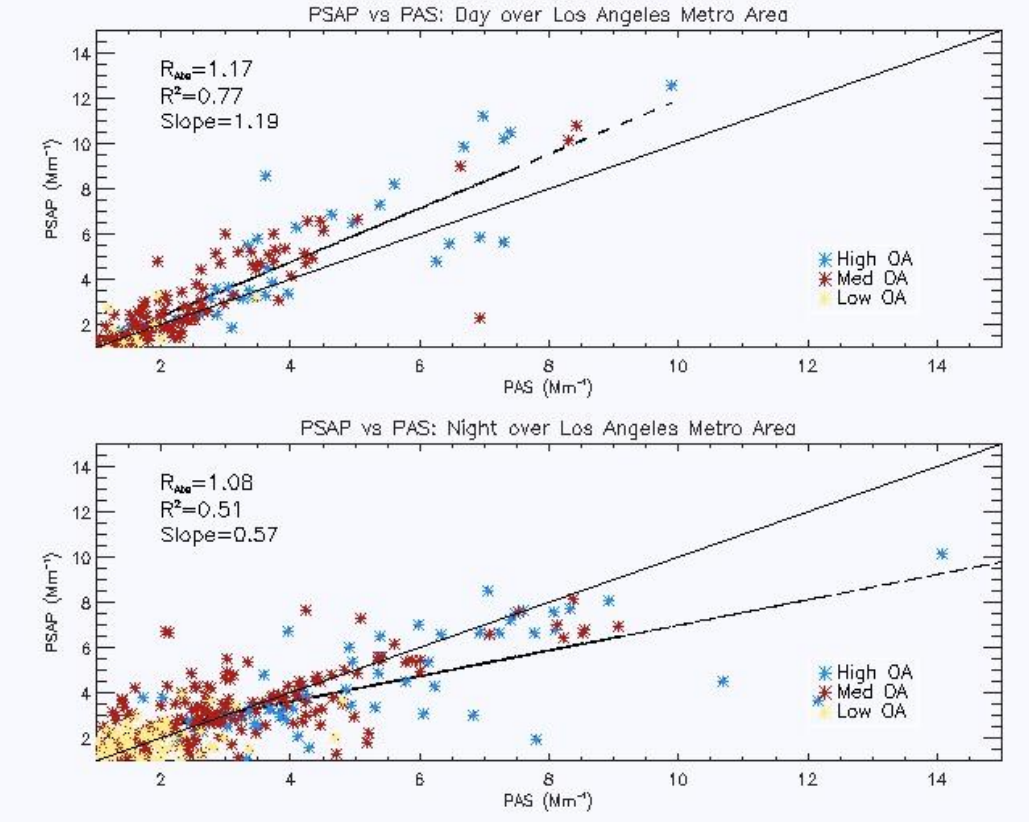

Figure 4.10: The regression between the PSAP and PAS during flights within the defined Los Angeles metro region (figure 4.8) during the daytime (top) and nighttime (bottom) flights. For the first time in analysis, a bias to the filter-based PSAP appears (top), suggesting potential differences in day versus night σ_{ap} measurements.

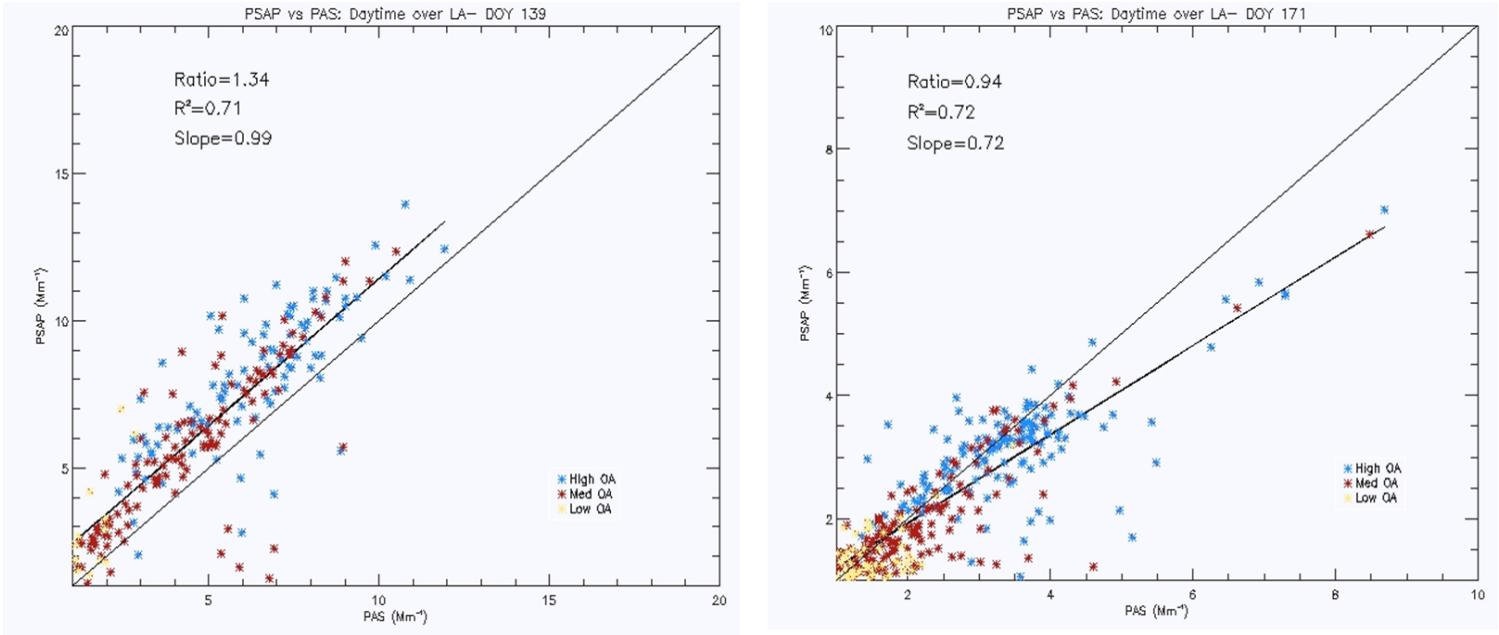

Figure 4.11: Regressions of the PSAP and the PAS for daytime flights over the Los Angeles metro region. A bias to the filter-based PSAP appears on May 19 (DOY 139; right), but is not apparent on June 20th (DOY 171; left). This difference indicates other factors of influence must be considered to determine cause of bias.

The breakdown of the two daytime flights over the LA region (excluding the flight back to Colorado on June 22, 2010 (DOY 173) due to lack of time spent within the area) is shown in figure 4.11. It is immediately striking that the observed bias is only present during May 19, 2010 (DOY 139) (figure 4.11; left) and is not apparent on June 20, 2010 (DOY 171) (figure 4.11; right). Separating the daytime flight data into the individual flights shows that the bias only occurs on DOY 139, where virtually equal levels of medium and high OA are observed. DOY 139 yields a R_{abs} of 1.34 and a slope of 0.99 with the linear fit to the data lying above the 1:1 line due to a substantial offset (~1.8). This hints at a fairly strong indication of some sort of bias. DOY 171, however, has a R_{abs} value of 0.94 and a slope of 0.72. Both daytime flights were generally in the same region and at the same time of day (12:00-18:00). This hints that there other factors to consider when determining whether or not the potential filter-based bias is dependent on photochemical activities and further demonstrates the wide-variety of influences that may impact a measurement. The presence of a PSAP bias on DOY 139 suggests that some aspect of the conditions on that day that did not exist or were not as prevalent on DOY 171.

The total mass spectra measured from the AMS are shown in figure 4.12. It's clear that there were significant observed differences in the AMS spectra on DOY 139 (left) and 171 (right).

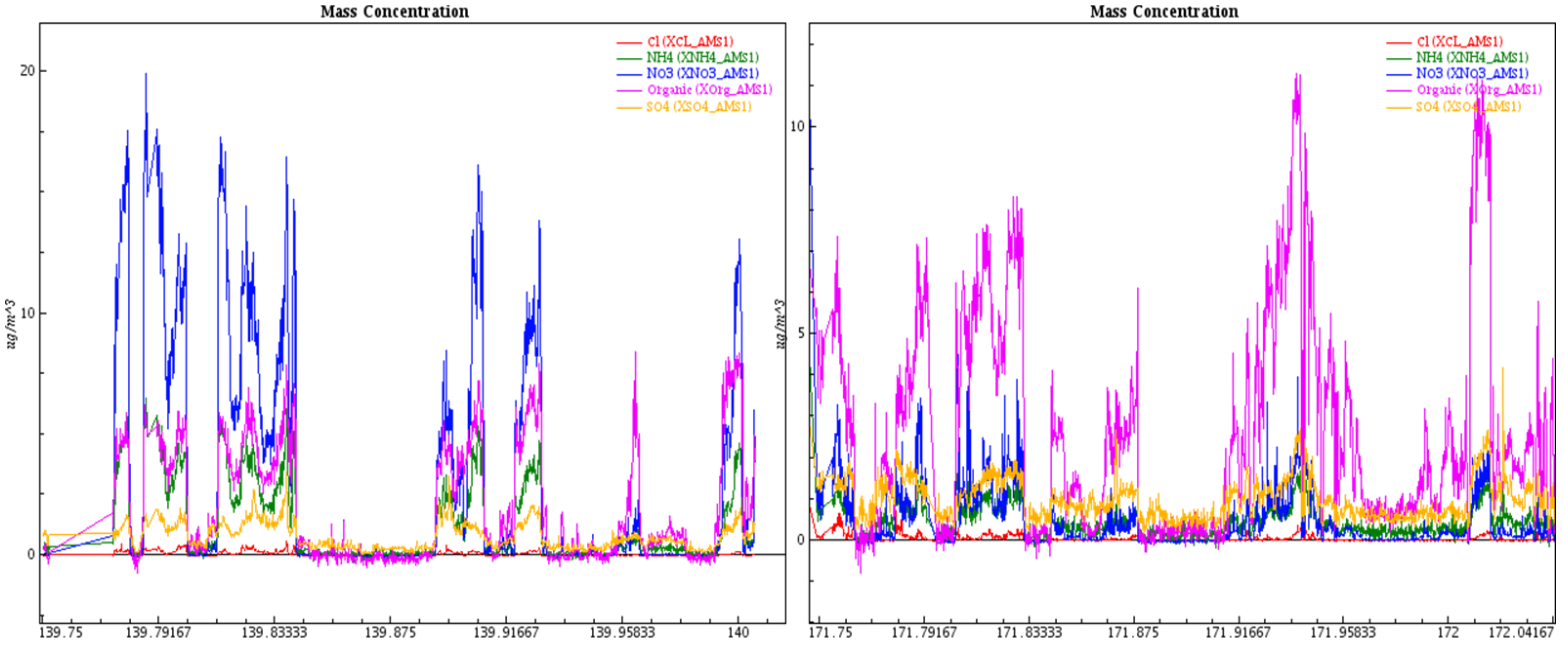

Figure 4.12: The total mass spectra from the AMS for DOY 139 (left) and DOY 171 (right). Significant differences in the NO_3^-/ OA may indicate different processing histories and could potentially be utilized as a proxy for the atmospheric age of sampled particles.

Most notably, the ratio of nitrate (NO_3^- ;blue line) to OA (pink line) mass appears to be higher on DOY 139 and lower on DOY 171. As seen in figure 4.12, the levels of organics were comparable for both days; however, the elevated levels of NO_3^- on DOY 139 may hint at a difference in the age of the sample. The increased levels of NO_3^- suggest a higher level of oxidation within the aerosol, suggesting that the aerosol sampled on DOY 139 differed in processing history from that of DOY 171. Although NO_3^- correlates well with aged air masses, the presence of nitrate does not stand alone as an indication of an aged aerosol (Ulbrich et al., 2009). This could be related to emissions of nitrate from anthropogenic combustion sources or agricultural regions outside the metro area. In order to truly establish if the NO_3^- is due to oxidation, further analysis involving gas phase sample constituents would be appropriate. For instance, the ratio of NO_3^- to CO could potentially be used as a proxy to define oxidation, as CO is a prevalent gas in the atmosphere with an atmospheric lifetime around one year (Seinfeld and Pandis, 2006). The oxygen to carbon ratio (O:C ratio) could also be investigated, as aged air masses will typically have higher O:C values (Ng et al., 2010). Alternatively, the utilization of the ratio of NO_z ($NO_y - NO_x$) to NO_y (gas-phase reactive nitrogen) as a determinant of the transition to an aged particle for this field campaign is considered by Langridge et al. (2012; paper submitted). This ratio will be around zero for freshly emitted NO_x and around one for aged, highly oxidized samples which would be associated with HNO_3.

Another means for determining the age of the sample plume could be through the distinction between oxygenated organic aerosol (OOA) and hydrocarbon-like organic aerosol (HOA) (this technological ability is available within the AMS instrumentation; however, data were not available for this particular campaign). The OOA and HOA observed will vary based on the meteorological and mass transport conditions, abundance of secondary OA precursors, and level of aging due to photochemical processes. Various influences such as 24-hour temperature fluctuations, movements of air masses, or proximity to industrial emissions affect the observed OOA and HOA properties (Ng et al., 2010). These properties could be relevant to the suggested organics bias as the age of the particles will have effects on hydroscopic tendencies and volatility of any developed coatings (Moosmüller et al., 2009). For instance, when a BC particle is first emitted, it is hydrophobic in nature. As the particle ages, a coating of organics can develop around the particle, altering the nature of the original material. An affinity for water develops as

the particle ages, typically developing within the timespan of one day (Cooke and Wilson, 1996; Moosmüller et al., 2009). If the aerosols sampled on DOY 139 were more aged than those sampled on DOY 171 (and therefore, more susceptible to a liquid-like coating), the source of the bias could be related to the alteration of the particles as deposited on the filter (Subramanian et al., 2007). It is possible that the particles collected on DOY 171 were more freshly-emitted, hydrophobic materials that did not exhibit this morphing characteristic upon filter deposition. Levels of observed BC were considerable for these two days, with DOY 171 exhibiting more significant fluctuations, possibly relating to fresher source material. However, this conclusion is only speculation as further investigation into this insight is limited by the availability of relevant data.

It can also be noted in figure 4.11 that the medium and high OA material appears to exhibit the same level on influence on the bias. This raises the question if the bias is related to the OA level at all, or if the exhibited bias is due to some other factor. As mentioned in section 4.1.1, it is possible the bias is caused by pressure-related influences from changes in altitude. However, the dependence on altitude was considered, but limiting data only observed within 500-700m in height did not remove the bias.

Another opportunity to investigate a potential organics bias occurred outside of the Los Angeles region on June 22nd, 2010 (DOY 173). During this particular flight, higher levels of organics were observed. The flight documented pollution plumes over the city of Las Vegas, as well as aged plumes from distant forest fires in New Mexico and Colorado. Figure 4.13 depicts a segment of a flight on DOY 173, which was the transit flight back to the NOAA facilities in Colorado. This particular segment was chosen not only for the higher levels of organic material, but also the close-to-level horizontal flight pattern maintained during the peaks in absorption. This flight provides the opportunity to analyze any potential pressure-related discrepancies in measurements. During this time, it does not appear that the PSAP absorption measurements are markedly higher than the PAS. In fact, it is interesting to note that the PAS absorption is slightly higher than the PSAP absorption at various moments in this flight segment, including when the highest organic mass concentration (14 µg m^{-3} (based on 30 second average)) is observed at.

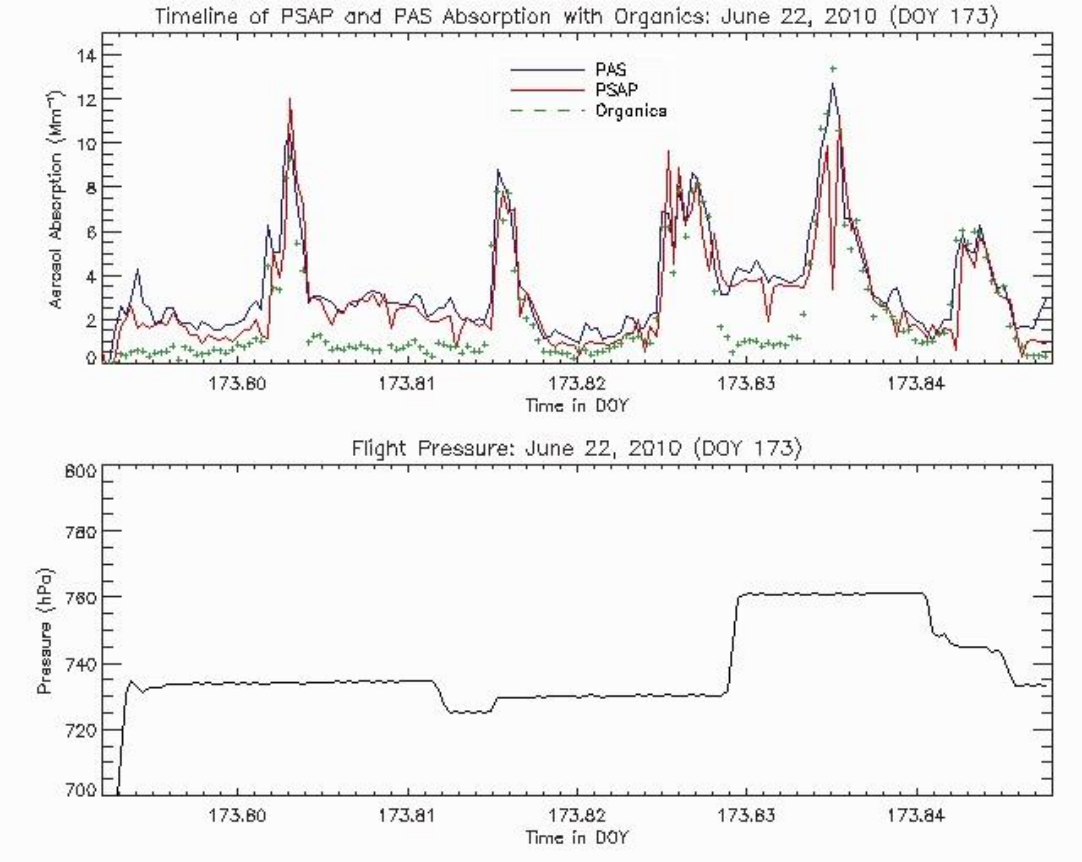

Figure 4.13: A flight segment for June 22nd, 2010 (DOY 173) depicting the PSAP and PAS measurements, as well as the observed levels of organics (top). Levels of OA are on the same scale as absorption but in μg m^{-3}. This segment was not only chosen for the higher levels of OA, but also the near level-flight pattern. This may reduce the potential for any pressure-related discrepancies.

This particular segment is the observation of a forest fire plume from New Mexico. During the organic mass concentration peaks, both the PAS and the PSAP remain very close in agreement but alternate in which has higher reported absorption. This is the period where the highest levels of organics for the analyzed portion of the CalNex campaign are seen and where one might expect to see indications of the potential filter-based bias due to organic aerosol. A short time later, even greater levels of organics were observed, reaching almost 20 μg m^{-3}. Unfortunately, not all data were available for analysis during this time and further investigation was not possible. These peaks are further investigated in figure 4.14, where the linear regression between the PSAP and PAS measurements during these specific peaks are analyzed.

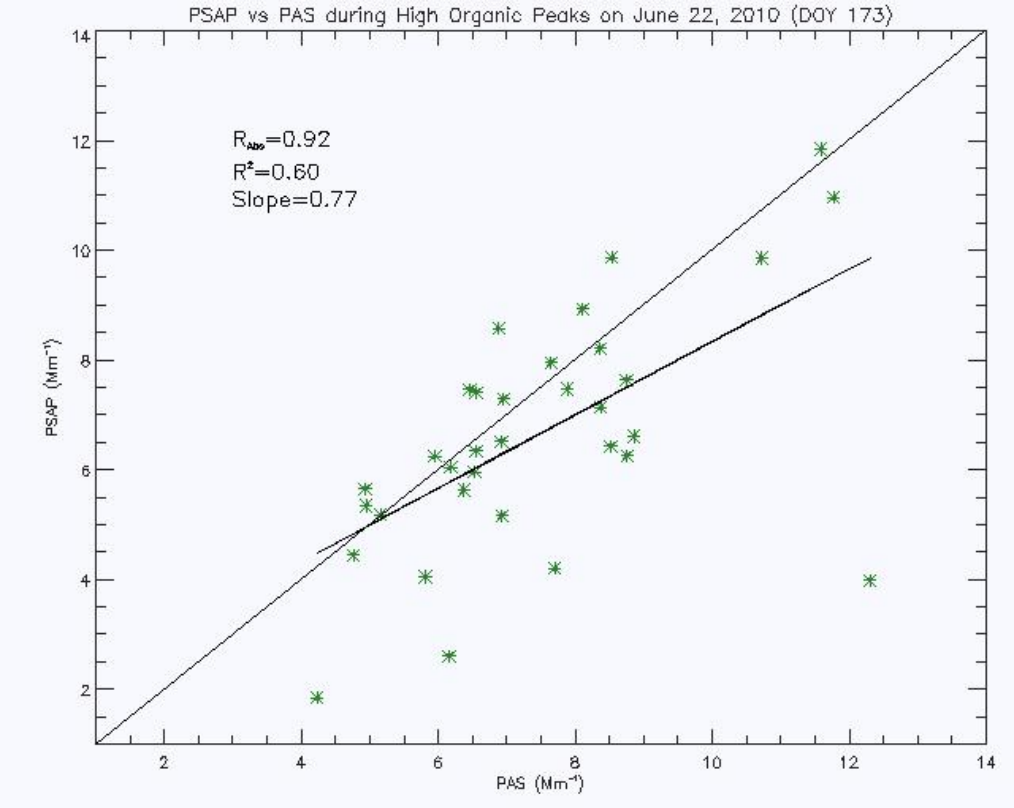

Figure 4.14: The regression between the PSAP and the PAS during the highest observed levels of OA in the analyzed CalNex flights, reaching a peak of 14 µg m^{-3}. Despite this peak, a bias to the filter-based PSAP does not result.

Figure 4.14 shows the relationship between the PSAP and the PAS during the period of high organics on DOY 173. During the highest level of organics seen within the analyzed data, the R_{abs} value is lowered from all flights to 0.92, and the slope is decreased to 0.77. Again, the potential bias does not appear to be present. In fact, a R_{abs} value of 0.92 implies that the PAS σ_{ap} was about 10% higher than the PSAP σ_{ap}. This is an interesting finding, as having observed the potential for an organic bias during a daytime flight in Los Angeles, it would seem reasonable to assume the bias would be present during the apex of observed OA levels. This further implies that there are a number of influences to consider when analyzing the conditions that occur during measurement and their possible effects on the outcome. For example, figure 4.15 considers the total organics as a part of the entire aerosol mass concentration.

In the Lack et al. (2008) paper which first described a potential bias in filter-based measurements due to artifacts from OA, only the amount of OA was considered. However, the

closer investigation of the mass fraction of organics (e.g. total organic mass/total AMS mass) could potentially be an important aspect to consider as well.

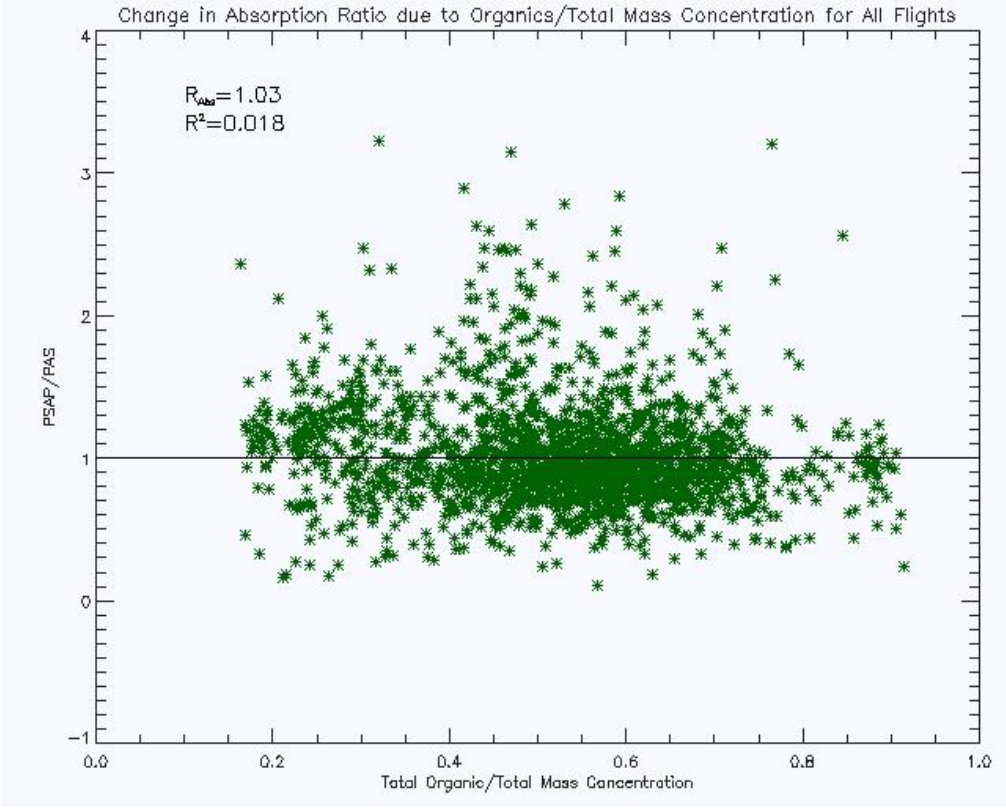

Figure 4.15: The change in R_{abs} as a function of organic mass fraction, where the OA mass is normalized by dividing the total AMS mass concentration. The data appears to be a bit noisy, but R_{abs} appears to fluctuate around 1.

Figure 4.15 shows the change in the R_{abs} as a function of organic mass fraction. For this, the total quantity of organics is normalized by dividing the total amount of mass concentration (including Cl^-, NH_4^+, SO_4^-, and NO_3^-). The data appears to be a bit noisy, but the R_{abs} fluctuates around the value of 1. It is apparent that the region between 0.4 and 0.8 of total organics/total concentration and below a R_{abs} of 1 is where an abundance of data falls and remains the closest to unity. As evidenced by figure 4.15, the total amount of organics relative to the total AMS concentration does not appear to affect the R_{abs} in any systematic way. This remains an important finding, as the potential for the amount of OA relative to the total AMS mass as an influence of a bias was overlooked in the Houston data. However, as demonstrated by the differences in organics by region, it could become an issue of greater importance within other locales (see figure 5.1 in section 5 for further illustration of this). The large variability in the composition of global

aerosols implies that the [OA] / [total AMS] could exert a more substantial influence on a regional basis.

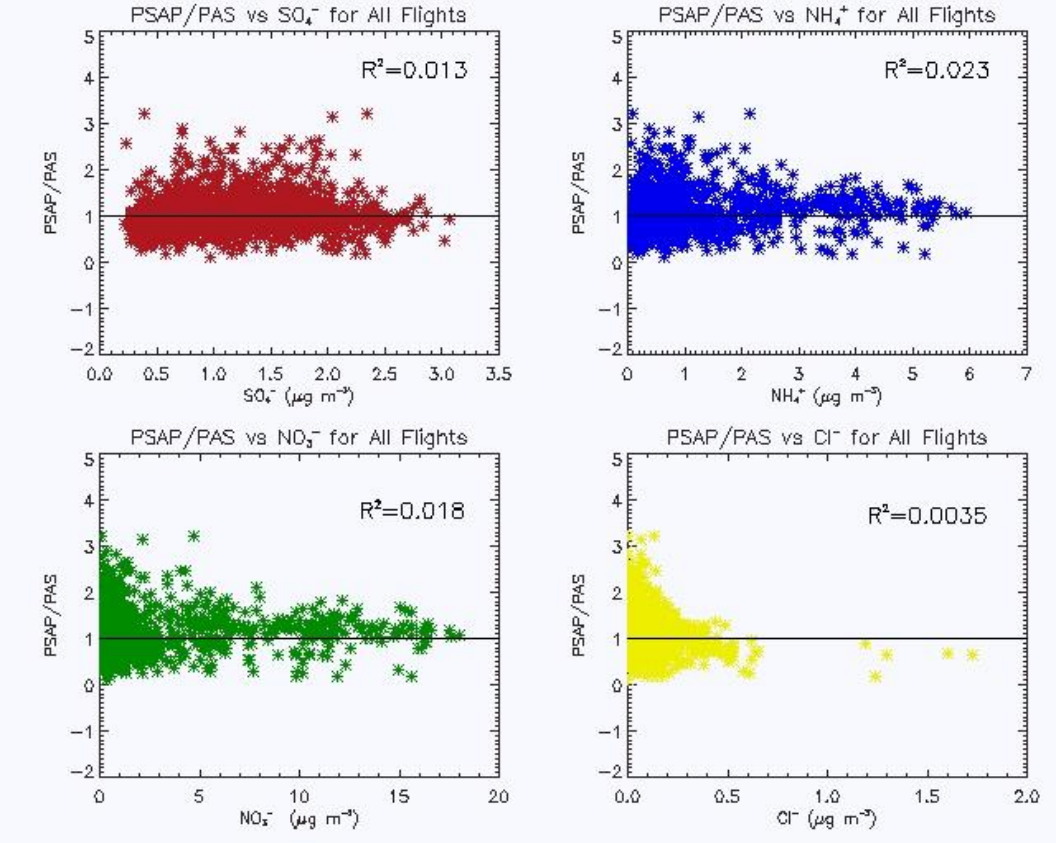

Figure 4.16: The change in R_{abs} as a function of the 4 other AMS components ($SO4^-$, $NH4^+$, $NO3^-$, and Cl^-) for all the analyzed CalNex flights. It does not appear that these AMS components effect R_{abs} in a systematic way.

The influences of the other AMS components are considered individually in figure 4.16. As is evident by the R^2 values of 0.013, 0.023, 0.018, and 0.0035 for SO_4^-, NH_4^+, NO_3^-, and Cl^- respectively in figure 4.16, non-OA components of the AMS do not yield significant influence on the ratios of the PSAP and PAS σ_{ap}. These ions are all hygroscopic; however, since the instruments were operated under low RH, liquid water would be assumed to have a minimal effect. This is to be expected, as the absorption by aerosols is said to be enhanced through the liquid-like coatings that encompass atmospheric organic aerosols, due to the potential to spread upon filter deposition (Subramanian et al., 2007). None of these other AMS mass concentration components would be expected to possess such a coating, and therefore, would not create the same potential issues proposed for organic concentrations. As discussed earlier, the presence of these materials remains important to consider, since they yield an indication of sources and

atmospheric processing history. The lack of effect of these AMS components could be due to analyzing all flight collectively, as influence may vary based on conditions during each flight (as discussed previously for DOY 139).

4.1.3: CTS Correction Comparison with Bond Correction

As mentioned in section 2.6.2, another concern of uncertainty with filter-based measurements and the comparison to other methods for absorption measurement is the applications of empirical corrections schemes to yield final values of σ_{ap}. It is commonplace for the Bond Correction to be utilized for the adjustment of filter-based absorption measurements. However, faults in this empirical calculation have the potential to cause further errors in measurement, limiting the accuracy in derived σ_{ap} (Bond et al., 1999; Virkkula et al., 2005a; Lack et al., 2008). For this reason, various other methods of correction have been considered, with the CTS correction algorithm the focus for this investigation (section 2.2.3b). It is possible that addressing the uncertainties associated with the empirical corrections could give rise to a more consistent absorption measurement from filter-based instruments.

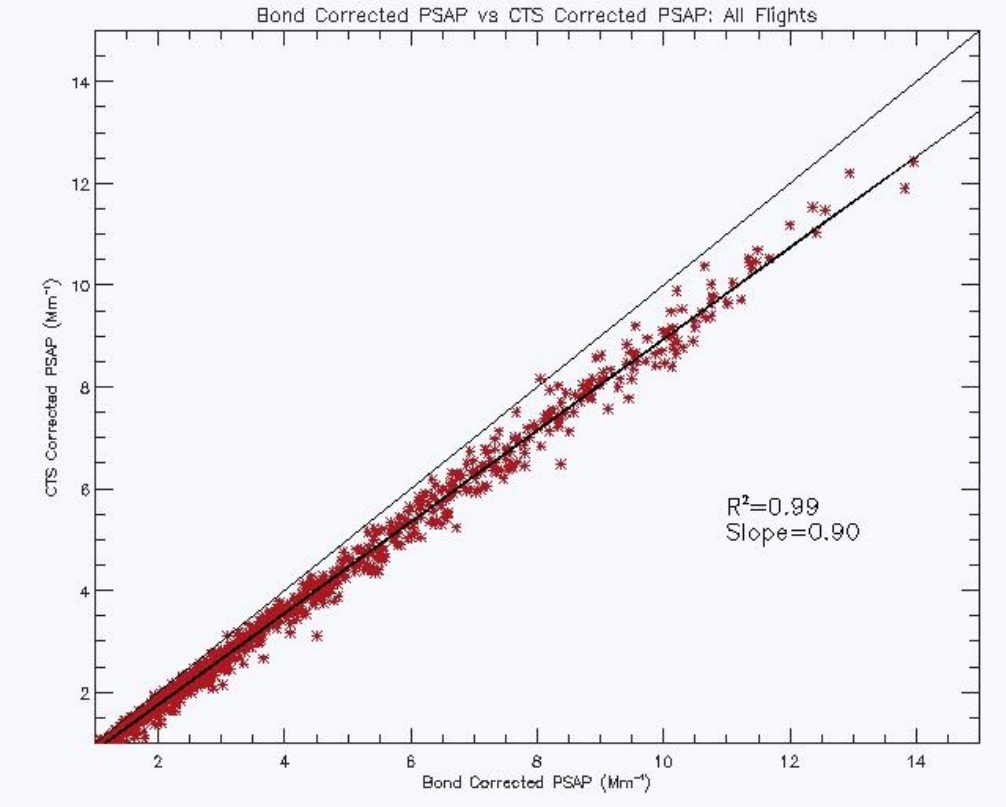

Figure 4.17: The regression between the CTS corrected PSAP and the Bond corrected PSAP for all flight analyzed in CalNex. From this figure, the use of the CTS correction instead of the Bond correction does not display obvious benefits.

The previous results for CalNex PSAP and PAS comparison have utilized the Bond et al. (1999) correction scheme to correct the PSAP data. Further assessment of PSAP to PAS measurement agreement can be performed utilizing the CTS correction scheme. Figure 4.17 shows a comparison of the PSAP data for both correction algorithms. With an R^2 value of 0.99 and a slope of 0.90, the Bond Corrected PSAP and the CTS Corrected PSAP are within 10% of each other. This difference could prove significant in some applications, if the conditions that hinder the accuracy of the regularly-used Bond Correction are the cause. It is obvious from figure 4.17 that the CTS correction will not significantly change the output from the Bond correction, as both corrections follow closely with each other. This is informative, as any noteworthy divergences under 'normal' conditions might discourage the utilization of the novel correction scheme.

Despite reaching a conclusion that the suggested PSAP bias to organics is not apparent within the majority of the CalNex data, it is important to consider all potential ways in which the suggested bias could be identified. In a continuation of the CTS versus Bond correction scheme analysis, the novel CTS correction scheme for filter-based measurements is applied to the CalNex PSAP data to determine if a more theoretically rigorous/complex correction leads to an identification of bias in the PSAP measurements (figure 4.18).

Figure 4.18 shows the companion figure to 4.7, where the PSAP versus the PAS regression is considered based on levels of OA. When compared with the Bond correction shown in figure 4.7, it can be seen that the R_{abs} ($\sigma_{ap,CTS}$/ σ_{PAS}) values, as well as the correlation and slope values shift only very slightly for this dataset. With the application of the CTS correction scheme to the PSAP data, as opposed to the regularly-utilized Bond Correction, shifts the agreement for all flights from an R^2 value of 0.70 to 0.63 and the slope from 0.80 to 0.71. While this 10% difference appears to not be a considerable difference, this provides insight towards its potential application for PSAP corrections. As such, any obvious benefits of using the CTS correction over the Bond correction for the CalNex dataset are not clear from these results. The resulting R_{abs} values are not significantly different compared with those obtained with the utilization of the Bond correction.

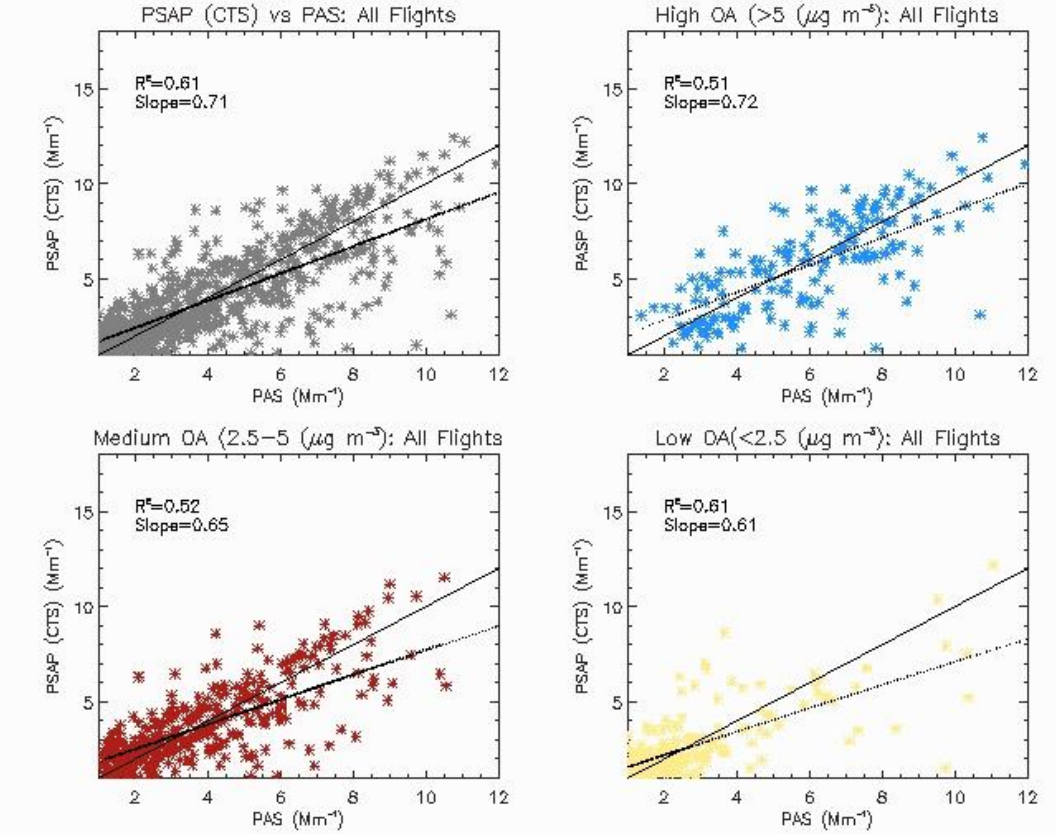

Figure 4.18: The regressions for the CTS corrected PSAP and the PAS for all flights (top left), with the OA levels distinguished in the three categories utilized for analysis (described previously in table 4.2). As can be seen in these figures, the utilization of the CTS correction versus the Bond correction for filter-based measurements does not yield obvious benefit to this analysis.

Table 4.4: The R_{abs} ($\sigma_{ap,CTS}$/ σ_{PAS}) values obtained using the CTS correction (top), with the companion measurements from table 4.3 with R_{abs} ($\sigma_{ap,Bond}$/ σ_{PAS}) values with Bond correction for all analyzed CalNex flights.

	All Flights	High OA	Medium OA	Low OA
Absorption Ratio (R_{abs}) using CTS correction	1.05 (± 0.41)	0.99 (± 0.35)	1.06 ±0.41)	1.08 (±0.46)
Absorption Ratio (R_{abs}) using Bond correction	1.02 (± 0.38)	1.04 (± 0.58)	1.07 ±0.38)	0.97 (±0.37)

Both the high OA and low OA R_{abs} values shift, from 1.04 to 0.99 and 0.97 to 1.08, respectively. These shifts are not monumental by any means, but still yield further insight into the uncertainties associated with ambient aerosol measurements. The application of the CTS correction scheme versus the Bond Correction scheme to the CalNex flights does not yield a conclusive "better option" between the two. Despite this, it does demonstrate how considering alternative methods from what is commonly applied could provide beneficial results in atmospheric aerosol measurement.

4.2: Laboratory Results and Discussion

Table 4.5: Initial results from the NOAA laboratory experiment, showing mean σ_{ep} and σ_{sp} from the CAPS and the nephelometer, the mean σ_{ap} from filter-based instruments and the mean σ_{ap} from the difference method reference for each of the four runs analyzed. All wavelengths are reported at the red (656 nm). Standard deviations and SSA are also given.

Aerosol Type	CAPS σ_{ep} Mean (Mm^{-1})	Neph σ_{sp} Mean (Mm^{-1})	Ref σ_{ap} Mean (Mm^{-1})	PSAP σ_{ap} Mean (Mm^{-1})	CLAP σ_{ap} Mean (Mm^{-1})	SSA Mean
White	508.7(±190.5)	536.6(±196.9)	-27.9	-2.01 (±1.95)	0.09 (±2.81)	1.06
Black	99.9 (±21.8)	47.7(±11.7)	52.3	54.8 (±12.8)	47.9 (±11.5)	0.48
Mixed (Grey)	463.8 (±55.5)	456.1 (±55.6)	7.7	42.3 (±9.81)	37.4 (±7.80)	0.98
White on Grey	107.78(±75.1)	112.79(±78.4)	-5.01	2.82 (±1.67)	2.55 (±1.99)	1.05

Table 4.5 shows the mean σ_{ep} and σ_{sp} from the CAPS and the nephelometer, the mean σ_{ap} from filter-based instruments and the mean σ_{ap} from the difference method reference for each of the four runs analyzed here. All values are reported at the red (656 nm) wavelength. The run's average SSA (calculated from the nephelometer scattering and CAPS extinction) is also listed for better comprehension of run characteristics. The PSAP and CLAP are Bond corrected for the laboratory dataset, with the CTS correction utilized only for the comparison in section 4.2.2. There are obvious discrepancies found between the reference σ_{ap} obtained via the difference method and the filter-based methods. Here, the white, mixed, and white on grey runs yield reference σ_{ap} values that are vastly different those observed by the PSAP and CLAP. These results will be explored further, with discussion to follow in 4.2.3.

4.2.1: Filter-based Comparison

Originally, the intentions for the CalNex campaign was to provide an analysis of how well the PSAP and CLAP measure in comparison to each other. This sort of information is vital, as the phasing out of PSAP instruments in the NOAA network is scheduled to occur over the coming years. As it is intended that the CLAP become the standard filter-based instrument for absorption measurement in the NOAA observatories and laboratories, understanding the potential differences between these two filter-based instruments is vital. As mentioned, the CalNex campaign did not enable this sort of comparison due to issues with the CLAP deployment; however, results from filter-based instrumentation measurements are given from the laboratory experiment and a NOAA measurement station in the global network. As filter-based instruments are such an essential device for global aerosol absorption measurements, the inter-comparison of performance of the same instrument class can yield better understanding of associated

measurement uncertainty. As has already been discussed, filter-based instruments, such as the CLAP and PSAP, do not measure true σ_{ap} and require empirical corrections to yield a measured σ_{ap}. In order to lessen the uncertainty associated with filter-based σ_{ap}, further observation of differences in measurement can provide opportunity for improved instrument capacity (Müller et al., 2009).

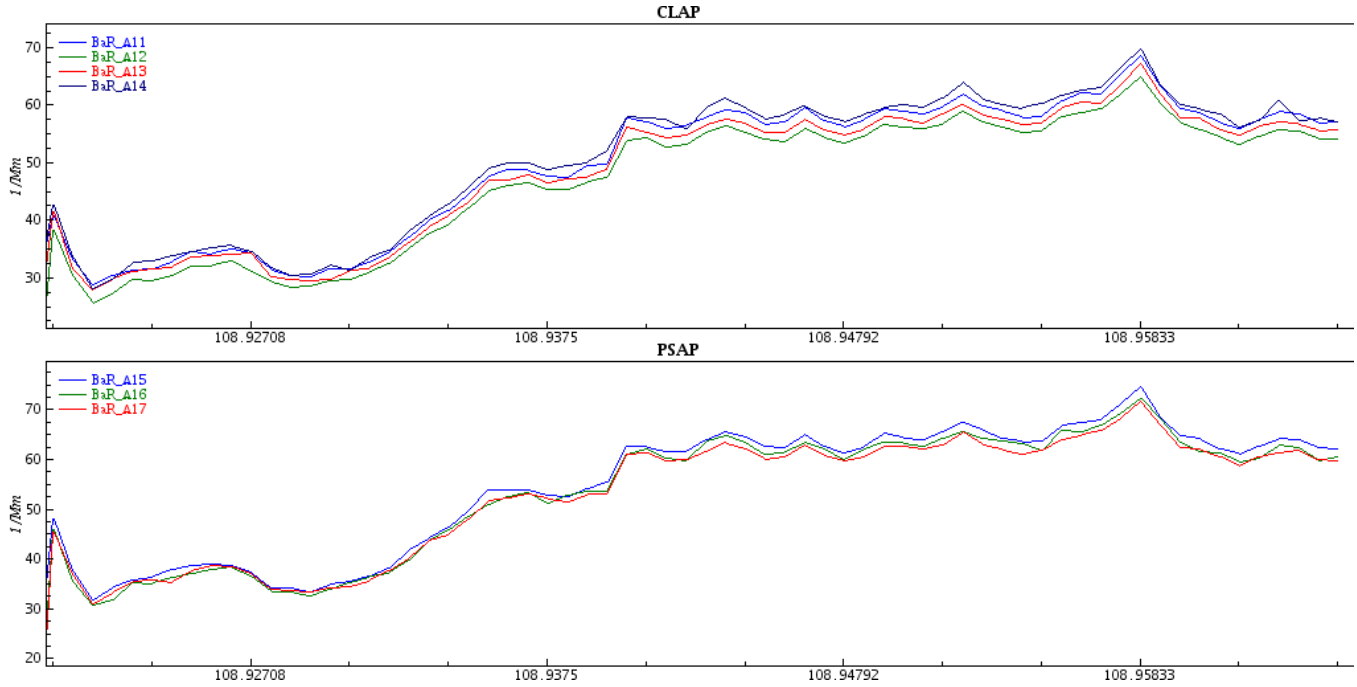

Figure 4.19: Time series of the 4 CLAP and 3 PSAP σ_{ap} measurements during the black aerosol run in the NOAA laboratory experiment. As expected, the instruments follow closely in structure and magnitude, with slight shift due to unit-to-unit variability.

A comparison of these two instruments is given in figure 4.19, where the time series of measured absorption from all of the CLAPs and PSAPs at 656 nm during a black aerosol run is shown. The structure and magnitude of the absorption data is similar for both the PSAP and CLAP measurements. The slight variation in instrument outputs can be attributed to the unit-to-unit variability associated with each instrument. It would not be expected that each instrument would yield exactly identical measurements. However, figure 4.19 shows the definite similarities in instrument output.

For the same black aerosol run, the linear regression between PSAP (#1) and CLAP (#1) is given in appendix figure A3. With a slope of 1.11, an R^2 value of 0.99, and a R_{abs} ($\sigma_{ap,CLAP}/\sigma_{ap,PSAP}$) of 0.87, it is clear that the PSAP and CLAP are closely linked in measurement of σ_{ap}.

Measurements of the grey aerosol run yielded similar results with a R_{abs} of 0.88, an R^2 of 0.99, and a slope of 1.25 (appendix figure A4). It is clear that the PSAP and the CLAP are closely correlated when absorbing aerosol are present within the sampled air.

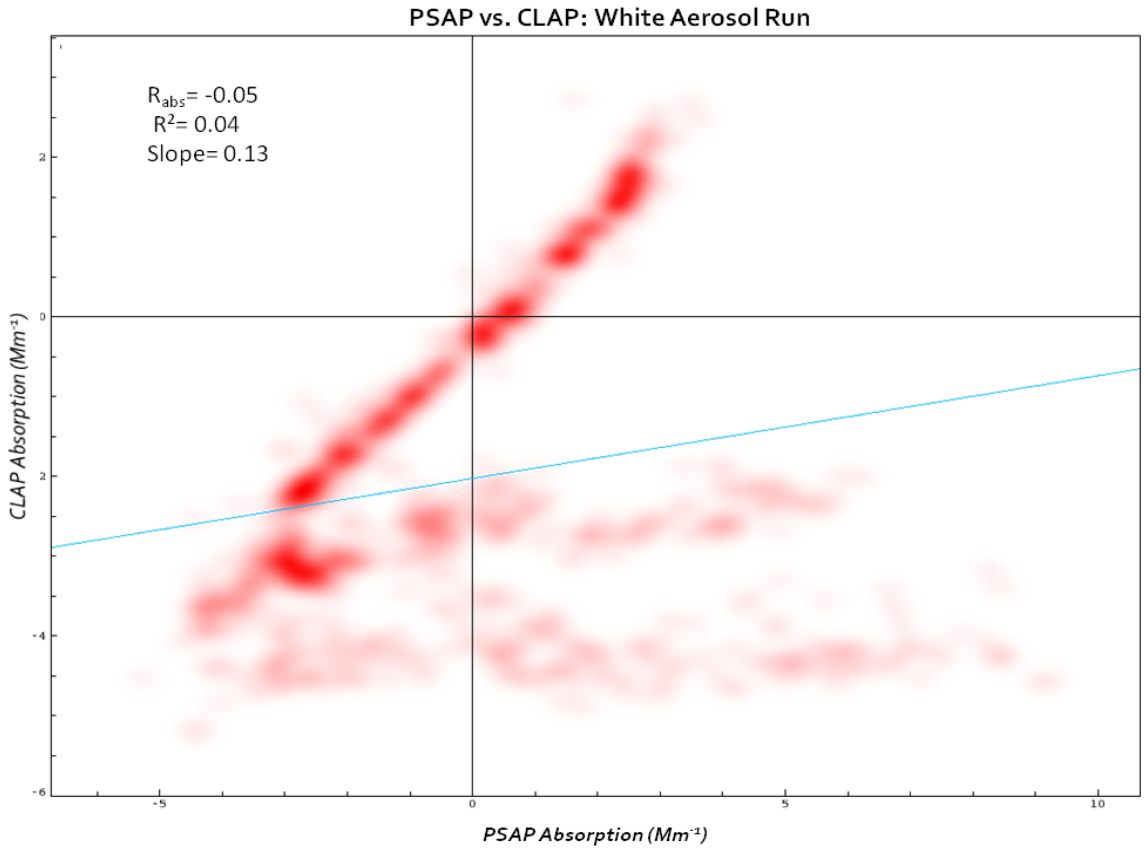

Figure 4.20: The regression between the CLAP (#1) and PSAP (#1) for the white aerosol run in the NOAA laboratory experiment. It is apparent that lower values of σ_{ap} yield difficulties in distinguishing instrument performance. Compliment figures for the grey and black aerosol run given in appendix figure A3 and A4.

In contrast to this, figure 4.20 shows the filter-based regression during a white run. With a R_{abs} of -0.05, an R^2 of 0.04, and a slope of 0.13, it is immediately apparent that the relationship between the two is less defined than it was for the black and grey runs. This is due to an issue that has already been discussed in the CalNex results, i.e. low absorption levels make the differences between the two more difficult to discern. During a white aerosol run, where scattering is essentially equal to extinction, the measured absorption levels are assumed to be the apparent absorption coefficient (Bond et al., 1999). If the aerosol is a completely scattering one, such as the ammonium sulfate utilized in white runs, any measured absorption will be due to the influence of loading scattering particles on the filter.

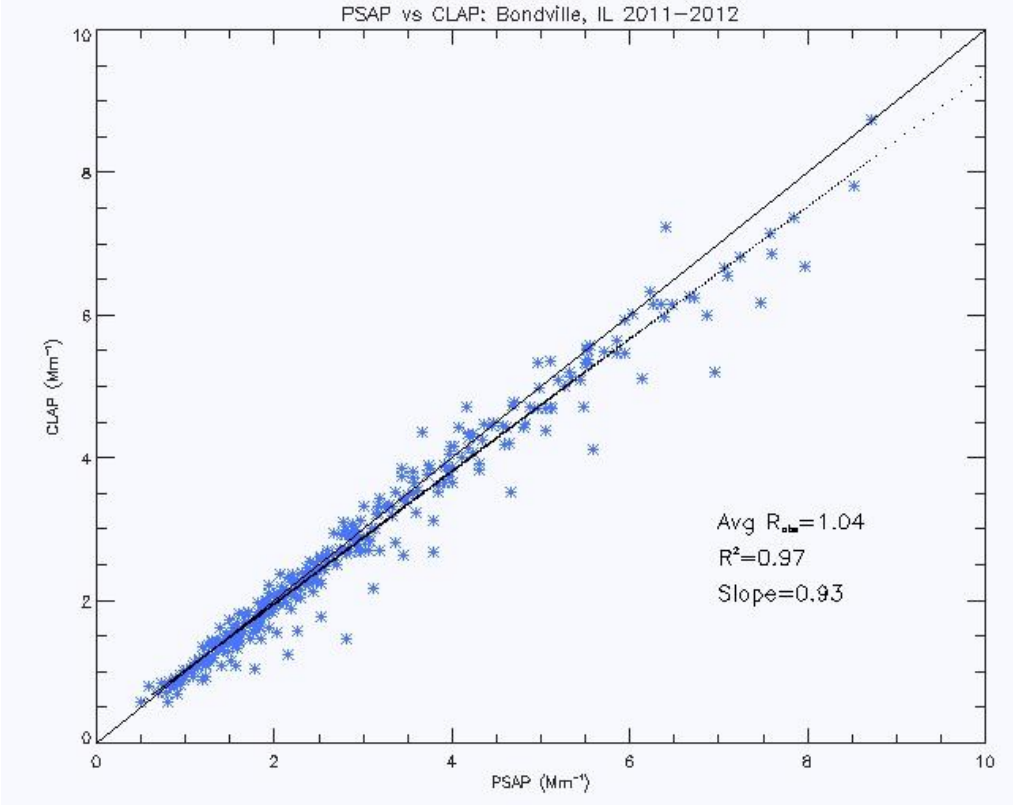

Figure 4.21: The regression between the CLAP and PSAP instruments at the Bondville, Illinois observatory. This location yields good agreement between the filter-based instruments, as there is a significant concentration of absorbing aerosol for measurement. "Cleaner" regions (such as the Summit observatory in the Greenland) do not yield as strong of correlation.

Figure 4.21 is a comparison of the PSAP and CLAP in ambient field conditions measured at the Bondville, Illinois observatory. The figure is based on the daily averages over the one year period from January 1st, 2011 to January 1st, 2012. In areas where there is significant aerosol to be measured, such as in Bondville, the PSAP and the CLAP track well. This is evident with a slope of 0.93 and a correlation of 0.97. In other locations where the air is extremely clean (such as the Summit station in Greenland), the differences between the two instruments is difficult to measure due to the low observed absorption coefficients.

For further insight into unit-to-unit variability in the CLAP and PSAP instruments, a precision analysis is considered. To achieve this, the standard deviation over the mean is plotted as a function of the σ_{ap} mean. Figure 4.22 is the precision of both the CLAP and the PSAP together for the black aerosol run after all corrections and edits are applied. The standard deviation over the mean as a function of the mean σ_{ap} during the run shows the stability in instrument outputs in

comparison to each other. The stability of instrument output near a value of 0.05 indicates good relation between the instruments utilized in this laboratory experiment.

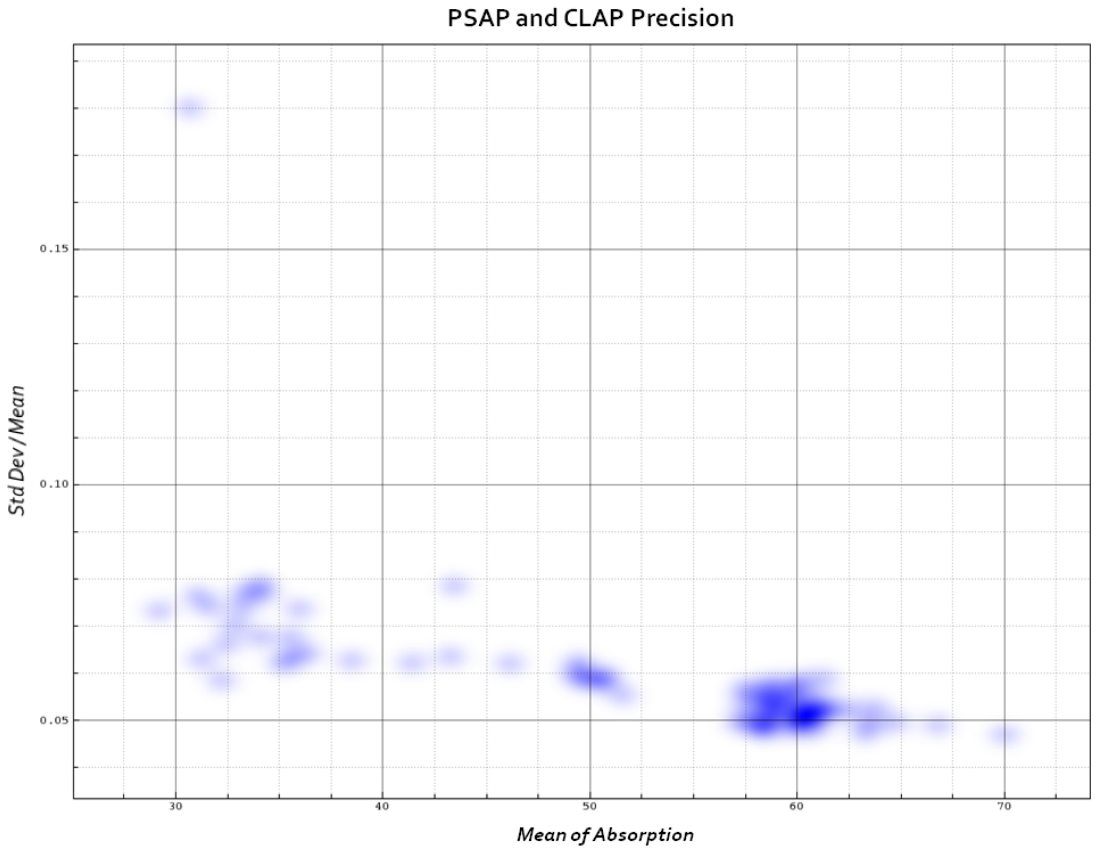

Figure 4.22: The precision analysis between the CLAP (#1) and the PSAP (#1) during the black aerosol run in the NOAA laboratory experiment. The standard deviation/ mean as a function of the mean σ_{ap} shows the stability of the instruments relative to another during the run.

This indicates that with lower σ_{ap} values, the precision between the instruments will also decrease. Had this figure shown a greater degree of variability in its spread, the precision of the instruments in contrast to each other would be questionable. Figure 4.22 is the CLAP and the PSAP together after all edits and corrections were applied. However, this analysis was also conducted for raw data without corrections in order to observe actual instrument output. The results of this analysis did not yield significantly different answers for the precision analysis, and therefore were not included.

A crucial aspect of this filter-based, laboratory inter-comparison lies in the use of the same model of PSAP and CLAP utilized in NOAA's observation network. In this regard, the statistics on instrument noise and precision gained within this study will be directly useful to those

utilizing the same manufacturer's model of instruments at long term measurement sites (Müller et al., 2011).

4.2.2: CTS Correction Comparison to Bond Correction

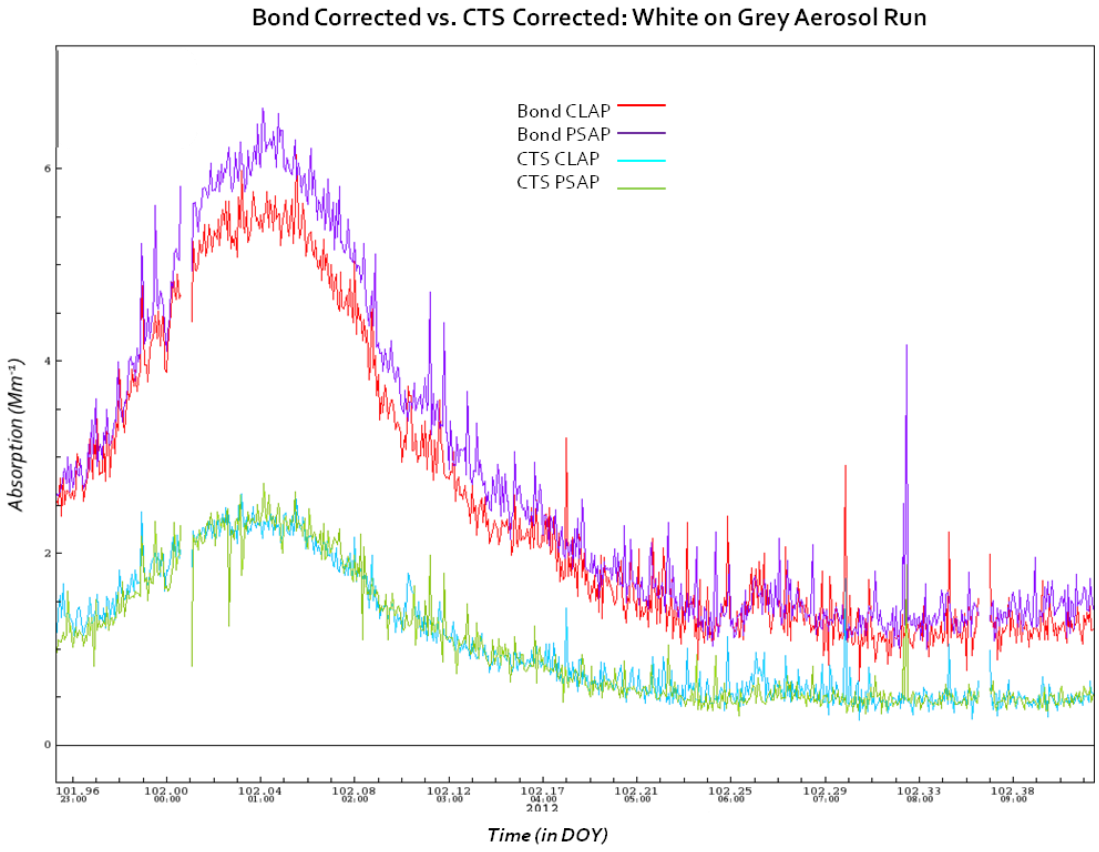

Figure 4.23: The time series of σ_{ap} for the CTS corrected and Bond corrected CLAP (#1) and PSAP (#1) during the white on grey aerosol run in the NOAA laboratory experiment. The utilization of the Bond correction during these conditions have potential overestimations of σ_{ap}, as stated by (Bond et al. (1999); Virkkula et al. (2005a); Sheridan et al (2005); Ogren (2010). This run yields an excellent example of the potential benefits of utilizing the CTS correction scheme rather than the Bond correction.

As mentioned in section 2.6.2, the Bond correction scheme has been questioned for accuracy in a number of absorption conditions (Bond et al., (1999); Virkkula et al., (2005a); Sheridan et al., (2005); Ogren (2010)). Here, a significant change in sampling condition is considered. Figure 4.23 is the time series of the CLAP and PSAP, corrected with both the Bond and the CTS correction schemes for the white on grey aerosol run. During the peak, the σ_{sp} is around 270 Mm^{-1}, leveling off at around 70 Mm^{-1} as the influence of residual absorption decreases. It is clear that the CTS corrected σ_{ap} is significantly lower than the Bond corrected, with an evident overestimation of σ_{ap} by the Bond corrected measurements. This is further explored in the regressions to follow in figure 4.24 and appendix figure A5.

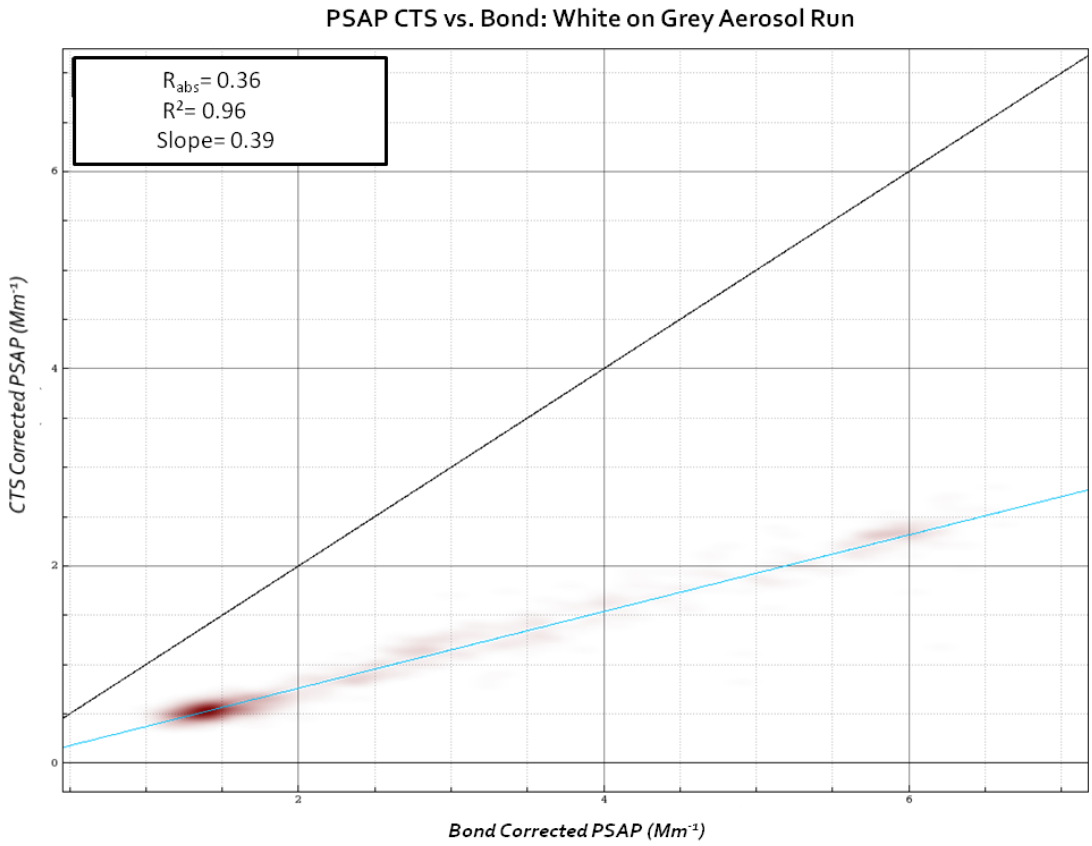

Figure 4.24: The regression between the CTS corrected PSAP (#1) and the Bond corrected PSAP (#1) for the white on grey aerosol run in the NOAA laboratory experiment. A potential overestimation by the Bond correction scheme is apparent during the changing conditions of this laboratory run. Compliment figures are given for the CLAP (#1) in appendix figure A5.

Further comparison of the discrepancy is shown in figure 4.24, where the results of the Bond corrected PSAP versus the CTS corrected PSAP are depicted for the white on grey run. As mentioned, these abruptly-changed conditions have been shown to yield uncertain absorption measurements when the Bond correction is utilized. It's clear that Bond correction absorption values are higher than those obtained when the measurements are corrected with the CTS. With a R_{abs} ($\sigma_{ap,CTS}/ \sigma_{ap,Bond}$) of 0.36 and a slope of 0.38, it is clear that there is a large potential overestimation by the Bond corrected PSAP. However, the two correction schemes remain closely correlated with an R^2 of 0.96. The CLAP results for the two correction schemes (figure A5) are comparable, with a R_{abs} of 0.41, an R^2 of 0.98, and a slope of 0.43.

In contrast to the white on grey aerosol run, the black aerosol run yields much better agreement between the two correction schemes. Figure 4.25 displays the time series of the CTS and Bond

corrected PSAP and CLAP for black aerosol run. Similar to results from the CalNex campaign, the CTS and Bond corrections are more similar than in the abruptly-changed conditions of the white on grey aerosol run.

Figure 4.26 gives the CTS and Bond corrected PSAP for the black aerosol run, yielding comparable results to the CalNex CTS regression in figure 4.17. As mentioned, the outcome of the two corrections schemes is more alike with a stable input of absorbing aerosol.

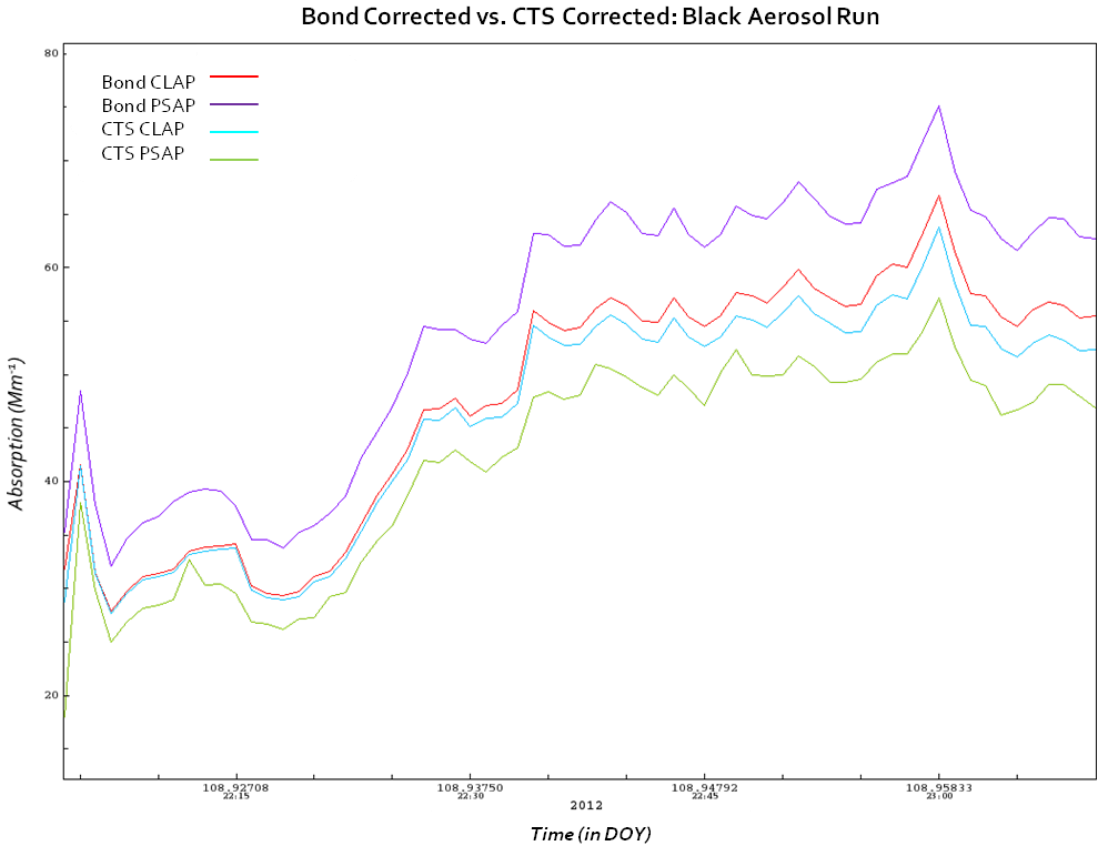

Figure 4.25: The σ_{ap} time series for the CTS corrected and Bond corrected PSAP (#1) and CLAP (#1) instruments during the black aerosol run in the NOAA laboratory experiment. A clear benefit to utilizing the CTS correction over the Bond correction is not obvious in highly absorbing conditions.

The R_{abs} of 0.77 and slope of 1.05 shows that the CTS correction yields a slightly higher σ_{ap} than the Bond corrected PSAP in this run. The correlation remains high with an R^2 of 0.98. The CLAP showed similar results (appendix figure A6) with a R_{abs} of 0.96, and R^2 of 0.99, and a slope of 0.92. Figures 4.24 and 4.26 show the variation in the CTS versus Bond corrected PSAP and CLAP for the 2 analyzed runs. It is not only clear that the measurements exhibit greater

noise in the white on grey aerosol run, but also that the difference between the two applied schemes is greater during this time.

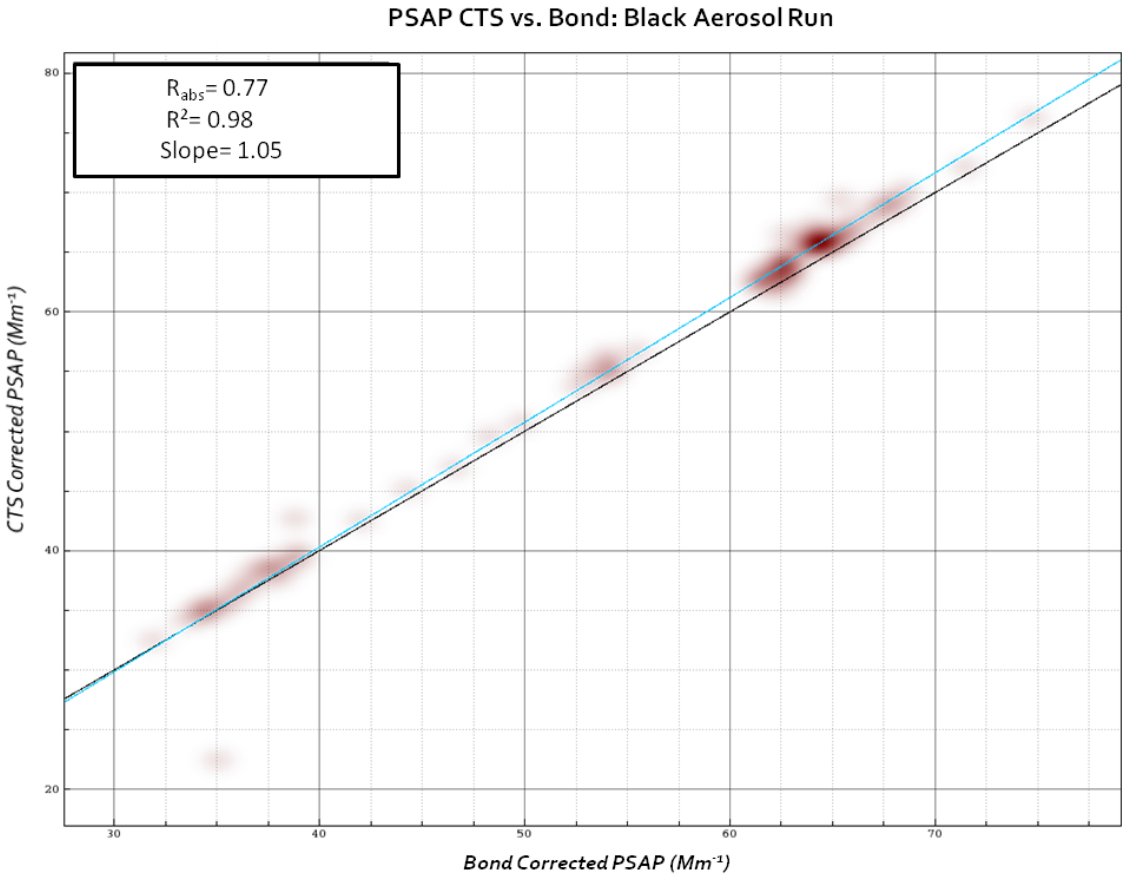

Figure 4.26: The regression between the CTS corrected PSAP (#1) and the Bond corrected PSAP (#1) for the black aerosol run in the NOAA laboratory experiment. As can be seen, the outcome of the two corrections schemes is more alike with a stable input of absorbing aerosol. The companion figure for the CLAP (#1) is given in the appendix figure A6.

This is to be expected, since the CTS correction scheme aims to provide greater accuracy in σ_{ap} values from filter-based instruments in when the properties of deposited particles significantly vary from newly sampled particles; a circumstance where the Bond correction falters (Müller et al., 2012; draft in progress). The time series shown in figure 4.23 provides an excellent illustration of why the CTS correction was developed. During the observed peak of σ_{ap}, the Bond corrected PSAP measures around 6 Mm^{-1}. Alternatively, the CTS corrected PSAP measures around 2 Mm^{-1}. This factor of 2-3 difference shows how the CTS correction scheme will systematically lower the σ_{ap} during these periods where Bond typically overestimates from the lack of consideration for what has previously been deposited on the filter. The regression of the CTS versus Bond corrected PSAP for the white on grey is given in figure 4.24, where the R^2

yields a high correlation of the two at 0.95, despite the R_{abs} of 0.36 and a slope of 0.39. Conversely, the regression generated for the black aerosol run shows that the CTS versus Bond correction schemes yield almost more similar σ_{ap} results with a R_{abs} of 077 and a slope of 1.05. The R^2 also indicates high relation of the two correction schemes at 0.98. As can be seen in figure 4.25 and figure 4.26, the use of CTS during sampling of aerosol with consistent optical properties and beginning with a clean filter is not as clearly beneficial as when used in conditions such as those depicted in figure 4.23 and 4.24.

4.2.3: Difference Method as a Reference Absorption

Müller et al. (2011) states that the measurement of aerosol absorption typically yields a greater amount of uncertainty than that of extinction or scattering. Both extinction and scattering occur in higher magnitudes than absorption, making them easier properties to measure. As σ_{ap} is typically a very small fraction of σ_{ep} (on the order of 10% in highly absorption regions (Seinfeld and Pandis, 2006)), the accurate measurement of absorption is a greater challenge. It is immediately apparent from table 4.5 that discrepancies were observed in the lab experiment with the difference method as the reference σ_{ap} measurement. Both the white and grey aerosol runs produce a reference σ_{ap} that greatly differs from the filter-based σ_{ap} values. The white aerosol run yields a reference σ_{ap} of -27.9 Mm^{-1}, where the PSAP and the CLAP σ_{ap} are -2.01 $Mm^{-1}$and 0.90 Mm^{-1}, respectively. The results for the grey run are similar; with the reference σ_{ap} at 7.7 $Mm^{-1}$and the PSAP and CLAP σ_{ap} at 42.3 Mm^{-1} and 37.4 Mm^{-1}, respectively. In both cases the σ_{sp} measured by the nephelometer was likely higher than the actual scattering and/or the σ_{ep} from the CAPS was likely lower than the actual extinction. It would be expected during a white aerosol run that σ_{sp} and σ_{ep} would be almost exactly the same, since the aerosol is a highly-scattering one. An SSA of 1.05 indicates that the absorption is completely negligible and that extinction is entirely driven by scattering. Similar to that, the SSA of 0.98 during the grey run indicates conditions dominated by scattering.

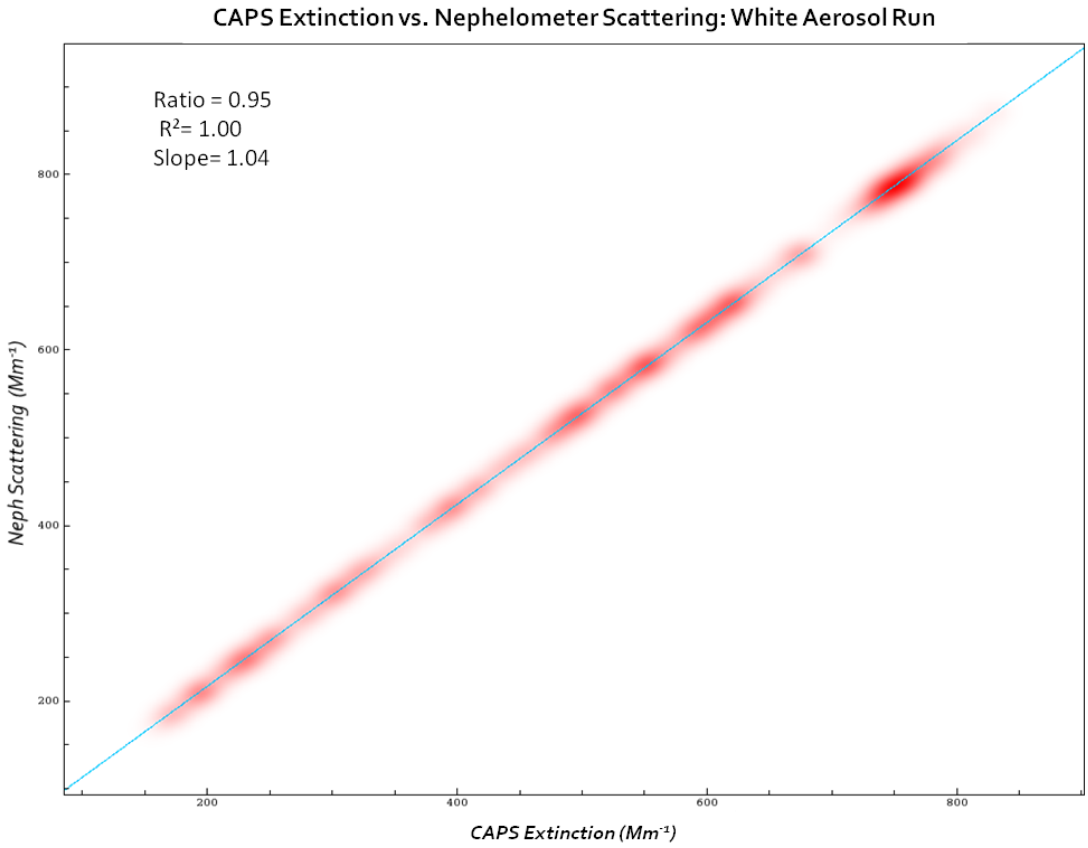

Figure 4.27: Regression between the nephelometer scattering and the CAPS extinction during the white aerosol run of the NOAA laboratory experiment. During an almost entirely scattering aerosol run, it would be expected that the ratio between scattering and extinction would be 1. The 5% discrepancy has the potential to cause inconsistencies in the reference σ_{ap}.

Figure 4.27 shows the strong relationship between the scattering of the nephelometer versus the extinction of the CAPS during a white aerosol run. When measurements are made with an aerosol that is almost entirely a scattering material, it would be expected scattering should be approximately equal to extinction, as absorption in this scenario is negligible. This is apparent with an R^2 value of 1.0 and a slope of 1.04. However, during a white aerosol run, the ratio between extinction and scattering would be expected to be 1. This indicates the nephelometer scattering measurement is 5% higher than the CAPS extinction.

What can be seen in figure 4.28 is that the scattering is measuring just above the extinction; a physical impossibility that would lead to a negative absorption coefficient. On a white aerosol run, these two instruments should report nearly identical values for scattering and extinction, as extinction will be almost entirely consisting of scattering. The discrepancy observed between the two in the white aerosol run is around 5%.

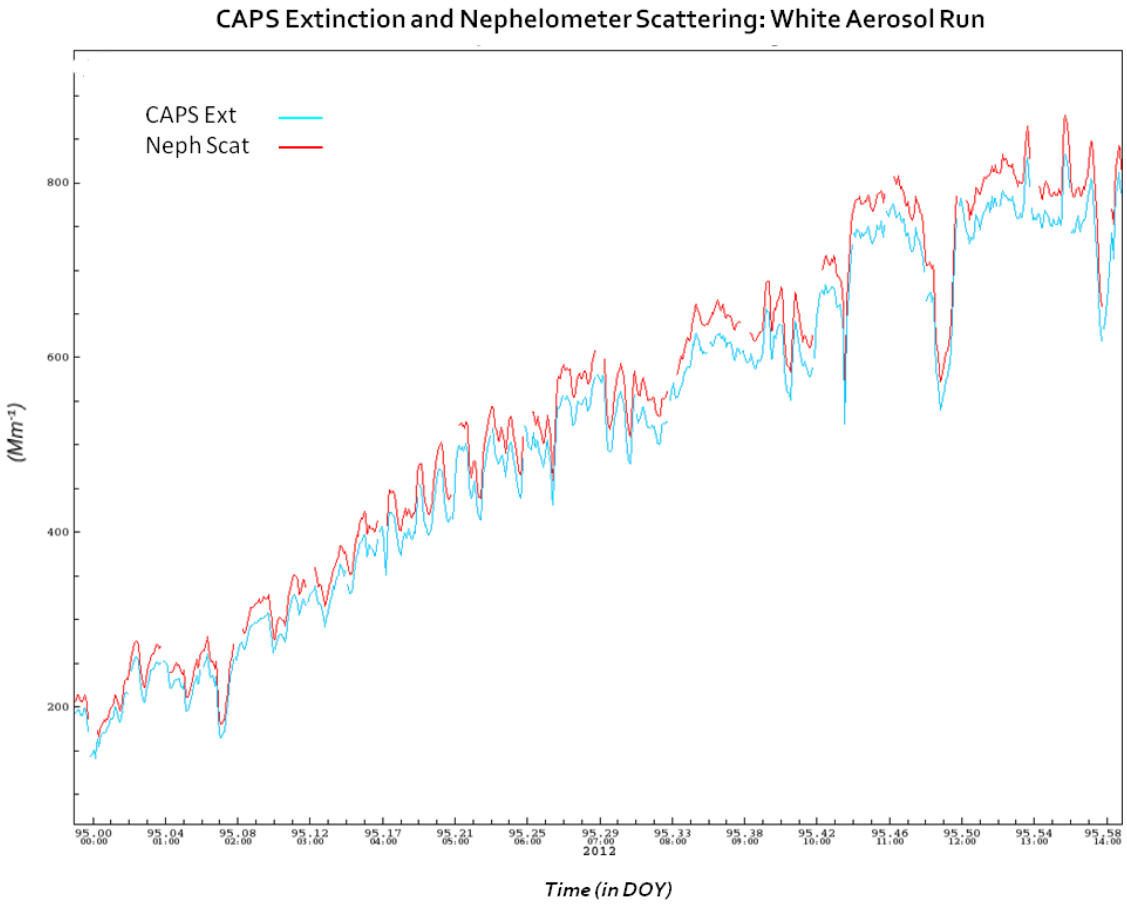

Figure 4.28: Time series of scattering by the nephelometer and extinction by the CAPS for the white aerosol run. The scattering is measured above extinction should be a physical impossibility, as it will yield a negative absorption value.

This around 5% uncertainty between the CAPS and the Nephelometer can yield large inconsistencies in the reference absorption measurement when compared to the filter-based instruments. Further analysis from the grey run, where the extinction was typically greater than scattering, yielded results that suggested that using the difference method as a reference absorption was unwarranted (appendix figures A7 and A8). The difference between these very close measurements, along with fluctuations of which instrument was higher in measurement, leads to a noisy output that does not appear to track the measurements of the filter-based instruments at all. The reference σ_{ap} for this run appears choppy and inconsistent with measurements of the filter-based instruments. What these results clearly indicate is that true insight into utilizing the CAPS/nephelometer difference as a reference method until the σ_{ep} and σ_{sp} discrepancy is resolved.

There are a number of possible reasons for such a difference between the reference σ_{ap} and the filter-based σ_{ap}. One reason could be related to the calibrations of the instruments utilized to obtain the difference method $\sigma_{ap,}$ which has the potential to yield large errors in measurement (Müller et al., 2009; Massoli et al., 2009b). The nephelometer periodically requires a full calibration process and frequent span checks, to evaluate whether the instrument calibration is shifting. Additionally nephelometer background measurements are established through the frequent measurement of scattering by filtered air. However, the nephelometer yielded an excellent span check prior to the start of the study, and an almost excellent span check in the middle of the study and the last full calibration was within the reasonable timeframe of 6 months and span check within 1 month. Moreover, the filtered-air background readings during the experimental runs had not fluctuated substantially and the changes were considered negligible. With that, the CAPS calibration was verified with the sampling of scattering CO_2 gas and subsequent analysis of measurements.

Another possibility relates to the adjustment of measurements to STP conditions and instrument uncertainties in their temperature (T) and pressure (ρ) measurements. The nephelometer and CAPS temperature were compared and the ~5° C difference observed between the CAPS and the nephelometer (nephelometer T was higher) was expected due to heat generation by the nephelometer light source. The pressure values reported by the nephelometer and CAPS were virtually identical. It was found that, collectively, the differences in temperature and pressure would have yielded less than 1% of the discrepancy. It is also possible that the wavelength adjustment applied to the nephelometer scattering measurements to match the CAPS wavelength of 656 nm introduced some error. Interpolating the nephelometer from 550 nm and 700 nm to 656 nm could possibly have been a contributor to discrepancy. However, subsequent calculations based on the aerosol size distribution and scattering obtained via the Mie theory (Bohren and Huffman, 1983) verified the legitimacy of the utilized mathematics.

An additional sampling error could have stemmed from losses of aerosol in the sampling lines. The aerosol sampling lines originated within a hood-ventilated workbench on one side of the room, travelled across the ceiling, and extended downward to the mixing chamber. The largest potentials for particle losses would have occurred at the junction points, where the tubing turned. The amount and sharpness of sampling line bends within were minimized as much as possible;

however, potential losses via diffusion of smaller particles to tubing, sedimentation and deposition of larger particles, and impaction of particles against sampling line turns are essentially unavoidable (Hinds, 1999). Depending on the flow rate, particle size, material of the tubing, sample line length, etc., the amount of particle loss can be calculated through the utilization of the penetration equation given in Hinds, 1999. The relevant losses to the CAPS and the nephelometer would have occurred from the mixing chamber to the instrument inlets and are considered negligible in practice, due to their close proximity and short travel distance.

However, the issue of greatest concern for this experimentation appeared to lie within the truncation correction. As described in section 2.4.3, there are a number of truncation corrections to consider when deciding how to correct for this known instrument limitation. Originally for this experiment, the Anderson and Ogren (1998) correction for "no cut" in the aerosol size distribution was applied to the dataset. This correction increases the scattering by particles due to their larger sizes. From this, a 10% discrepancy in σ_{ep} and σ_{sp} was observed in the white aerosol run. As this is an accumulation mode (diameter 0.1-1 μm) dataset, the decision was made to re-run the analysis applying the "submicron" correction factor. The result was a 5% decrease in the observed discrepancy.

Despite this reduction in the observed inconsistencies, this raises an interesting factor for consideration: what is the appropriate truncation correction? The Anderson and Ogren (1998) correction for the TSI nephelometer has associated uncertainties, cited as up to a 30% uncertainty for larger, highly absorbing particles (Massoli et al., 2009b). Bond et al. (2009) also states that the regularly-applied truncation correction to the TSI nephelometer correction (i.e., Anderson and Ogren (1998) may have a bias towards estimated scattering by 1-5% if the absorbing aerosol is either very strongly absorbing or weakly absorbing "brown carbon." The study states that Anderson and Ogren (1998) correction should retain its accuracy for a wide scale of atmospheric aerosols. However, uncertainty becomes greater (up to 5%) if they are aerosol measured at or nearby a significant source of absorbing aerosol; for example, near traffic regions (or in laboratory experiments with highly absorbing aerosol). Due to the strong size dependence of the correction, Bond et al. (2009) recommends utilizing the Mie theory calculations for specific size distributions to estimate C_{ts}. In this regard, further discrimination in the selection of which correction factors are being applied could be necessary (i.e. other factors

in Anderson and Ogren, 1998; Moosmüller and Arnott, 2003; Massoli et al., 2009b; Bond et al., 2009). However, this investigation was beyond the scope of the experimental design, requiring extensive analysis and unfamiliar mathematical applications. As this presented potential for entirely new scientific questions from the original experimental aim, it was decided that the further exploration of variance in truncation corrections should become priority in future experimentation.

After the consideration of a large list of potential reasoning and methodology for reducing the discrepancy, it was decided by the NOAA aerosols group to develop a correction factor for the extinction measurements to reduce the discrepancy demonstrated during the white aerosol run. This is not an uncommon practice and has been duplicated in other experimental research (Bond et al., 1999). In the Bond et al. (1999) experimentation, where the correction for filter-based measurements was developed, a similar σ_{ep} correction of 1.05 was applied. For this study and the NOAA laboratory study, the justification for the application of the σ_{ep} adjustment requires assumptions. First, the accuracy of the reference σ_{ap} is then tied to the accuracy of the nephelometer. Second, the laboratory-generated white aerosol is assumed to be completely scattering.

The regression developed in figure 4.27 was created for the entirety white aerosol runs within the experiment and then was forced through the origin. The slope of the linear model forced through the origin was then recalculated, yielding a correction coefficient of 1.046 to be applied to the σ_{ep}. After the utilization of this correction, the regression was redeveloped to include the correction factor, yielding a slope of 0.99, an R^2 of 0.99, and ratio of 0.99. From this, the analysis of laboratory data was recreated with the correction factor of 1.046 applied to the σ_{ep} for the entire dataset.

Table 4.6 gives the corrected σ_{ep} and corrected reference σ_{ap} for the utilized laboratory runs. It can be seen that the inconsistency is greatly reduced for the white run, which is the aim of the correction factor. If the σ_{ep} and σ_{sp} do not align during a white aerosol run, the potential for utilizing the difference method for a reference σ_{ap} is questionable (appendix figures A7 and A8). The shift in other run values comes in conjunction with the adjustment of the white run discrepancy, where σ_{ep} and σ_{sp} are meant to be at unity with each other.

Table 4.6: The results and standard deviations for the corrected σ_{ep} and corrected reference σ_{ap} for the utilized laboratory runs. The inconsistency between the σ_{ep} and σ_{sp} is greatly reduced for the white run with the correction, yielding a more relatable reference σ_{ap}.

Aerosol Type	CAPS σ_{ep} Mean (Mm^{-1})	Corrected σ_{ep} Mean (Mm^{-1})	Neph σ_{sp} Mean (Mm^{-1})	Ref σ_{ap} Mean (Mm^{-1})	Corrected Ref σ_{ap} Mean (Mm^{-1})	PSAP σ_{ap} Mean (Mm^{-1})	CLAP σ_{ap} Mean (Mm^{-1})
White	508.7(±190.5)	**532.2(±199.3)**	536.6(±196.9)	-27.9	**-4.47**	-2.01 (±1.95)	0.09 (±2.81)
Black	99.9 (±21.8)	**105.6(±22.8)**	47.7(±11.7)	52.3	**56.9**	54.8 (±12.8)	47.9 (±11.5)
Mixed (Grey)	463.8 (±55.5)	**485.6(±58.1)**	456.1 (±55.6)	7.7	**29.1**	42.3 (±9.81)	37.4 (±7.80)
White on Grey	107.78(±75.1)	**112.7(±77.5)**	112.79(±78.4)	-5.01	**-0.05**	2.82 (±1.67)	2.55 (±1.99)

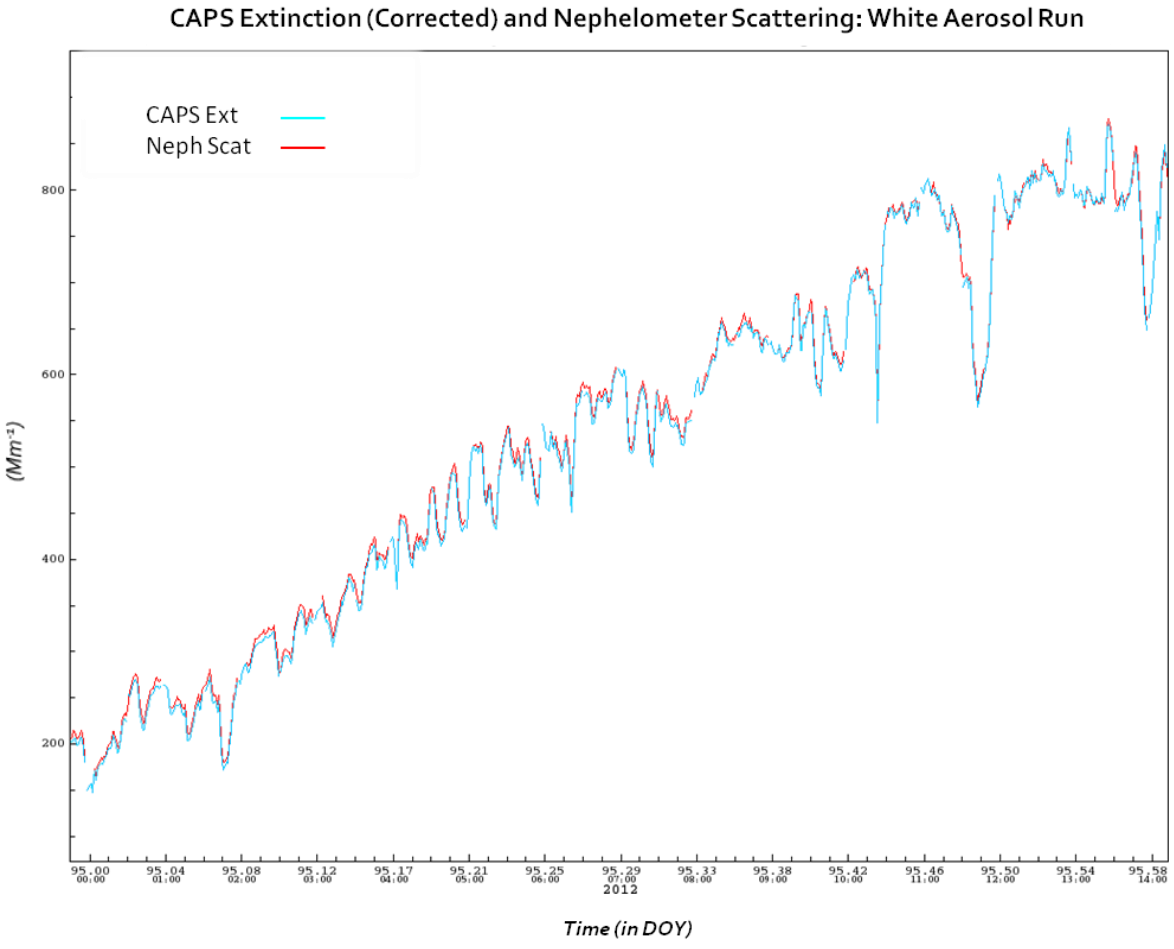

Figure 4.29: The time series for the scattering from the nephelometer and the extinction from the CAPS for the white aerosol run after the correction factor has been applied. With the discrepancy resolved, a more relatable reference σ_{ap} is provided for the NOAA laboratory experiment.

Figure 4.29 shows the corrected σ_{ep} and the σ_{sp} for the white aerosol run, as previously depicted in figure 4.28. After the correction factor is applied, the corresponding values of the CAPS extinction and the nephelometer scattering are more consistent with each other, which is what would be expected. From this, a reasonable reference σ_{ap} can be utilized for the laboratory experimentation and further analysis with the difference method as a reference σ_{ap} becomes justified.

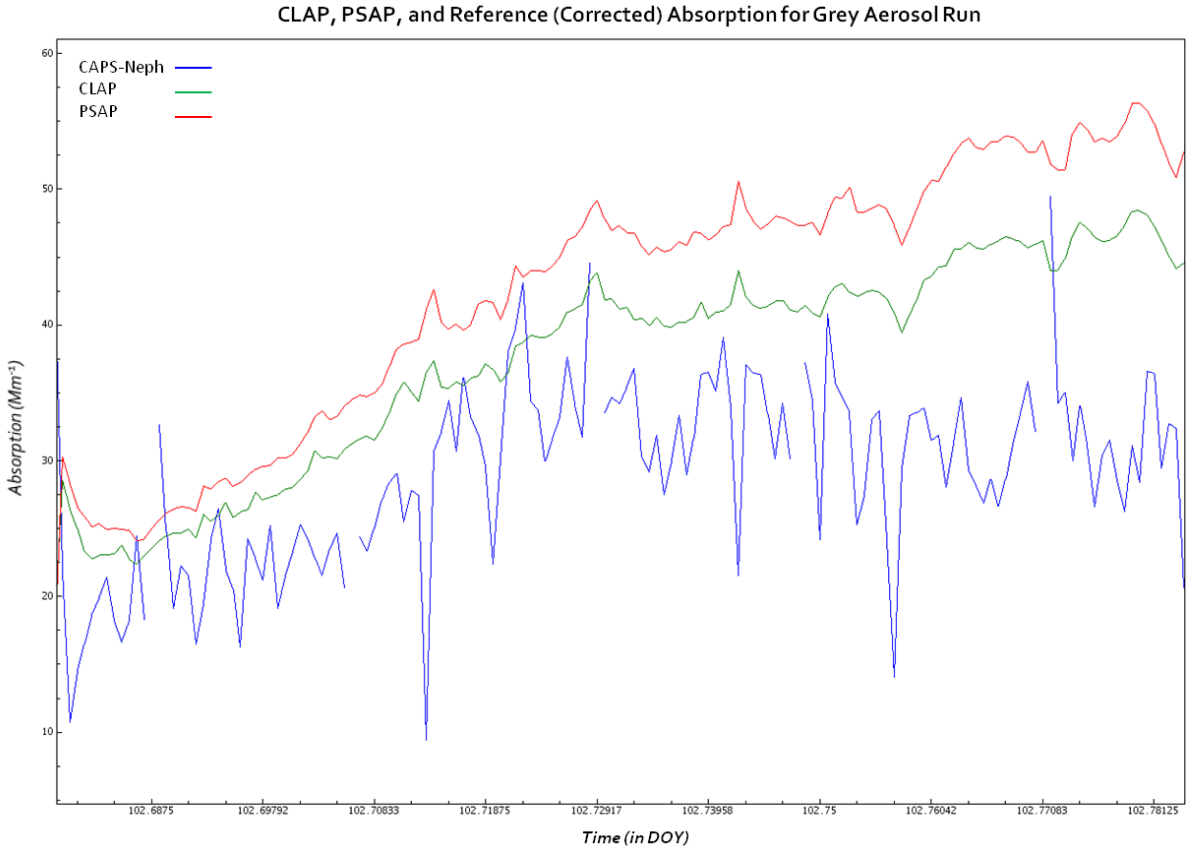

Figure 4.30: Time series of the CLAP (#1), PSAP (#1), and reference σ_{ap} for the grey aerosol run, where the σ_{ep} measured by the CAPS has been adjusted with the correction factor. The alignment of the filter-based σ_{ap} and the reference σ_{ap} remains imperfect; however, improved from time series shown in figure appendix figure A7.

Figure 4.30 shows the time series of the PSAP, CLAP, and reference σ_{ap} during the grey aerosol run, after the σ_{ep} measured by the CAPS has been corrected. It can be seen that the alignment between the filter-based σ_{ap} and the reference σ_{ap} is not perfect, but this is to be expected. This is also a low-absorbing aerosol run, with an SSA of 0.98 and a scattering mean of 456.1 Mm^{-1}. In this regard, the precision of the filter-based methods may be decreased, as discussed earlier. However, the reference σ_{ap} does appear to be noisier than the filter-based $\sigma_{ap,}$ which is potentially

a result of being the subtraction of two larger numbers (σ_{ap} and σ_{sp}) to yield a smaller number (σ_{ap}).

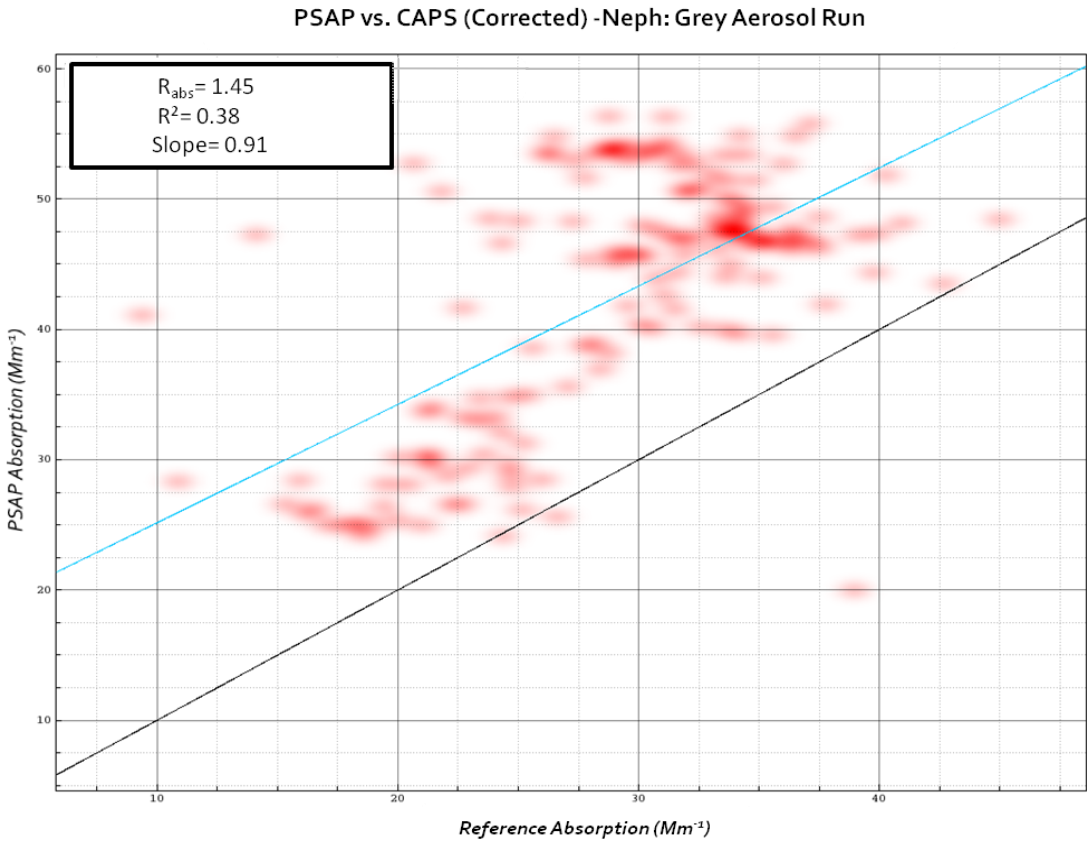

Figure 4.31: The regression between the PSAP (#1) and the reference σ_{ap} for the grey aerosol run, where the σ_{ep} measured by the CAPS has been adjusted using the correction factor.

Figure 4.31 shows the regression between the PSAP σ_{ap} and the reference σ_{ap}, where the σ_{sp} has been subtracted from the corrected σ_{ep}. The R_{abs} between the PSAP σ_{ap} and the reference σ_{ap} is 1.45, demonstrating that the filter-based measurement is consistently higher than the reference σ_{ap} for this run. However, the correlation between the two may not be so strong, with an R^2 value of 0.38. The best fit line is above the 1:1 line, with a slope of 0.91. The CLAP σ_{ap} versus the reference σ_{ap} yields similar results (appendix figure A9), with a R_{abs} of 1.28, an R^2 value of 0.40, and a slope above the 1:1 line of 0.72.

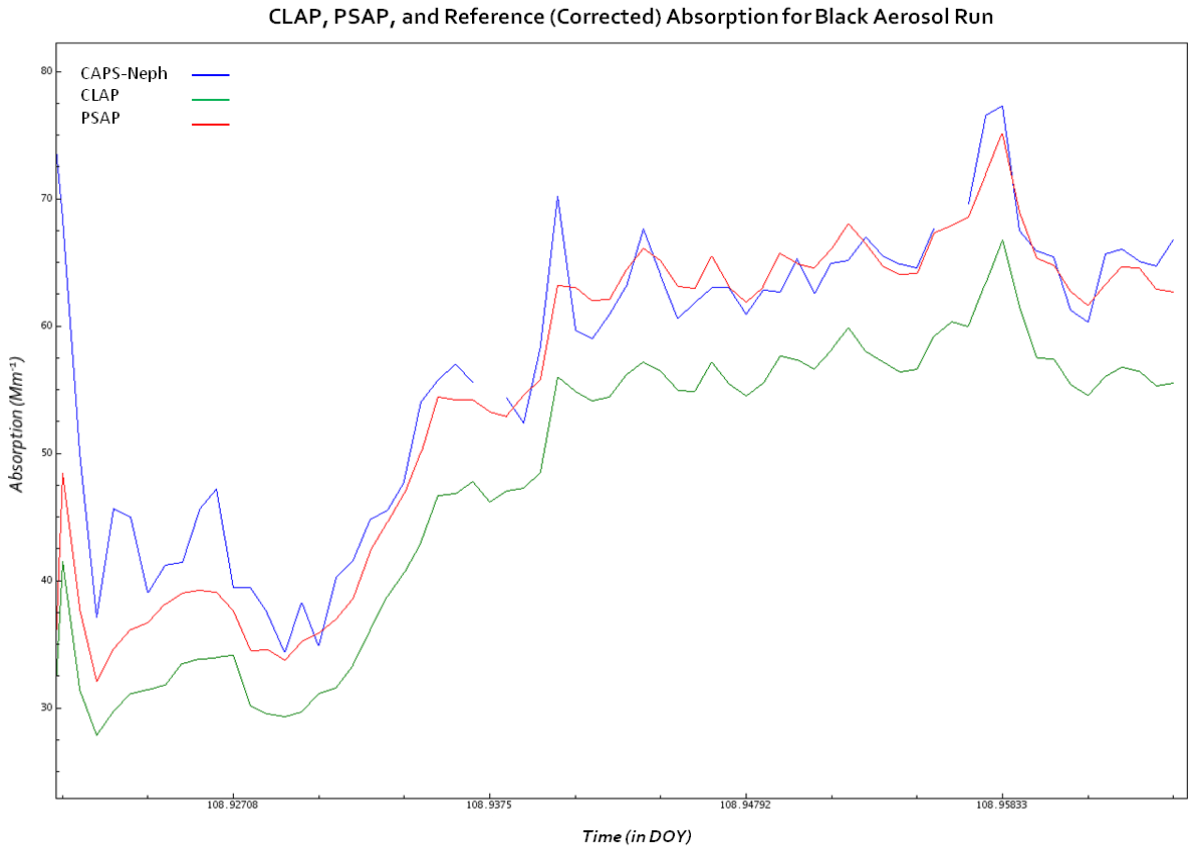

Figure 4.32: Time series of the CLAP (#1), PSAP (#1), and reference σ_{ap} for the black aerosol run, where the σ_{ep} measured by the CAPS has been adjusted with the correction factor.

Figure 4.32 shows the time series of the PSAP, CLAP, and reference σ_{ap} for the black aerosol run, which shows a more comparable reference σ_{ap} to that of the filter-based measurements. Again, a non-perfect comparison is found between the reference σ_{ap} and the filter-based $\sigma_{ap,}$ which is to be expected. However, in the higher absorption levels, the reference σ_{ap} is more relatable to the filter-based σ_{ap} than in the previous run. During the black run, the SSA was 0.48, with a mean σ_{sp} of 47.7 Mm^{-1}. This provides a greater difference in value between σ_{ep} and $\sigma_{sp,}$ and therefore, a less noisy reference $\sigma_{ap.}$

Figure 4.33 gives the regression between the PSAP σ_{ap} and the reference σ_{ap} with the corrected σ_{ep} for the black aerosol run. A more strongly associated relationship is depicted with a R_{abs} of 0.96, an R^2 of 0.78, and a slope of 1.0. The CLAP σ_{ap} also yields similar results (appendix figure A10) with a R_{abs} of 0.86, an R^2 of 0.80, and a slope of 0.94.

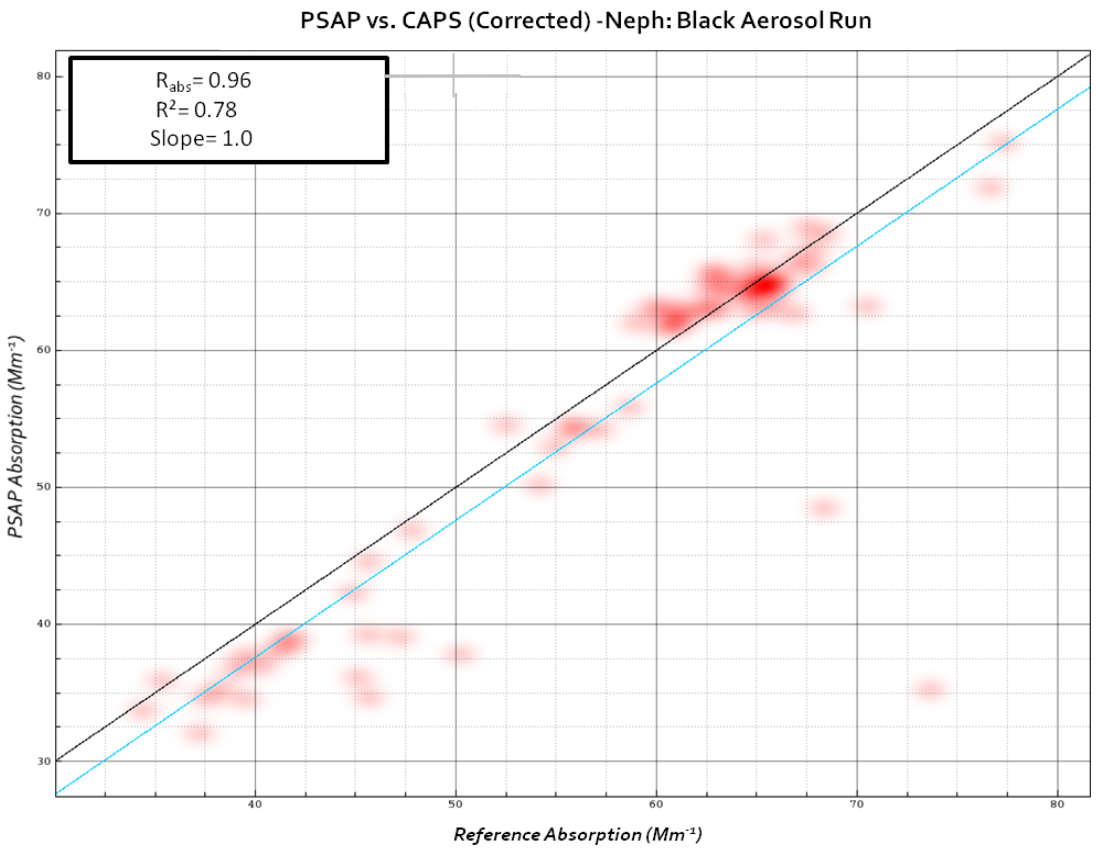

Figure 4.33: The regression between the PSAP (#1) and the reference σ_{ap} for the black aerosol run, where the σ_{ep} measured by the CAPS has been adjusted using the correction factor.

It should be noted that these sort of instrumental discrepancies when utilizing the difference method for the reference σ_{ap} is not necessarily uncommon. For example, ambient measurements that were obtained from the Storm Peak Laboratory (SPL; http://stompeak.dri.edu) in Steamboat Springs, Colorado in conjunction with the Storm Peak Laboratory Property Validation Experiment (STORMVEx) encountered similar inconsistencies in difference method measurements (Andrews et al., 2012; draft in progress). In this closure experiment aimed to obtain better estimation of the σ_{ep} through the PSAP + the nephelometer, the CAPS and the nephelometer were also found to measure within 5% of each other. In this case, the nephelometer was measuring just below the CAPS. However, it was found that the σ_{ap} obtained from CAPS – nephelometer was much nosier than the σ_{ap} measured by the PSAP. Regressions of the PSAP versus the CAPS – nephelometer suggested that the utilization of the difference method for a reference σ_{ap} was not ideal. This was due to the noise level observed in the reference σ_{ap}

compared to the PSAP σ_{ap}, which is similar to the results shown for the grey run in figures 4.30 and 4.31.

The utilization of the difference method for a reference σ_{ap} is widely-used and most often with high correlation to filter-based measurements. In the Reno Aerosol Optics Study (RAOS), Sheridan et al. (2005) utilized both the photoacoustic method and the difference method as a means of σ_{ap} reference. In this study, careful consideration went into determining what to use as the reference σ_{ap}, as it is pointed out that there is no clear definition in atmospheric studies on which methodology yields more robust results. For σ_{ep} measurements, the CRD and an Optical Extinction Cell (OEC; Virkkula et al., 2005a) were utilized in conjunction with the nephelometer. During their white aerosol run, the OEC σ_{ep} and the nephelometer σ_{sp} were shown to agree within 2% of each other within the red wavelength (660 nm). Both the photoacoustic spectrometer and the difference method σ_{ap} not only agreed very well with each other (within 3-7% over all three wavelengths), but agreed within 3% of the PSAP σ_{ap} for the atmospherically-relevant absorption levels. However, it was considered that the monitored conditions (i.e. consistently low RH, stable aerosol mixture, etc.) of a laboratory setting may have influenced the more-ideal agreement.

These cases, as well as the CalNex campaign and NOAA laboratory results, introduce the fundamental concern in the current measurement of atmospheric aerosols: there is no ideally-defined reference σ_{ap} methodology. These disagreements in σ_{ap} measurements arise from the wide array of elements to consider in atmospheric aerosol measurements.

5. Conclusions, Implications, and Future Work

5.1: Conclusions, Implications, and Future Work

The aim of this investigation was to investigate the a few scientific methods for obtaining the σ_{ap} of atmospheric aerosols and the associated uncertainties therein. The CalNex field campaign and the NOAA laboratory experiment provided unique opportunities for the comparison of instruments measuring the absorption by aerosols. Both established and novel techniques for the measurement of aerosol absorption were considered, as the coupling of these techniques is essential through inter-comparisons of simultaneous measurement.

Differences and similarities between the filter-based measurements and the in-situ measurements were observed both in the CalNex campaign and the NOAA laboratory experiment. Insight toward questions A and B were provided through comparisons of both techniques in a variety of sampling conditions. The most significant differences between the filter-based instruments, the in-situ techniques of the photoacoustic spectrometer, and the difference method appeared to occur during periods of lower σ_{ap} measurement. The biggest discrepancies in σ_{ap} measurement between the PSAP and PAS in the CalNex campaign occurred during flights where lower σ_{ap} was measured, such as when flown during the nighttime hours or over rural areas (DOY 151 or DOY 169). During these flights, low absorption resulted in greater uncertainty in signal-to-noise levels. This was also observed in the NOAA laboratory experiment when the generated aerosol yielded higher SSA levels and extinction was almost completely dominated by scattering (i.e. the white, grey, and white on grey runs). For instance, the regression between the PSAP and the reference σ_{ap} for the grey aerosol run yields a low correlation and higher R_{abs} value between the measurement techniques. This ambiguity in lower absorption measurements is an important issue for global aerosol absorption measurements. Even low levels of absorption in ambient air can have significant effects on localized meteorology and cloud dynamics (Ramanathan et al., 2001 and sources therein). Increasing instrument detection limits in lower absorption levels is an important potential for future work.

In contrast, the greatest agreement of σ_{ap} measurement occurs when higher levels of absorption occur. The time series from the DOY 167 flight in figure 4.2 is an excellent demonstration of the agreement in measurement by the PSAP and PAS during period of significant $\sigma_{ap.}$ Good relation between the PSAP, CLAP, and reference σ_{ap} is also observed during the black aerosol run of the NOAA laboratory experiment, where the time series (figure 4.32) shows imperfect, but relatable magnitude of $\sigma_{ap.}$ This also remains true for the filter-based comparison between the PSAP and CLAP. When there are absorbing aerosols present within the sampled air, the PSAP and the CLAP measure very similar amount of absorption and are highly correlated. This is to be expected, as they are essentially variations of the same instrument. The regression between the two types of instruments is comparable for the grey aerosol run, the black aerosol run as well as for long-term (1-year) measurements at the Bondville observatory. Filter-based comparisons demonstrate the similarities in absorption measurements by the CLAP and the PSAP. These sorts of studies are essential in better understanding of unit-to-unit variability, due to their inclusion within an international monitoring network, where reliability and correspondence in measurements is vital. Maintenance of common method of calibration, data collection, and data analysis is crucial for observations that will be utilized in global monitoring and climate predictions.

The most significant discrepancy between techniques occurred with the reference σ_{ap} obtained by the difference method in the NOAA laboratory experiment. The inconsistencies observed between the σ_{ep} and σ_{sp} in the white aerosol run, where these are expected to be nearly the same, provided an interesting illustration of how these uncertainties can proliferate in further analysis if not properly addressed. The long list of potential reasoning for the discrepancy yields insight on the large array of influences that may affect accuracy in measurement.

In the CalNex investigation, the PSAP and the PAS did not appear to have significant sensitivity to RH or pressure changes; however, results shown in figures 4.4 and 4.5 hint at the necessity for deeper analysis. The potential for further investigation of instrument accuracy during changes in ρ and RH could be conducted through the distinguishing of segments of level flight and analysis therein. It could be argued that the consideration of profile ascents and descents may have effect on instrument performance and therefore, would present implications on measurement validity. Instrument uncertainties may increase with instability of conditions (i.e. continued changes in ρ).

Occurrences where pressure is changed substantially within a defined timeframe could have an effect on measurement uncertainty.

Investigation for question C was focused on the CalNex data, where concentration of organic aerosol was measured. The bias attributed to high OA levels observed in the Lack et al. (2008) Texas campaign did not result in a similar bias in the CalNex flights. The heavily polluted regions investigated within the TexAQS/GoMACCS were based within the Houston shipping channel, which would create potential differences in sources, types, and levels of observed organic. It can be concluded that there is some difference in the type of organics observed within the Houston area versus the Los Angeles area. However, it is still interesting to note that while the bias was not obvious when all eight CalNex flights were considered, a bias was observed for a single daytime CalNex flight. Had the separation between OOA and HOA been available for this investigation, further inferences could have been made on whether the potential organics bias is related to the age and oxidation-level of the sampled aerosol. This could have implications in further research which aims to make observations with filter-based instruments in high OA regions. This may also provide further insight for assessment of station/observatory data that may question absorption data obtained from filter-based measurements during periods of high OA loading, such as Mexico City or Manchester U.K. during the summer (figure 5.1).

As is shown in figure 5.1 from Zhang et al. (2007), the atmospheric aerosol varies significantly globally. The sources, compositions, and amount of organic aerosols are not constant on a global basis. Thus, there is reason to further investigate this bias of filter-based instruments as a function of location, and therefore, different sources of aerosols types or compositions. It is completely plausible to consider that the potential PSAP bias to organics could be a regional occurrence, dependent on the type, source, and composition of local aerosol. Unfortunately, distinguishing between OOA and HOA is beyond the scope of this paper and inferences of influences by each cannot be made. However, this is a concept that should be explored in conjunction with the potential PSAP bias to organics.

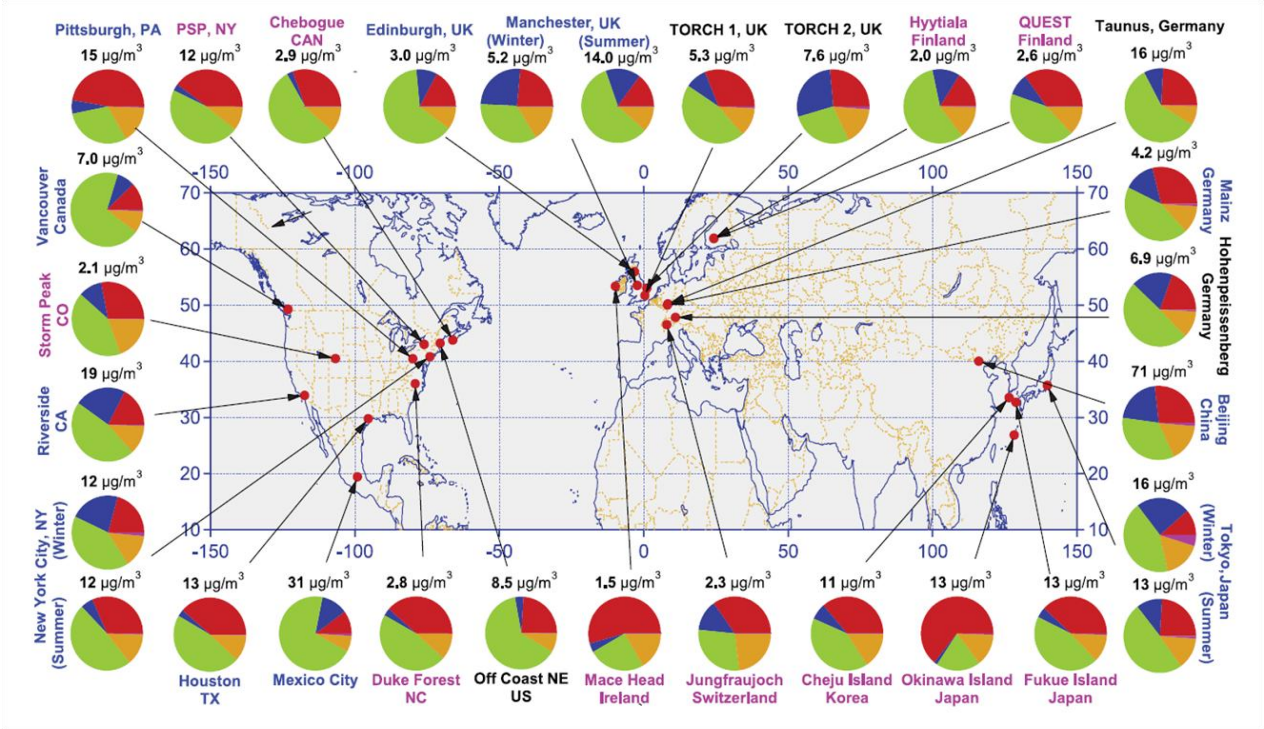

Figure 5.1: Variance in atmospheric aerosol composition based on global measurements by Zhang et al. (2007). With the wide array of measured OA (green in circles) on a global scale, further investigation of a potential filter-based bias is necessary on a regional basis. Sulfates (red), nitrate (blue), ammonium (orange) and chloride (purple) also given in pie charts. Figure reproduced by permission of the American Geophysical Union.

Finally, the utilization of the CTS correction scheme in the CalNex field campaign and the NOAA laboratory experiment provides insight for when the mathematically-intensive CTS correction is beneficial for filter-based instruments (question D). However, it's possible that question D would be better-asked as "during what sampling conditions can an advanced correction scheme reduce the differences between various methods of σ_{ap} measurements?" During periods of consistent aerosol σ_{ap} measurements, such as those observed in CalNex flights or the black aerosol run of the NOAA laboratory experiment, the clear benefit for CTS is not apparent. In CalNex, data were shifted on a slight scale, without much effect to measured results (figures 4.17 and 4.18). In the black aerosol run of the NOAA laboratory experiment, the CTS and Bond corrections yielded similar results (figure 4.25 and 4.26). However, as shown in figures 4.23 and 4.24, the NOAA laboratory experiment's white on grey run yields the greatest case for the utilization of the CTS correction. Figure 4.23 is an excellent illustration of why the calculation-intensive correction was developed. The potential overestimation by the Bond

correction in these changing conditions will affect the accuracy of σ_{ap} measurements if not properly addressed.

Within this investigation, an inter-comparison of absorption measurements, via differing methods in both atmospheric research and experimental design has been provided. A novel potential admission to the proposed filter-based bias to organic aerosols was observed, in that it is possibly related to the diurnal photochemical patterns of day and night atmospheric conditions. Also, the importance in detail-oriented investigations when considering possible discrepancies in measurement was demonstrated through both ambient field sampling and controlled laboratory conditions. These demonstrations of the filter-based, in-situ, and difference method yield some uncertainties that display the fundamental problem in aerosol measurements: there is no defined 'perfect' reference absorption measurement method. Each potential reference absorption method has associated uncertainties and inaccuracies. As such, further development through inter-comparisons of instruments and datasets is essential in order to reduce the uncertainty in absorption by atmospheric aerosol, and subsequent climate predictions.

IV. References

Agarwal, J.K. and G.J. Sem (1980). "Continuous-Flow, Single-Particle-Counting Condensation Nucleus Counter. *Journal of Aerosol Science,* 11: 343-357.

American Lung Association (2012). "State of the Air 2012." A report from the American Lung Association. 14-18 of 179 pgs. Accessed online at <stateoftheair.org> on March 30, 2012.

Anderson, T.L. and J.A. Ogren (1998). "Determining Aerosol Radiative Properties Using the TSI 3563 Integrating Nephelometer." *Aerosol Science and Technology,* 29: 57-69.

Anderson, T.L. et al. (2003). "Variability of Aerosol Optical Properties Derived from In Situ Aircraft Measurements during ACE-Asia." *Journal of Geophysical Research,* 108: 15-1-15-19.

Andrews, E. et al. (2012). "A Closure Experiment on Aerosol Absorption at Storm Peak Laboratory." Draft in progress.

Arnott, W. P., et al. (2003). "Photoacoustic and Filter-Based Ambient Aerosol Light Absorption Measurements: Instrument Comparisons and the Role of Relative Humidity." *Journal of Geophysical Research,* 108: 4034.

Arnott, W. P. et al. (2006). "Photoacoustic Insight for Aerosol Light Absorption Aloft from Meteorological Aircraft and Comparison with Particle Soot Absorption Photometer Measurements: DOE Southern Great Plains Climate Research Facility and the Costal Stratocumulus Imposed Perturbation Experiments." *Journal of Geophysical Research,* 111: D05S02, 16 pp.

Bond, T. C., T. L. Anderson, and D. Campbell (1999). "Calibration and Intercomparison of Filter-Based Measurements of Visible Light Absorption by Aerosols." *Aerosol Science and Technology*, 30: 582–600.

Bond, T.C. et al. (2009). "Truncation and Angular-Scattering Corrections for Absorbing Aerosol in the TSI 3563 Nephelometer." *Aerosol Science and Technology,* 43: 866-871.

Bohren, C.F. and D.R. Huffman (1983). Absorption and Scattering of Light by Small Particles. Wiley, New York.

Cappa et al. (2008). "Bias in Filter-Based Aerosol Light Absorption Measurements due to Organic Aerosol Loading: evidence from Laboratory Measurements." *Aerosol Science and Technology,* 42:1022-1032.

Charlson, R.J. et al. (1992). "Climate Forcing by Anthropogenic Aerosols." *Science,* 255: 423-430.

Cooke, W. F. and J.J.N. Wilson. (1996). "A Global Black Carbon Model." *Journal of Geophysical Research,* 101: 19-395-19-409.

DeCarlo, Peter F. et al. (2006). "Field-Deployable, High-Resolution, Time-of-Flight Aerosol Mass Spectrometer." *Analytical Chemistry.* 78: 8281-8289.

Feingold, G. et al. (2003). "First Measurements of the Twomey Indirect Effect using Ground-based Remote Sensors." 30, 6: 1287-1290.

Haywood, J. and O. Boucher (2000). "Estimates of the Direct and Indirect Radiative Forcing Due to Tropospheric Aerosols: A Review." *Reviews of Geophysics*, 38, 4: 513-543.

Hientzenberg, J. and R.J. Charlson (1996). "Designs and Applications of the Integrating Nephelometer: A Review." *Journal of Atmospheric and Oceanic Technology*, 13: 987-1000.

Hinds, William C. (1999). Aerosol Technology: Properties, Behavior, and Measurement of Airborne Particles (Second Edition). Wiley-Interscience Publication: Hoboken, New Jersey. Pages 121-138, 235-242.

Intergovernmental Panel on Climate Change (IPCC) (2007). Climate Change 2007: Working Group I: The Physical Science Basis: Summary for Policymakers. Figure SMP.2; Section 2.4 in AR4: Aerosols.

Jayne, J.T. et al. (2000). "Development of an Aerosol Mass Spectrometer for Size and Composition Analysis of Submicron Particles." *Aerosol Science Technology*, 33: 49-70.

Jimenez, J.L. et al. (2003) "Ambient Aerosol Sampling using the Aerodyne Aerosol Mass Spectrometer." *Journal of Geophysical Research*, 108: 8425-8438.

Kahn, R.A. et al (2009). "Atmospheric Aerosol Properties and Climate Impacts." (Chapter 1). Report by the U.S. Climate Change Science Program and the Subcommittee on Global Change Research. National Aeronautics and Space Administration. Washington D.C.

Lack, D. et al. (2006). "Aerosol Absorption Measurement Using Photoacoustic Spectroscopy: Sensitivity, Calibration, and Uncertainty Developments." *Aerosol Science Technology*, 40: 697-708

Lack et al. (2008). "Bias in Filter-Based Aerosol Light Absorption Measurements Due to Organic Aerosol Loading: Evidence from Ambient Measurements." *Aerosol Science and Technology*, 42: 1033-1041.

Lack, D. et al (2012). "Aircraft Instrumentation for Comprehensive Characterization of Aerosol Optical Properties, Part 2: Black and Brown Carbon Absorption and Absorption Enhancement Measured with Photoacoustic Spectroscopy." *Aerosol Science and Technology*, 46: 555-568.

Langridge, J.M. et al. (2011). "Aircraft Instrumentation for Comprehensive Characterization of Aerosol Optical Properties, Part 1: Wavelength-Dependent Optical Extinction and Its Relative Humidity Dependence Measured Using Cavity Ringdown Spectroscopy." *Aerosol Science and Technology*, 45: 1305-1318.

Langridge, J.M. et al. (2012). Submitted Paper: "Evolution of Aerosol Particles Impacting Visibility and Direct Climate Forcing in an Ammonia-rich Urban Environment."

Lu, Rong and Richard P. Turco (1994). "Air Pollutant Transport in a Costal Environment. Part I: Two Dimensional Simulations of Sea-Breeze and Mountain Effects." *Journal of Atmospheric Sciences*, 15: 2285-2308.

Magee Scientific: Aethalometers. www.mageesci.com. Accessed April 15, 2012.

Malm, W. C. et al. (1994). "Spatial and Seasonal Trends in Particle Concentration and Optical Extinction in the United States." *Journal of Geophysical Research*, 99: 1347-1370.

Massoli, P. et al. (2009a). "Aerosol Optical and Hydroscopic Properties during TexAQS-GoMACCS 2006 and their Impact on Aerosol Direct Radiative Forcing." *Journal of Geophysical Research,* 114: 1-17.

Massoli, P. et al. (2009b). "Uncertainty in Light Scattering Measurements by TSI Nephelometer: Results from Laboratory Studies and Implications for Ambient Measurements." *Aerosol Science and Technology*, 43: 1064-1074.

Massoli, P. et al. (2010). "Aerosol Light Extinction Measurements by Cavity Attenuated Phase-Shift Spectroscopy: Laboratory Validation and Field Deployment of a Compact Aerosol Particle Extinction Monitor." *Aerosol Science and Technology*, 44: 428-435.

Moosmüller, H. and W.P. Arnott (2003). "Angular Truncation Errors in Integrating Nephelometry." *Review of Scientific Instruments,* 74: 3492-3502.

Moosmüller H., R. Varma, and W.P. Arnott (2005). "Cavity Ring-Down and Cavity-Enhanced Detection Techniques for the Measurement of Aerosol Extinction." *Aerosol Science and Technology,* 39: 30-39.

Moosmüller, H., R.K. Chakrabarty, and W.P. Arnott (2009). "Aerosol Light Absorption and its Measurement: A Review." *Journal of Quantitative Spectroscopy and Radiative Transfer,* 10: 844-878.

Müller, T. et al. (2009). "Angular Illumination and Truncation of Three Different Integrating Nephelometers: Implications for Empirical, Size-Based Corrections." *Aerosol Science and Technology*, 43: 581-586.

Müller, T. et al. (2011). "Characterization and Intercomparison of Aerosol Absorption Photometers: Result of Two Intercomparision Workshops." *Atmospheric Measurement Techniques,* 4: 245-268.

Müller, T., A. Virkkula, and J.A. Ogren (draft). "Constrained Two-Stream Algorithm for Calculating Aerosol Light Absorption Coefficient from the Particle Soot Absorption Photometer."

Ng, N. L. et al. (2010). Organic Aerosol Components Observed in Northern Hemisphereric Datasets from Aerosol Mass Spectrometry." *Atmospheric Chemistry and Physics.* 10: 4625-4641.

NOAA Aerosol group homepage. www.ersl.NOAA.gov/gmd/aero. Accessed February 28, 2012

NOAA CLAP User's Manual (2012). Draft in progress.

NOAA Research Plan (2008). "2010 CalNex: Science and Implementation Plan." Research at the Nexus of Air Quality and Climate Change. Submitted 6 October 2008.

Ogren, J. (2010). "Comment on 'Calibration and Intercomparison of Filter-Based Measurements of Visible Light Absorption by Aerosols.'" *Aerosol Science and Technology,* 44: 589-591.

O'Keefe, Andrew and David A.G. Deacon (1988). "Cavity Ringdown Optical Spectrometer for Absorption Measurements Using Pulsed Laser Sources." *Review of Scientific Instruments,* 59: 2544-2555.

Oke, T.R. (1978). Boundary Layer Climates: Second Edition. Chapter 1: Energy Mass and Exchanges. University Press, Cambridge. 435 pp.

Petzold, A. and M. Schönlinner (2004). "Multi-Angle Absorption Photometry- A New Method for the Measurement of Aerosol Light Absorption and Atmospheric Black Carbon." *Journal of Aerosol Science,* 35: 421-441.

United States Census Bureau (2010). United States Census: 2010. Accessed online at <http://www.census.gov/> on March 24, 2012.

Ramanathan, V. and A.M. Vogelman (1997). "Greenhouse Effect, Atmospheric Solar Absorption, and the Earth's Radiation Budget: From the Arrhenius-Langley Era to the 1990's." *Ambio,* 26: 38-46.

Ramanathan, V. et al (2001). "Aerosols, Climate, and the Hydrological Cycle." *Science,* 294: 2119-2142.

Ramanathan, V. and G. Carmichael (2008). "Global and Regional Climate Changes due to Black Carbon." *Nature Geoscience,* 1: 221-227.

Rasool, S.I. and S. H. Schneider. "Atmospheric Carbon Dioxide and Aerosols: Effects of Large Increases on Global Climate." *Science,* 173, 3992: 138-141.

Raspet, R. et al. (2003). "Evaporation-Condensation Effects on Resonant Photoacoustics of Volatile Aerosols." *Journal of Atmospheric and Oceanic Technology,* 20:685-695.

Schwarz, J. P., et al. (2006). "Single-Particle Measurements of Midlatitude Black Carbon and Light-Scattering Aerosols from the Boundary Layer to the Lower Stratosphere."*Journal of Geophysical Research,*111.

Seinfeld, John H. and Spyros N. Pandis (2006). Atmospheric Chemistry and Physics: Air Pollution to Climate Change. Wiley-Interscience Publication. Hoboken, New Jersey.

Sheridan, P.J. et al. (2005). "The Reno Aerosol Optics Study: An Evaluation of Aerosol Absorption Measurement Methods." *Aerosol Science and Technology,* 39:1-16.

Smith, J.D. and D.B. Atkinson (2001). "A Portable Pulsed Cavity Ring-Down Transmissometer for Measurement of the Optical Extinction of the Atmospheric Aerosol." *Analyst,* 126:1216-1220.

Strawa, A.W. et al. (2003). "The Measurement of Aerosol Optical Properties Using Continuous Wave Cavity Ring-Down Techniques." *Journal of Atmospheric and Oceanic Technology,* 20: 454-465.

Stephens, M., et al. (2003). "Particle identification by Laser Induced Incandescence in a Solid State Laser Cavity." *Applied Optics,* 42: 3726–3736.

Subramanian, R. et al. (2007). "Yellow Beads and Missing Particles: Trouble Ahead for Filter-based Absorption Measurements." *Aerosol Science and Technology,* 41:630-637.

Twomey, S. (1974). "Pollution and the Planetary Albedo." *Atmospheric Environment,* 8: 1251-1256.

Ulbrich, M. et al (2009). "Interpretation of organic components from Positive Matrix Factorization of aerosol mass spectrometric data." *Atmospheric Chemistry and Physics:* 9, 2891-2918.

Virkkula, A. et al. (2005a). "A Three-Wavelength Optical Extinction Cell for Measuring Light Extinction and its Application to Determining Light Absorption Coefficient." *Aerosol Science and Technology,* 39: 52-67.

Virkkula, A. et al. (2005b). "Modification, Calibration, and a Field Test of an Instrument for Measuring Light Absorption by Particles." *Aerosol Science and Technology*, 39: 68-83.

Virtanen, A. et al. (2006). "Winter and Summertime Size Distributions and Densities of Traffic-related Aerosol Particles at a Busy Highway in Helsinki." *Atmospheric Chemistry and Physics,* 6: 2411-2421.

Wakimoto, Roger M. and James L. McElroy (1986). "Lidar Observation of Elevated Pollution Layers over Los Angeles." *Journal of Climate and Applied Meteorology,* 25:1583-1599.

Wang, S.C. and R.C. Flagan (1990). "Scanning Electrical Mobility Spectrometer." *Aerosol Science and Technology,* 13: 230-240.

Weingartner, E. et al. (2003). "Absorption of Light by Soot Particles: Determination of Absorption Coefficient by Means of Aethalometers." *Journal of Aerosol Science,* 34: 1445-1463

Wrobel, A et al. (2000). "Transport of Traffic-related Aerosols in Urban Areas." *Science of the Total Environment,* 257:199-211.

Zhang, Q. et al. (2007). "Ubiquity and Dominance of Oxygenated Species in Organic Aerosols in Anthropogenically-Influenced Northern Hemisphere Midlatitudes." *Geophysical Research Letters,* 34: L13801.

Zhu, Y. et al. (2002). "Study of Ultrafine Particles Near a Major Highway with Heavy-duty Diesel Traffic." *Atmospheric Environment,* 36: 4323-4335.

V. Appendices
A. Appendix: CalNex CLAP Discrepancies

As mentioned in section 2.6.1, the CLAP from the CalNex field campaign was not utilized in analysis. The original intention of the thesis was to base the comparison of the PAS in-situ technique to filter-based on measurements obtained from the CLAP. Developed by the aerosol group at NOAA, the CLAP instrument is a novel method for the measurement of σ_{ap} and data obtained from the instrument has not yet been published. However, due to very large inconsistencies on CLAP data obtained during the campaign, it was decided that CLAP data were unusable. A significant amount of work was devoted to investigating the cause of this discrepancy; however, the results of the examination remain inconclusive.

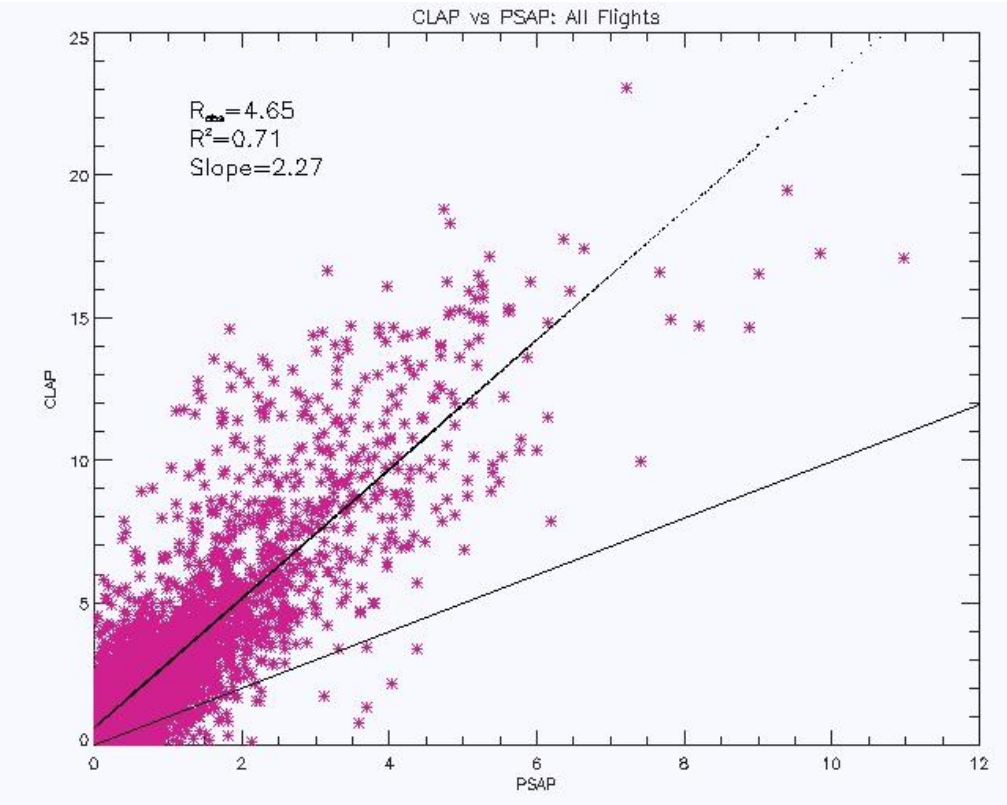

Figure A1: The regression between the CLAP and the PSAP utilized in the CalNex field campaign for analyzed all flights. A substantial inconsistency between the CLAP and PSAP measurements is apparent. This is not to be expected, as the CLAP and PSAP typically exhibit good relation in measurement.

Figure A1 gives the relationship between the CLAP and the PSAP for all analyzed flights in the CalNex field campaign. This large inconsistency between the two filter-based instruments is not typically observed (as evidenced by analysis conducted in section 4.2.1). It was found for the

entire CalNex dataset that the CLAP was consistently a factor of 2 higher than the PSAP, and 2-3 higher than the PAS. To investigate this, raw data was re-downloaded for both filter-based instruments and applied corrections (i.e. the Weiss and Bond corrections; equations 4 and 5) were calculated for small segments in Excel. These calculations were done in order to verify that the corrections were being applied correctly. Flow rates, spot sizes, and applied corrections were verified, and yet, the discrepancy remained.

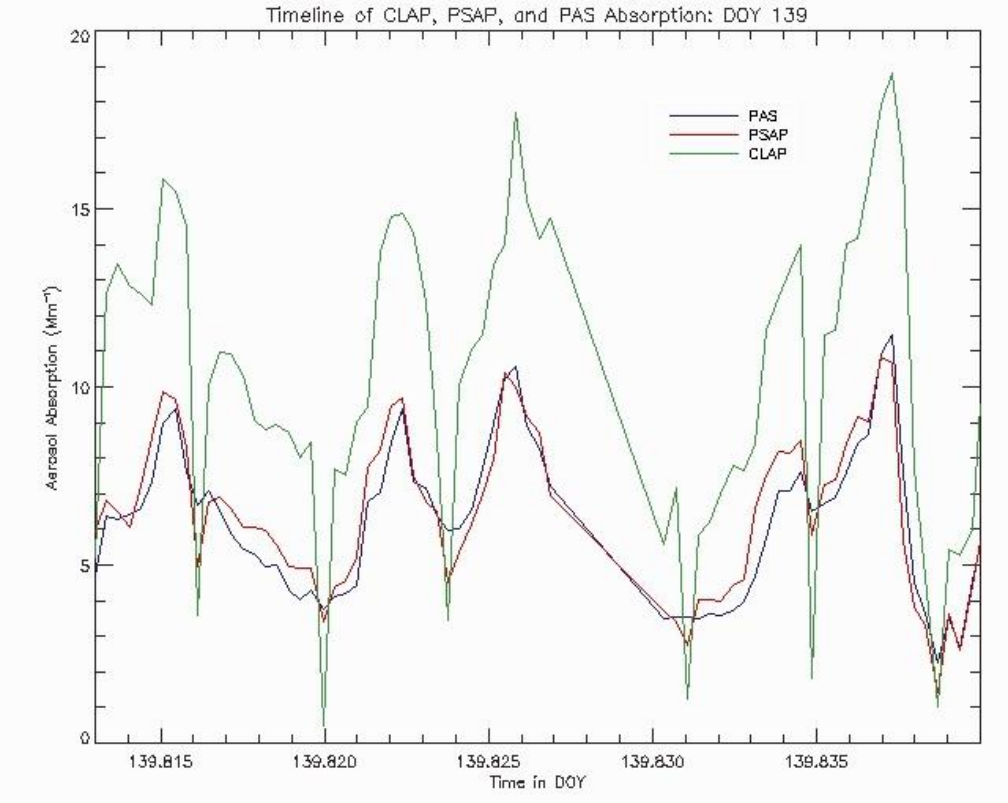

Figure A2: Time series example showing the large inconsistency in CLAP σ_{ap} compared to PSAP and PAS σ_{ap} for May 19th, 2010 (DOY 139). The measurements by the PSAP and PAS show good relation, while the CLAP yields measurements that are consistently higher.

Figure A2 is an example of a flight segment that depicts the CLAP discrepancy. This example for May 19th, 2010 (DOY 139) gives a typical example of the magnitude in which the CLAP measured above the PSAP and the PAS. A large number of reasons for the discrepancy were considered, but as it was the first field-deployment for the first manufactured CLAP, issues with measurement are to be expected.

B. Appendix: Other PSAP and CLAP Figures for NOAA Laboratory Experiment

B1. Figures from Filter-Based Comparison

Within the analysis in section 4.2.1, not all regressions were essential for the illustration of analysis findings. However, these figures are included here for further insight.

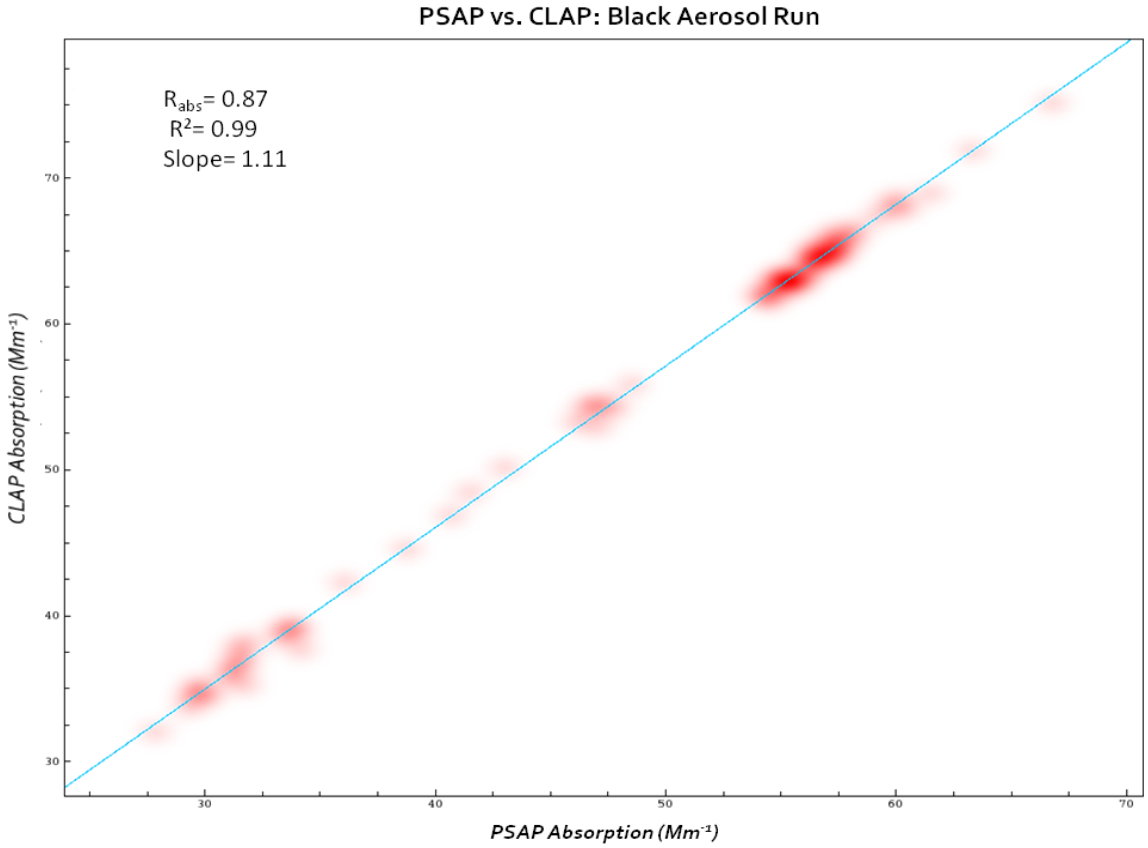

Figure A3: The regression between the CLAP (#1) and the PSAP (#1) σ_{ap} for the black aerosol run in the NOAA laboratory experiment.

For the black aerosol run, the linear regression between PSAP (#1) and CLAP (#1) is given in figure A3. With a slope of 1.11, an R^2 value of 0.99, and a R_{abs} ($\sigma_{ap,CLAP}$/ $\sigma_{ap,PSAP}$) of 0.87, it is clear that the PSAP and CLAP are closely linked in measurement of σ_{ap}.

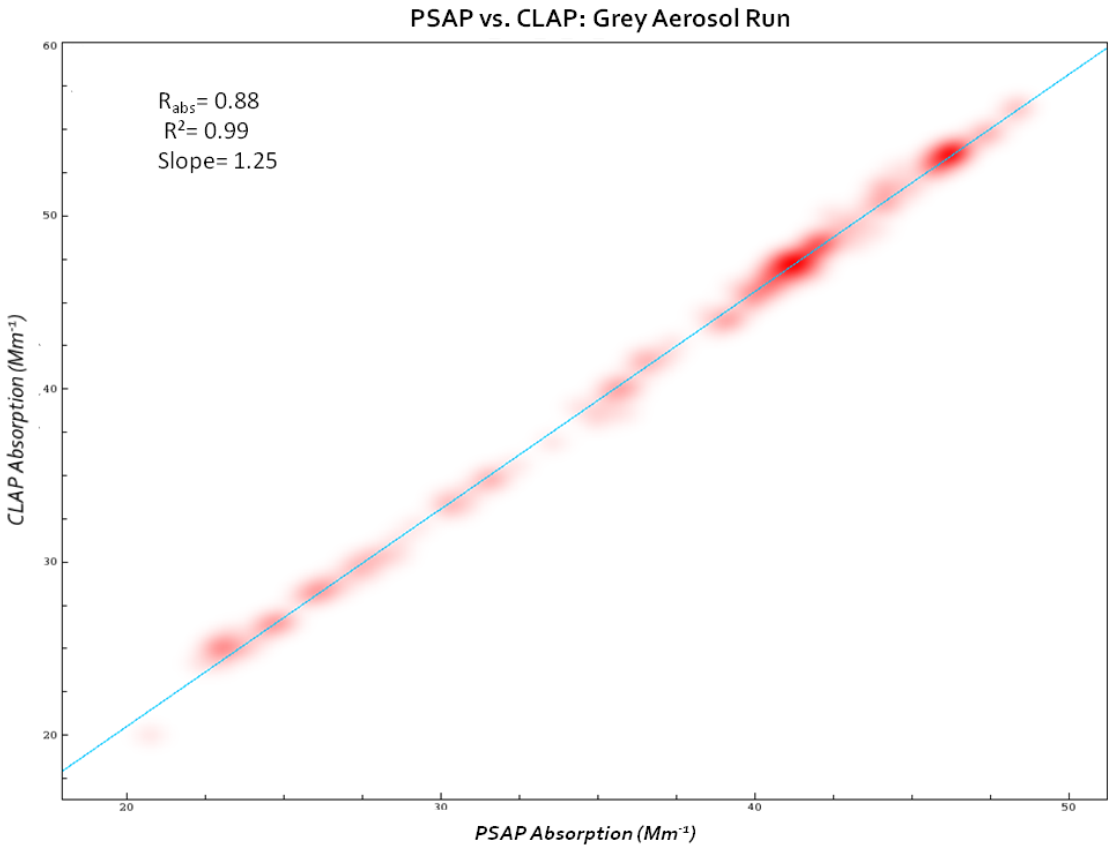

Figure A4: The regression between the CLAP (#1) and the PSAP (#1) σ_{ap} for the grey aerosol run in the NOAA laboratory experiment.

Figure A4 shows the linear regression for the CLAP and the PSAP for the grey aerosol run. With grey aerosol, the R_{abs} is 0.88, the slope is 1.25, and a strong correlation is shown with an R^2 value of 0.99. This is relevant to atmospheric research, as the conditions found during a grey aerosol run will be the most likely to be relatable to ambient conditions (on a regional basis).

B2: CTS Correction Comparison to Bond Correction for the CLAP

For the comparison between the CTS correction and the Bond correction for filter based instruments in the NOAA laboratory experiment, only the PSAP results were provided in analysis. Here, the similar results for the CLAP are given.

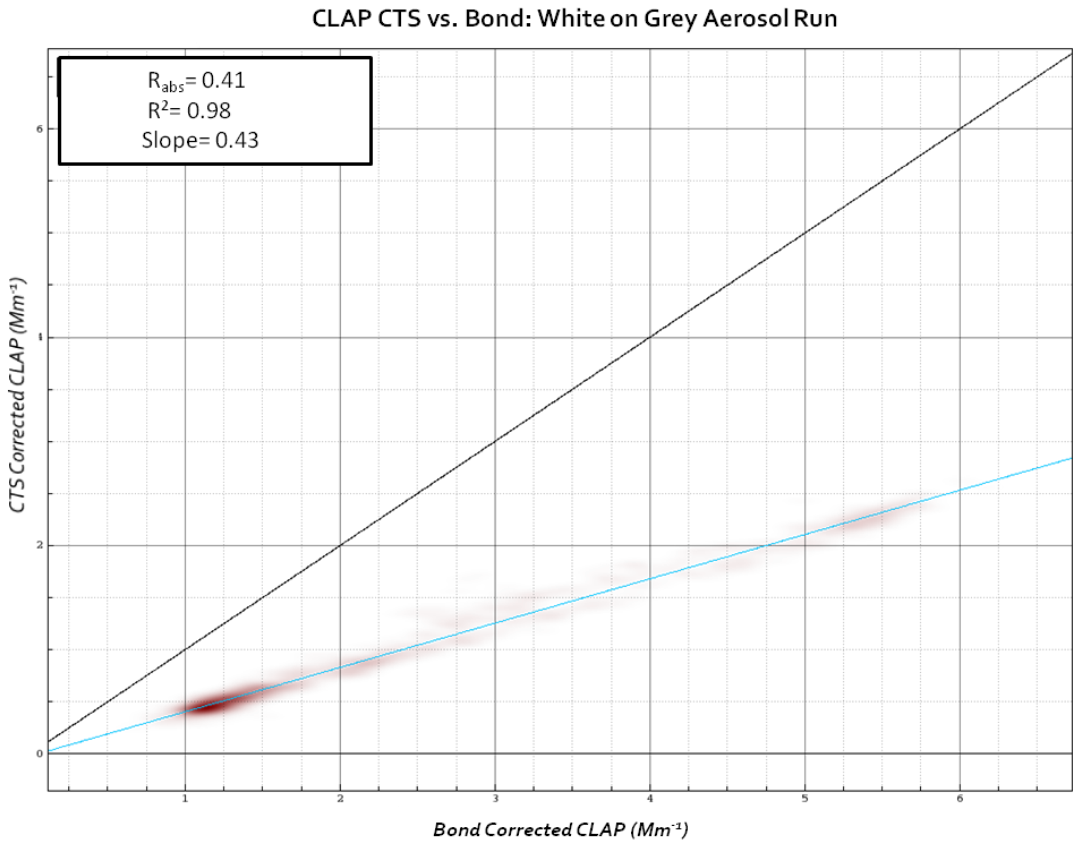

Figure A5: The regression between the CTS corrected CLAP (#1) and the Bond corrected CLAP (#1) σ_{ap} for the white on grey aerosol run in the NOAA laboratory experiment. An potential overestimation by the Bond correction scheme is apparent during the changing conditions of this laboratory run.

Figure A5 is the relationship between the CTS corrected CLAP (#1) and the Bond corrected CLAP for the white on grey run in the NOAA laboratory experiment. The R^2 value of 0.98 shows the strong correlation between the two correction schemes, despite the potential overestimation by the Bond corrected σ_{ap}. The possible benefit of utilizing the CTS correction during these changing conditions is evident with a R_{abs} ($\sigma_{ap,CTS}$/ $\sigma_{ap,Bond}$) of 0.41 and a slope of 0.43. Similar results to the PSAP, as seen in figure 4.24.

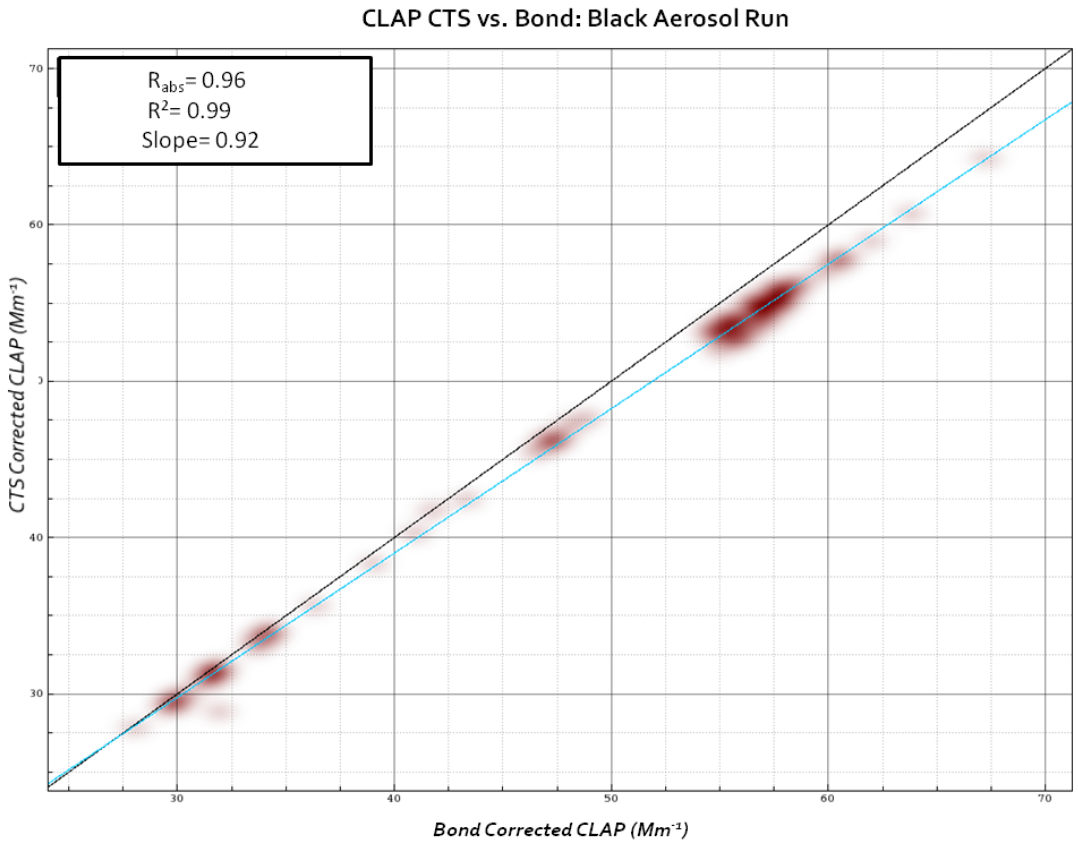

Figure A6: The regression between the CTS corrected CLAP (#1) and the Bond corrected CLAP (#1) σ_{ap} for the black aerosol run in the NOAA laboratory experiment. As can be seen, the outcome of the two corrections schemes is more alike with a stable input of absorbing aerosol.

As was shown in figure 4.26, the relationship between the CTS correction and the Bond correction more clear in consistent, highly absorbing conditions. With a R_{abs} of 0.96, an R^2 of 0.99, and a slope of 0.92, the benefit of utilizing the CTS correction is not as clear in these sampling conditions.

C. Appendix: NOAA Laboratory Discrepancy

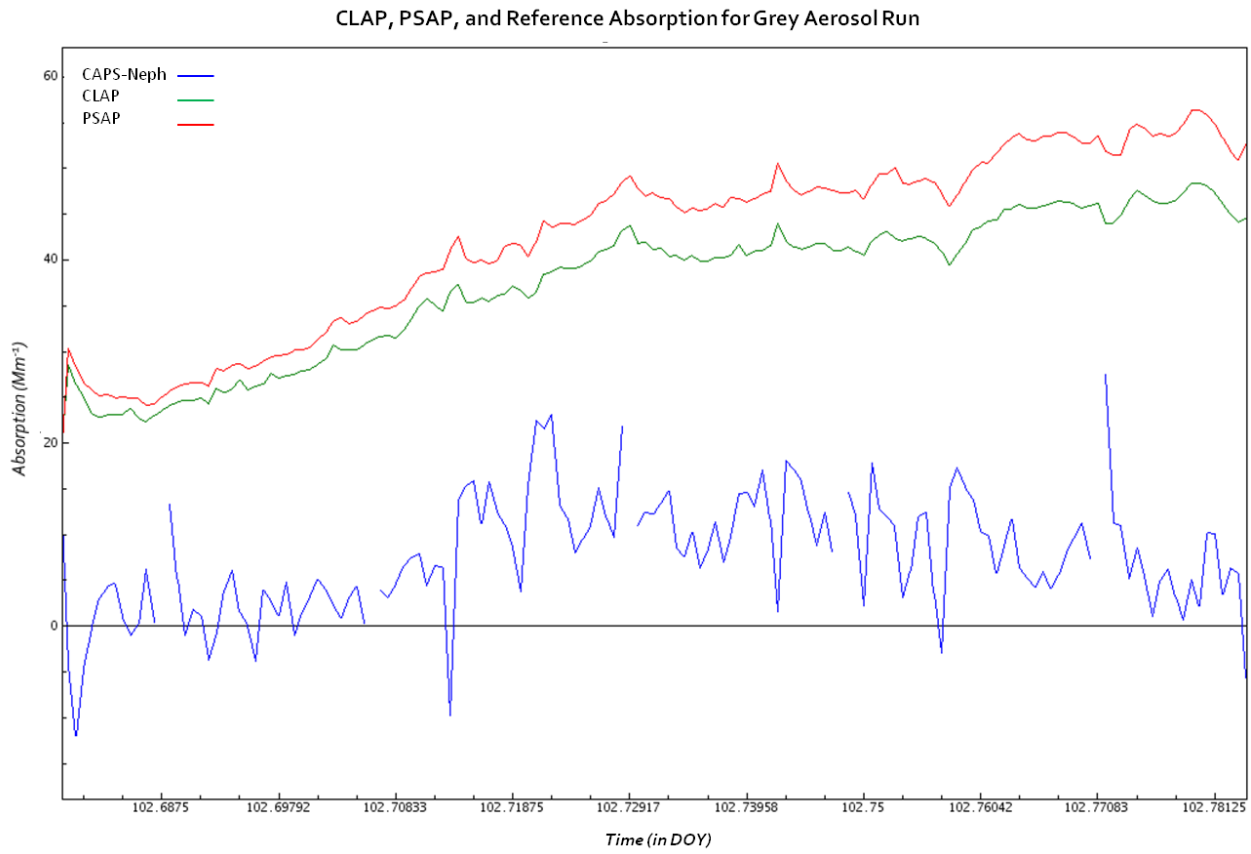

Figure A7: Time series of the CLAP (#1), PSAP (#1), and reference σ_{ap} for the grey aerosol run, where the σ_{ep} measured by the CAPS and the σ_{sp} measured by the nephelometer are inconsistent in measurement by about 5%.

Figure A7 demonstrates how the uncorrected 5% uncertainty between the CAPS extinction and the nephelometer scattering can yield large inconsistencies in the reference absorption measurement when compared to the filter-based instruments. In this grey run, the extinction was typically greater than the scattering, which is to be expected; however, the magnitudes were quite close. The difference between these very close measurements, along with fluctuations of which instrument was higher in measurement, leads to a noisy output that does not appear to track the measurements of the filter-based instruments at all. The reference σ_{ap} for this run appears choppy and inconsistent with measurements of the filter-based instruments. What these results clearly indicate is that true insight into utilizing the CAPS-nephelometer difference as a reference method until the σ_{ep} and σ_{sp} discrepancy was resolved.

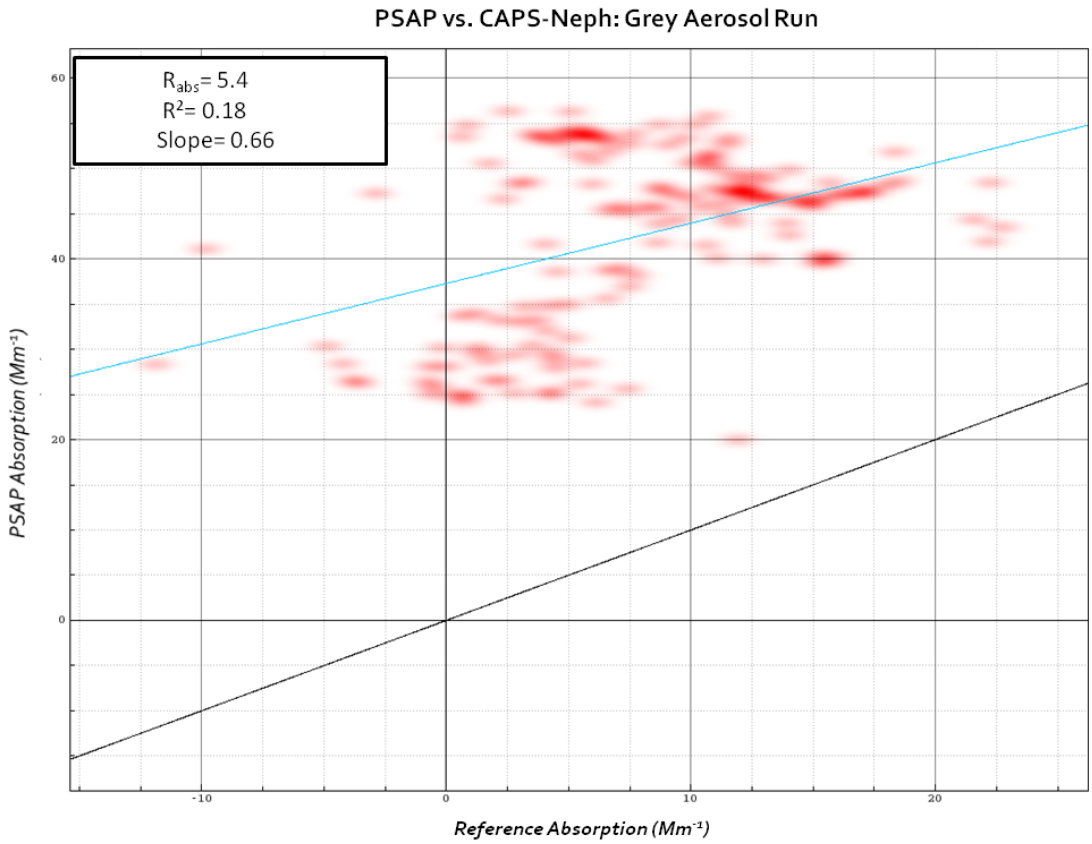

Figure A8: Regression between the PSAP (#1) σ_{ap} and the reference σ_{ap} for the grey aerosol run. The 5% discrepancy between the CAPS σ_{ep} and the nephelometer σ_{sp} provides a questionable reference σ_{ap}.

As figure A8 shows, the 5% discrepancy naturally leads to a comparison that does not yield much insight. With the best fit line of y = 0.66x + 37.38 and a R_{abs} ($\sigma_{ap,PSAP}$/ $\sigma_{ap,reference}$) of 5.4, the use of the CAPS – the nephelometer as a reference absorption method may have to be reconsidered. The CLAP yields similar results as the PSAP when compared to the reference absorption values, with a best fit line of y = 0.53x + 33.31 and a R_{abs} of 4.8. The lack of correlation is apparent in the very low R^2 values of 0.18 for the PSAP and 0.19 for the CLAP to the reference $\sigma_{ap.}$ Possible reasons for the large inconsistencies in filter-based measurement to the reference σ_{ap} were discussed in section 4.2.3.

D. CLAP Figures with Corrected Reference Measurements from NOAA Laboratory Experiment

In section 4.2.3, the comparison of the filter-based σ_{ap} measurements to the corrected reference σ_{ap} measurements were given with the PSAP results. Here, similar results for the CLAP are provided.

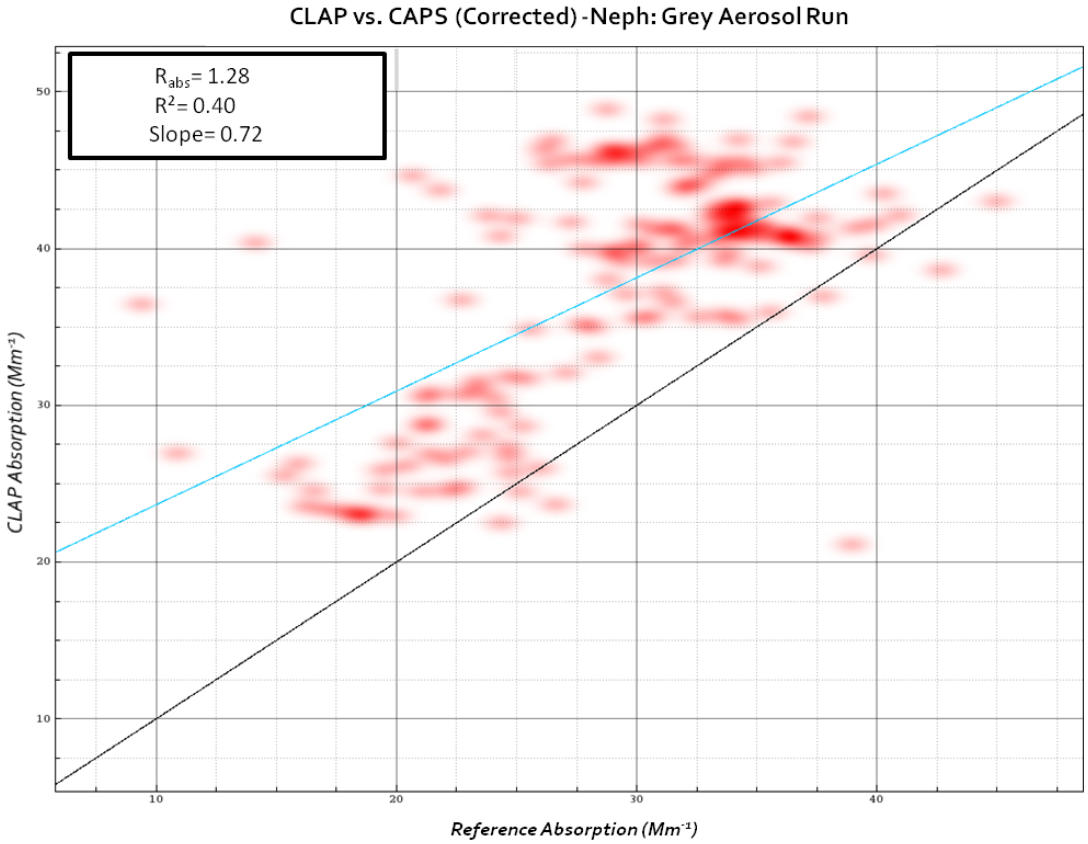

Figure A9: The regression between the CLAP (#1) and the reference σ_{ap} for the grey aerosol run, where the σ_{ep} measured by the CAPS has been adjusted using the correction factor.

Similar to the PSAP results, the CLAP measures consistently higher than the reference σ_{ap}. The R_{abs} ($\sigma_{ap,CLAP}$/ $\sigma_{ap,reference}$) is 1.28, with a slope of 0.72. The R^2 of 0.40 demonstrates a potentially weaker correlation between the filter-based σ_{ap} and the reference σ_{ap}.

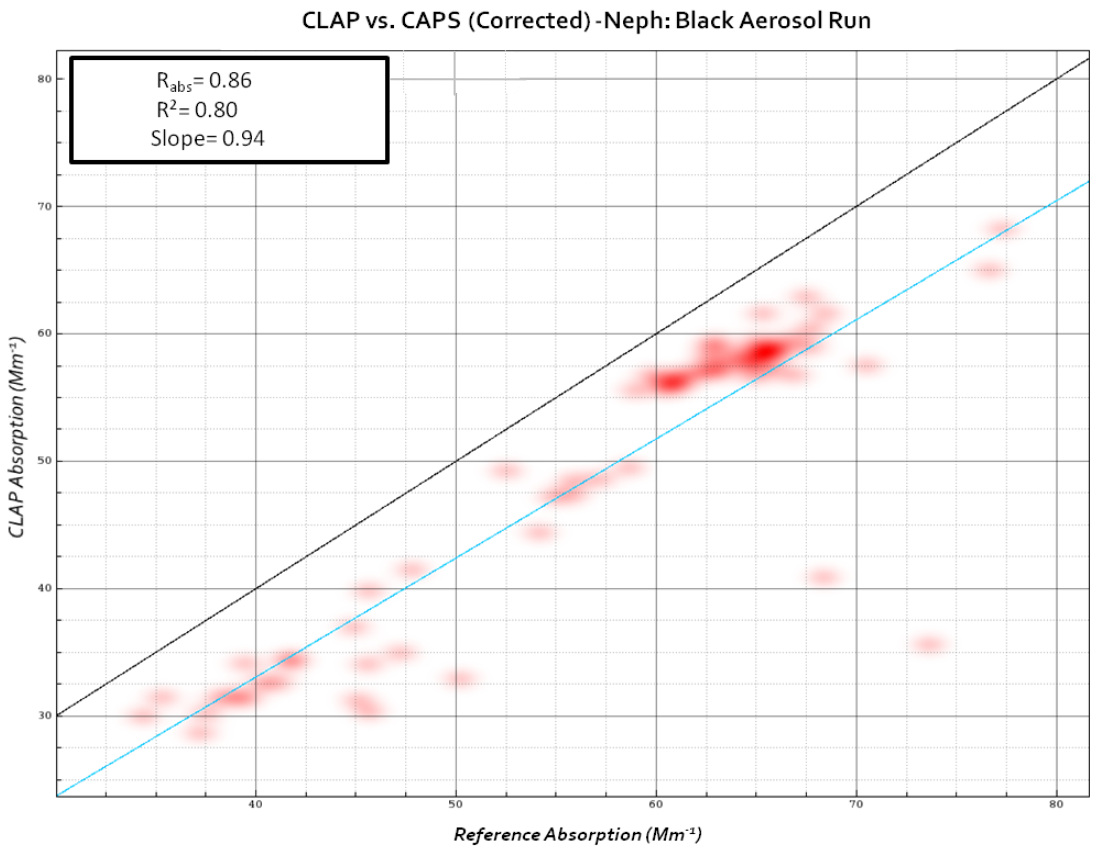

Figure A10: The regression between the CLAP (#1) and the reference σ_{ap} for the black aerosol run, where the σ_{ep} measured by the CAPS has been adjusted using the correction factor.

The relationship between the filter-based CLAP σ_{ap} and the reference σ_{ap} appears to be stronger in the highly absorbing conditions. Similar to the PSAP, the R_{abs} decreased from the grey run from 1.25 to 0.86. The correlation becomes stronger with an R^2 value of 0.80. The slope of the best-fit line becomes 0.94.

Institutionen för naturgeografi och ekosystemvetenskap, Lunds Universitet.

Student examensarbete (Seminarieuppsatser). Uppsatserna finns tillgängliga på institutionens geobibliotek, Sölvegatan 12, 223 62 LUND. Serien startade 1985. Hela listan och själva uppsatserna är även tillgängliga på LUP student papers (www.nateko.lu.se/masterthesis) och via Geobiblioteket (www.geobib.lu.se)

The student thesis reports are available at the Geo-Library, Department of Physical Geography and Ecosystem Science, University of Lund, Sölvegatan 12, S-223 62 Lund, Sweden. Report series started 1985. The complete list and electronic versions are also electronic available at the LUP student papers (www.nateko.lu.se/masterthesis) and through the Geo-library (www.geobib.lu.se)

199 Herbert Mbufong Njuabe (2011): Subarctic Peatlands in a Changing Climate: Greenhouse gas response to experimentally increased snow cover
200 Naemi Gunlycke & Anja Tuomaala (2011): Detecting forest degradation in Marakwet district, Kenya, using remote sensing and GIS
201 Nzung Seraphine Ebang (2011): How was the carbon balance of Europe affected by the summer 2003 heat wave? A study based on the use of a Dynamic Global Vegetation Model; LPJ-GUESS
202 Per-Ola Olsson (2011): Cartography in Internet-based view services – methods to improve cartography when geographic data from several sources are combined
203 Kristoffer Mattisson (2011): Modelling noise exposure from roads – a case study in Burlövs municipality
204 Erik Ahlberg (2011): BVOC emissions from a subarctic Mountain birch: Analysis of short-term chamber measurements.
205 Wilbert Timiza (2011): Climate variability and satellite – observed vegetation responses in Tanzania.
206 Louise Svensson (2011): The ethanol industry - impact on land use and biodiversity. A case study of São Paulo State in Brazil.
207 Fredrik Fredén (2011): Impacts of dams on lowland agriculture in the Mekong river catchment.
208 Johanna Hjärpe (2011): Kartläggning av kväve i vatten i LKAB:s verksamhet i Malmberget år 2011 och kvävets betydelse i akvatiska ekosystem ur ett lokalt och ett globalt perspektiv
209 Oskar Löfgren (2011): Increase of tree abundance between 1960 and 2009 in the treeline of Luongastunturi in the northern Swedish Scandes
210 Izabella Rosengren (2011): Land degradation in the Ovitoto region of Namibia: what are the local causes and consequences and how do we avoid them?
211 Irina Popova (2011): Agroforestry och dess påverkan på den biofysiska miljön i Afrika.
212 Emilie Walsund (2011): Food Security and Food Sufficiency in Ethiopia and Eastern Africa.

213 Martin Bernhardson (2011): Jökulhlaups: Their Associated Landforms and Landscape Impacts.
214 Michel Tholin (2011): Weather induced variations in raptor migration; A study of raptor migration during one autumn season in Kazbegi, Georgia, 2010
215 Amelie Lindgren (2011) The Effect of Natural Disturbances on the Carbon Balance of Boreal Forests.
216 Klara Århem (2011): Environmental consequences of the palm oil industry in Malaysia.
217 Ana Maria Yáñez Serrano (2011) Within-Canopy Sesquiterpene Ozonolysis in Amazonia
218 Edward Kashava Kuliwoye (2011) Flood Hazard Assessment by means of Remote Sensing and Spatial analyses in the Cuvelai Basin Case Study Ohangwena Region –Northern Namibia
219 Julia Olsson (2011) GIS-baserad metod för etablering av centraliserade biogasanläggningar baserad på husdjursgödsel.
220 Florian Sallaba (2011) The potential of support vector machine classification of land use and land cover using seasonality from MODIS satellite data
221 Salem Beyene Ghezahai (2011) Assessing vegetation changes for parts of the Sudan and Chad during 2000-2010 using time series analysis of MODIS-NDVI
222 Bahzad Khaled (2011) Spatial heterogeneity of soil CO2 efflux at ADVEX site Norunda in Sweden
223 Emmy Axelsson (2011) Spatiotemporal variation of carbon stocks and fluxes at a clear-cut area in central Sweden
224 Eduard Mikayelyan (2011) Developing Android Mobile Map Application with Standard Navigation Tools for Pedestrians
225 Johanna Engström (2011) The effect of Northern Hemisphere teleconnections on the hydropower production in southern Sweden
226 Kosemani Bosede Adenike (2011) Deforestation and carbon stocks in Africa
227 Ouattara Adama (2011) Mauritania and Senegal coastal area urbanization, ground water flood risk in Nouakchott and land use/land cover change in Mbour area
228 Andrea Johansson (2011) Fire in Boreal forests
229 Arna Björk Þorsteinsdóttir (2011) Mapping *Lupinus nootkatensis* in Iceland using SPOT 5 images
230 Cléber Domingos Arruda (2011) Developing a Pedestrian Route Network Service (PRNS)
231 Nitin Chaudhary (2011) Evaluation of RCA & RCA GUESS and estimation of vegetation-climate feedbacks over India for present climate
232 Bjarne Munk Lyshede (2012) Diurnal variations in methane flux in a low-arctic fen in Southwest Greenland
233 Zhendong Wu (2012) Dissolved methane dynamics in a subarctic peatland
234 Lars Johansson (2012) Modelling near ground wind speed in urban environments using high-resolution digital surface models and statistical methods
235 Sanna Dufbäck (2012) Lokal dagvattenhantering med grönytefaktorn

236 Arash Amiri (2012)Automatic Geospatial Web Service Composition for Developing a Routing System
237 Emma Li Johansson (2012) The Melting Himalayas: Examples of Water Harvesting Techniques
238 Adelina Osmani (2012) Forests as carbon sinks - A comparison between the boreal forest and the tropical forest
239 Uta Klönne (2012) Drought in the Sahel – global and local driving forces and their impact on vegetation in the 20th and 21st century
240 Max van Meeningen (2012) Metanutsläpp från det smältande Arktis
241 Joakim Lindberg (2012) Analys av tillväxt för enskilda träd efter gallring i ett blandbestånd av gran och tall, Sverige
242 Caroline Jonsson (2012) The relationship between climate change and grazing by herbivores; their impact on the carbon cycle in Arctic environments
243 Carolina Emanuelsson and Elna Rasmusson (2012) The effects of soil erosion on nutrient content in smallholding tea lands in Matara district, Sri Lanka
244 John Bengtsson and Eric Torkelsson (2012) The Potential Impact of Changing Vegetation on Thawing Permafrost: Effects of manipulated vegetation on summer ground temperatures and soil moisture in Abisko, Sweden
245 Linnea Jonsson (2012). Impacts of climate change on Pedunculate oak and Phytophthora activity in north and central Europe
246 Ulrika Belsing (2012) Arktis och Antarktis föränderliga havsistäcken
247 Anna Lindstein (2012) Riskområden för erosion och näringsläckage i Segeåns avrinningsområde
248 Bodil Englund (2012) Klimatanpassningsarbete kring stigande havsnivåer i Kalmar läns kustkommuner
249 Alexandra Dicander (2012) GIS-baserad översvämningskartering i Segeåns avrinningsområde
250 Johannes Jonsson (2012) Defining phenology events with digital repeat photography
251 Joel Lilljebjörn (2012) Flygbildsbaserad skyddszonsinventering vid Segeå
252 Camilla Persson (2012) Beräkning av glaciärers massbalans – En metodanalys med fjärranalys och jämviktslinjehöjd över Storglaciären
253 Rebecka Nilsson (2012) Torkan i Australien 2002-2010 Analys av möjliga orsaker och effekter
254 Ning Zhang (2012) Automated plane detection and extraction from airborne laser scanning data of dense urban areas
255 Bawar Tahir (2012) Comparison of the water balance of two forest stands using the BROOK90 model
256 Shubhangi Lamba (2012) Estimating contemporary methane emissions from tropical wetlands using multiple modelling approaches
257 Mohammed S. Alwesabi (2012) MODIS NDVI satellite data for assessing drought in Somalia during the period 2000-2011
258 Christine Walsh (2012) Aerosol light absorption measurement techniques: a comparison of methods from field data and laboratory experimentation